Social touch promotes interfemale communication via activation of parvocellular oxytocin neurons

Yan Tang, Diego Benusiglio, Arthur Lefevre, Louis Hilfiger, Ferdinand Althammer, Anna Bludau, Daisuke Hagiwara, Angel Baudon, Pascal Darbon, Jonas Schimmer, et al.

Social touch promotes inter-female communication via activation of parvocellular oxytocin neurons

Yan Tang[1*$], Diego Benusiglio[1*], Arthur Lefevre[1,2]*, Louis Hilfiger[2]*, Ferdinand Althammer[1,3], Anna Bludau[4], Daisuke Hagiwara[1], Angel Baudon[2], Pascal Darbon[2], Jonas Schimmer[1], Matthew K. Kirchner[3], Ranjan K. Roy[3], Shiyi Wang[1], Marina Eliava[1], Shlomo Wagner[5], Martina Oberhuber[6], Karl K. Conzelmann[6], Martin Schwarz[7], Javier E. Stern[3], Gareth Leng[8], Inga D. Neumann[4@], Alexandre Charlet[2@#] and Valery Grinevich[1,3@#]

[1]Department of Neuropeptide Research in Psychiatry, Central Institute of Mental Health, Medical Faculty Mannheim, University of Heidelberg, 68159 Mannheim, Germany
[2]Centre National de la Recherche Scientifique (CNRS) and University of Strasbourg, UPR3212, Institute of Cellular and Integrative Neurosciences, 67084 Strasbourg, France
[3]Center for Neuroinflammation and Cardiometabolic Diseases, Georgia State University, Atlanta GA 30303, USA
[4]Department of Neurobiology and Animal Physiology, University of Regensburg, 93040 Regensburg, Germany
[5]Sagol Department of Neurobiology, University of Haifa, Mt. Carmel, Haifa 31905, Israel
[6]Max von Pettenkofer-Institute Virology, Faculty of Medicine and Gene Center, Ludwig Maximilians University 81377 Munich, Germany.
[7]Institute for Experimental Epileptology and Cognition Research, University of Bonn Medical Center, D-53127 Bonn, Germany
[8]Centre for Discovery Brain Sciences, University of Edinburgh, Edinburgh EH8 9XD, UK

[$]Present address: Department of Biomedical Sciences, Faculty of Biology and Medicine, University of Lausanne, 1005 Lausanne, Switzerland

[*]Equal first authors
[@]Equal senior authors

[#]Corresponding authors:
Alexandre Charlet, PhD
Institute of Cellular and Integrative Neurosciences,
INCI CNRS UPR3212
8, Allée du Général Rouvillois
67000 Strasbourg, France
Phone: (33) 6070 825 06
E-mail: acharlet@unistra.fr

Valery Grinevich, MD, PhD
Department of Neuropeptide Research in Psychiatry
Central Institute of Mental Health
Medical Faculty Mannheim
University of Heidelberg
J5, Mannheim, 68159
Germany
Phone: (49) 621 1703 2995
E-mail: valery.grinevich@zi-mannheim.de

Abstract

Oxytocin is a great facilitator of social life, but although its effects on socially-relevant brain regions have been extensively studied, oxytocin neuron activity during actual social interactions remains unexplored. The majority of oxytocin neurons are magnocellular neurons, which simultaneously project to the pituitary and forebrain regions involved in social behaviors. Here, we show that a much smaller population of oxytocin neurons, parvocellular neurons that do not project to the pituitary but which synapse onto magnocellular neurons, is preferentially activated by somatosensory stimuli. This activation is transmitted to the larger population of magnocellular neurons, which consequently show coordinated increases in their activity during social interactions between virgin female rats. Selectively activating these parvocellular neurons promotes social motivation, whereas inhibiting them reduces social interactions. Thus, parvocellular oxytocin neurons, receive somatosensory inputs to control social behavior by coordinating the responses of the much larger population of magnocellular oxytocin neurons.

INTRODUCTION

The hypothalamic neuropeptide oxytocin (OT) promotes various types of social behavior[1–3]. OT is mainly synthesized in neurons of the paraventricular (PVN) and supraoptic (SON) nuclei of the hypothalamus. The vast majority of these neurons project to the posterior pituitary, where OT is secreted into the blood for essential physiological effects, such as suckling-induced milk let-down and for regulating uterine contractions during birth[4]. In parallel, these neurons project axonal collaterals to forebrain regions[5] that express OT receptors (OTRs), including the central nucleus of the amygdala, nucleus accumbens, lateral septum, hippocampus, and medial prefrontal cortex[6,7]. Studies employing microdialysis to measure OT concentrations within socially-relevant brain regions revealed that OT is released in the bed nucleus of stria terminalis, lateral septum, and central nucleus of amygdala during social investigation of a conspecific [2,8,9]. However, to date, no direct measurement of OT neuron activity during actual social interaction of freely moving conspecifics has been performed, although it was recently reported that social approach triggers calcium release in PVN OT neurons in immobilized, head-fixed male mice[10].

Several studies suggest that female-female interactions are predominantly mediated via somatosensory inputs[11,12], while other interactions such as male-male, male-female or parental contact may rely on other sensory modalities. However, whether those sensory stimulations can activate OT neurons is unknown since, to this date, there has been no direct recording of activity from identified OT neurons during actual social behavior. In an attempt to address these points, in the current study, we performed *ex vivo* and *in vivo* manipulation of OT neurons activity primarily in the PVN - the main source of OT in the brain[5] - to decipher their involvement in the modulation of social interaction in freely-moving female rats.

RESULTS

PVN OT neurons are activated upon social interaction

To identify OT neurons electrophysiologically, we injected a recombinant adeno-associated virus (rAAV-OTp-ChR2-mCherry) bilaterally into the PVN to induce expression of the light-sensitive ion channel Channelrhodopsin-2 (ChR2) under the control of the OT promoter[5,13]. This resulted in 90.4% of ChR2-expressing neurons being OT-positive, showing the high specificity of the infection in the PVN (**Extended Data Fig. 1a**). We then recorded individual neurons in the PVN using implanted tetrodes combined with an optic fiber to identify the OT neurons by their electrophysiological response to blue-laser pulses, similar to methods in[14].

In total, we recorded 90 neurons in 10 adult female rats at the diestrus phase of the ovarian cycle, while monitoring the behavior of the rats and their ultrasonic vocalizations during both *open field (OF) exploration* and *free social interactions* (FSI) (**Fig. 1a-b**). Fifteen of these neurons (in 5 animals) were stringently identified as single OT neurons (**Extended Data Fig. 1e**). In the open field arena, the patterns of spiking activity of these neurons (**Fig. 1d, Extended Data Fig. 2d**) were indistinguishable from those of OT neurons observed under basal conditions in anesthetized rats, as these neurons displayed typical OT neurons characteristics[15]. Specifically, they all display low rate of tonic firing (~1 Hz) with a low index of dispersion of spikes (<1) and a distribution of interspike intervals consistent with random spike generation subject to a prolonged relative refractory period. In contrast, during episodes of FSI with an unfamiliar conspecific, the same neurons fired at a higher rate (mean increase 1.5 ± 0.4 spikes/s, $p = 0.001$, $n = 15$; **Fig. 1c-d**) and more irregularly; the second-by-second firing rates showed a high index of dispersion, reflecting the prominent occurrence of clusters of spikes (**Fig. 1d, Extended Data Fig. 1n**).

As revealed by cross-correlation analysis, OT neurons also displayed increased synchronicity during FSI (mean pairwise correlation: open field, 0.10 ± 0.04; FSI 0.40 ± 0.08, $p = 0.001$, **Extended Data Fig. 1k-l**). In anesthetized rats, adjacent OT neurons showed no such cross-correlated activity. We also recorded local field potentials in the PVN and found a significant

increase of oscillatory power in the theta (5-10 Hz) frequency band during FSI (**Extended Data Fig. 1f-h**). The spike activity of OT neurons tended to be phase-locked with theta oscillations during FSI, but not in the open field arena (**Extended Data Fig. 1i-j**). In contrast to OT neurons, non-OT PVN neurons did not show an increase in spiking activity when comparing exploratory behavior and social interaction (**Extended Data Fig. 2e-g**).

Thus, during free social interaction with actual physical contact, OT neurons in the PVN were more active and exhibited frequent clusters of spikes, and this activity was correlated amongst the OT neurons.

Social physical contact increases PVN OT neuron activity

To examine which component of social interaction activates these neurons, we first recorded their neuronal activity during a *chambered social interaction* (CSI)[16]. In this setup, experimental and stimulus rats were separated by a transparent wall with small holes (7.5 mm) in it, allowing rats to see, sniff and hear each other, but not to touch each other (CSI, **Fig. 1e**).

OT neurons showed little change in spiking activity between CSI and baseline recordings in OF (CSI: 1.4 ± 0.4 spikes/s; open field: 1.0 ± 0.2 spikes/s, $p = 0.14$; **Fig. 1f**). When the wall was removed to allow free social interaction (FSI), the same OT neurons displayed a significant increase in activity (FSI: 3.0 ± 0.4 spikes/s, $p < 0.001$; **Fig. 1f**), accompanied by an increase in index of dispersion (FSI, 3.2 ± 0.4; CSI, 1.3 ± 0.3, $p = 0.006$ vs FSI; open-field, 0.9 ± 0.2, $p = 0.004$ vs FSI). To estimate the amount of oxytocin axonal release due to the increase in firing rate together with the altered firing pattern, we employed an activity (spike) dependent model of oxytocin secretion[17] (**Extended Data Fig. 2h-j**) that quantitatively captures the features of stimulus-secretion coupling at the nerve terminals.

To dissect which sensory modalities activate OT neurons during FSI, we categorized rat social behaviors into "*sniffing*", "*head-to-head*" and "*crawled on top*" *or* "*being crawled*" events and

constructed peristimulus time histograms (PSTH) of spiking activity before, during, and after the onset of each sequence (**Fig. 1g-h**). "*Crawled on top"* and "*being crawled"* induced the greatest increases in firing rates ($p = 0.036$, $p = 0.024$, respectively; **Supplementary Video 1**), while "*sniffing"*, "*chasing"*, and "*head-to-head"* events induced lesser, non-significant changes (**Fig. 1h; Extended Data Fig. 2a-c**). In addition, ultrasonic vocalizations during FSI revealed the appearance of bands between 40 and 90 kHz known to be related to social communication in rats[18] (**Extended Data Fig. 3a-b**), but we found no time-locked (in ranges up to ± 5 s) correlation between OT neuron activity and ultrasonic vocalizations (**Extended Data Fig. 3c-e**). Although we were not able to discriminate USV individual calls between the two conspecifics, we hypothesized that OT neurons were activated mainly by physical contacts and investigated this further by modeling gentle, non-nociceptive mechanical stimuli.

Gentle non-nociceptive mechanical stimuli trigger OT neuron activation

To test whether somatosensory stimulation itself is sufficient to increase OT cell activity, we performed controlled tactile stimulations using compressed air delivery ("airpuffs") in isoflurane anaesthetized rats as in[19] (**Fig. 2a**). Stimulation of the skin on the dorsal body region by airpuffs (at three sites) reproducibly activated 19 out of 23 (83 %) recorded PVN OT neurons (mean increase 1.3 ± 0.5 spikes/s, mean *$p = 0.021$, **Fig. 2a-b** and **Extended Data Fig. 4a-b**).

Airpuffs applied to the abdominal skin produced little or no changes in their activity (mean change 0.5 ± 0.3 spikes/s., $p = 0.33$), and there were no detected effects after stimulation of the anogenital area or the whiskers pad (**Extended Data Fig. 4c**). For a potential involvement of the olfactory system in PVN OT neurons activation during social interaction, we exposed female rats to either a neutral odor (clean bedding) or to a socially relevant odor (urinated-on female beddings). We found that the exposure to odorants did not elicit significant changes in firing rate or in spike distribution ($p = 0.34$, $p = 0.48$ respectively, **Extended Data Fig. 4d-f**) in any of the recorded OT neurons.

There was also no difference upon presentation of neutral odor. Hence, we concluded that somatosensory inputs are the dominant signals that activate PVN OT neurons during social interactions.

ParvOT neurons respond to gentle non-nociceptive mechanical stimuli

Although the overwhelming majority of OT neurons in the PVN (97%) are magnocellular (magnOT) neurons, there is also a population of parvocellular OT (parvOT) neurons (~3%) that do not project to the pituitary[20], but which are crucial for the transmission of nociceptive signals to the magnOT cells[13].

To study whether parvOT neurons are also activated by *non*-nociceptive stimuli, applying airpuffs to conscious rats trained and adapted for short-term immobilization. For this purpose, we first used rats that had been injected systemically with the retrograde tracer Fluorogold™ to label all neurons in the brain that project outside the blood-brain barrier, including in particular magnOT, but not parvOT neurons. To identify neurons strongly activated by airpuffs, we used the expression of *c-fos* as an indicator of activated OT neurons. Previous studies have found that *c-fos* expression is activated in non-identified OT neuron cell type following social interaction in voles[21], mice[22] and rats[23]. Immunocytochemistry revealed the presence of *c-fos* in 30% of parvOT neurons in the PVN of stimulated rats (average 12.4 ± 3 neurons per PVN/hemisphere, n = 4, **Fig. 2c, Supplementary Table 1a**), but not in magnOT neurons or in any OT neurons in non-stimulated control rats, indicating that airpuffs specifically applied to the dorsal body region seem to predominantly activate parvOT neurons. In a second step, we labeled parvOT neurons retrogradely by injecting the canine adenovirus serotype 2 (CAV2-Cre)[24] into the SON, and concomitantly injected the Cre-responder rAAV expressing mCherry under the control of the OT promoter into the PVN. In line with our previous results, airpuffs induced *c-fos* expression exclusively in retrogradely-labeled

mCherry-positve OT neurons (average 47.6%, 7.5 ± 3 neurons per PVN/hemisphere, n = 4, **Fig. 2d, Supplementary Table 1b**).

To explore the role of parvOT neurons in social interaction and their response to gentle non-nociceptive mechanical stimuli (airpuffs), we chose to manipulate their activity via virally-expressed DREADDs. To this end, we used a similar Cre-dependent viral-based strategy employing OTp-DIO-hM4D(Gi)-mCherry and OTp-DIO-hM3D(Gq)-mCherry rAAVs (**Fig. 2e-f**). As a first step, we verified the efficiency of DREADDs in modulating of parvOT neuron activity *ex vivo*, showing that hM3D(Gq)-CNO-induced parvOT activation significantly increased the spontaneous AP frequency (baseline 0.85 ± 0.39 Hz vs CNO 1.31 ± 0.51 Hz, n = 9; p = 0.0039; **Extended Data Fig. 5a-c**) and the number of evoked APs (16.18 ± 3.89 AP vs CNO 22.55 ± 5.66 AP, n = 11; p = 0.0314; **Extended Data Fig. 5d-f**). Consistent with this, hM4D(Gi)-CNO-induced inhibition (10μM, 6min) significantly decreased both the spontaneous AP frequency (baseline 1.38 ± 0.38 Hz vs CNO 0.36 ± 0.18 Hz, n = 7; p = 0.0469; **Extended Data Fig. 5g-i**) and the number of evoked action potentials (APs) (baseline 13 ± 2.02 AP vs CNO 7.75 ± 2.03 AP, n = 11; p = 0.0007; **Extended Data Fig. 5j-l**).

Following the *ex vivo* results, we next performed *in vivo* recording in anaesthetized animals to better understand the airpuff-induced activation of parvOT. For this purpose, PVN parvOT activity was imaged using the GCaMP6s reporter using fiber photometry[25] (**Fig. 2e-h**). Then, rats were injected with the DREADD ligand CNO (3 mg/kg i.p.) and OT neurons Ca^{2+} transients were analyzed. Chemogenetic activation of the parvOT neurons enhanced the Ca^{2+} response to airpuffs (45 ± 9 % increase of area under the curve (AUC), p = 0.03, **Fig. 2i**). Conversely, chemogenetic inhibition of the parvOT neurons reduced the response to airpuffs (65 ± 5% decrease of AUC, p = 0.009 compared to control, **Fig. 2j**).

Thus, we concluded that gentle non-nociceptive mechanical stimulation of the dorsal region activates parvOT neurons, which we hypothesized may drive the activity of the larger population of magnOT neurons.

Intra-PVN connectivity of parvOT and magnOT neurons

To validate this hypothesis, we first looked for direct synaptic contact of parvOT neurons onto magnOT somata and/or dendrites via injection of OTp-DIO-GFP rAAV into the PVN and Cav2-Cre into the SON to specifically label parvOT neurons (**Extended Data Fig. 6a-b**) in analogy to[13]. For three-dimensional reconstruction of interposition between axons of parvOT neurons and somato-dendritic domains of magnOT neurons, we employed the IMARIS technique[26,27]. This approach allows precise identification of the location of synaptic contact by quantifying overlap with synaptophysin(SYN)-immunoreactive puncta. By performing IMARIS-assisted Sholl analysis, we found synaptic-like contacts of parvOT neurons with magnOT somas and dendrites (**Fig. 3a**, **Extended Data Fig. 6**, 6 dendritic contacts, 124 somatic contacts, n=354) as well as an average chance of innervation of 34.9% (**Fig. 3b**), indicating that approximately 1/3 of PVN magnOT neurons receive parvOT input. Based on these anatomical observations, we performed patch-clamp recording for functional validation of parvOT-magnOT neuron connection via rAAV-OTp-DIO-ChR2-mCherry (to label specifically parvOT) and rAAV-OTp-Venus (to label all OT neurons) injected into the PVN and Cav2-Cre injected into the SON (**Fig. 3g**). First, we confirmed the magnOT nature of recorded neurons through the presence of a hyperpolarizing transient outward rectification as well as a weak low threshold depolarization (**Fig. 3h**), by comparison to the electrophysiological properties of identified parvOT neurons (**Fig. 3c-f**). We observed that stimulation of parvOT neurons evoked responses in 45% of recorded magnOT neurons (9/20; **Fig. 3i**) with a significant increase of PSC frequencies (baseline 0.158 ± 0.055 Hz vs ChR2 0.346 ± 0.15 Hz, n = 9; $p < 0.01$; **Fig. 3i**). Next, we aimed to visualize Ca^{2+} variations in magnOT neurons upon DREADD-mediated activation of parvOT neurons via rAAV-OTp-DIO-hM3D(Gq)-mCherry and

rAAV-OTp-GCaMP6s injected in the PVN and Cav2-Cre into SON (**Fig 4a-d**). After application of CNO (10 µM, 1 min), we observed that 40 ± 8% of recorded magnOT neurons responded to parvOT hM3D(Gq) stimulation, confirming again described anatomical connectivity (**Fig. 3b, i; 4d**). In responsive neurons, the number of Ca^{2+} transients were significantly increased, a result mirrored by the increase of areas under the curves (**Fig. 4d**). However, the width of these Ca^{2+} transients did not show any significant change, indicating that parvOT-induced magnOT activity does not trigger long-lasting Ca^{2+} transients, but several bursts of sharp Ca^{2+} peaks, as observed in the example traces (**Fig 4b**). This feature was further confirmed by plotting the time course of Ca^{2+} event probability, showing that the probability of observing magnOT Ca^{2+} transients are increased during 4 minutes after the *ex vivo* CNO treatment (**Fig. 4c**). These data indicate that parvOT neurons synapse on magnOT neurons within the PVN to drive their activity, as similarly reported for SON magnOT neurons *in vivo*[13].

Magnocellular neurons and their release of OT into blood are controlled by parvOT neurons

Using similar viral strategies, we expressed DREADDs - hM3D(Gq) or hM4D(Gi) - specifically in parvOT and injected rAAV OTp-GCaMP6s in the PVN to express the Ca^{2+} indicator GCaMP6s in all PVN OT neurons (1193/1371 OT neurons expressed GCaMP6s, 87 ± 4%, n = 4; **Fig 4p**). This allowed us to monitor the global activity of PVN OT neurons via fiber photometry in isoflurane-anesthetized rats upon activation / inhibition of parvOT neurons. Activation of parvOT cells induced an increase in Ca^{2+} fluorescent signal of PVN OT neurons population approximately 30 min after CNO injection (i.p. 3 mg/kg) and lasting for more than 2 hours (**Fig 4e-h**). Conversely, inhibition of parvOT neurons decreased Ca^{2+} fluorescent signals of the general population 30 min after CNO injection and the effect lasted for more than 2 hours (**Fig 4i-l**). Administration of CNO did not have any effect on Ca^{2+} signal in control animals lacking the DREADD receptors (**Fig 4m-o**). Considering that the contribution of parvOT neurons to the OT population Ca^{2+} signal is negligible (**Extended Data Fig. 7a-e**), those results suggest that changes in parvOT neuron activity

directly influence the firing pattern of large populations of PVN magnOT neurons. The similar kinetics of Ca^{2+} signal fluctuations after CNO activation of parvOT PVN neurons together with airpuff application were detected during recording of magnOT neurons in the SON, which does not contain parvOT neurons (**Extended Data Fig. 7f-o**).

To investigate if parvOT-induced magnOT activity is followed by actual OT release, we analyzed neurohypophysial OT release after chemogenetic activation of parvOT neurons. We performed blood sampling from the jugular vein before and after CNO injection (3 mg/kg**; Fig. 4q**) and found a significant increase in plasma OT 45 min ($p = 0.00093$ versus basal; $p = 0.0036$ versus OTp-mCherry control) and 90 min ($p = 0.002$ versus basal; $p = 0.0017$ versus OTp-mCherry control; **Fig. 4r**) after i.p. CNO injections.

Taken collectively, these results indicate that parvOT neurons tightly control magnOT neuron activity *in vivo* to regulate peripheral OT release.

Differential neural inputs to parvOT and PVN magnOT neurons

The above findings suggest that parvOT neurons act as 'first responders to somatosensory input' conveying information to the rest of the PVN OT neuronal population (i.e., magnOT neurons). Hence, we asked whether parvOT neurons receive more synaptic inputs than PVN magnOT. In an attempt to assess potential differences of synaptic inputs to parvOT and magnOT neurons, we used IMARIS to quantify the total amount of SYN fluorescence at somata and dendrites. In order to perform an unbiased analysis, we created spheres that precisely engulfed magnOT and parvOT somata and accounted for individual variances in cell roundness and surface area (see Methods). We found statistically significant differences both at the soma (**Fig. 5a**) and dendritic locations (**Fig. 5b**, at two different locations, 5µm and 20µm from the soma) and analyzed a total of 104 neurons (parvOT=56, magnOT=48) suggesting that parvOT neurons might receive more overall synaptic input.

Next, to uncover the origin of synaptic inputs to parvOT and magnOT neurons, we employed the retrograde trans-synaptic EnvA-pseudotyped G deletion-mutant rabies virus (Rb-GFP[28]). To specifically distinguish inputs to parvOT and magnOT, we used a double conditional approach, which allows to retrotrace inputs to OT neurons that project to an area of choice (SON for parvOT and posterior pituitary for magnOT) (see Methods, **Fig. 5c,e**).

In both groups of rats, we found GFP expressing neurons in numerous brain regions, including the septum, medial preoptic area, and amygdala (**Fig. 5d,f** and **Extended Data Fig. 8h**), demonstrating that parvOT and magnOT neurons receive a large number of common inputs (**Supplementary Table 2**). However, we detected the presence of GFP neurons in the paraventricular nucleus of thalamus, insula and habenula only after the infection of parvOT neurons (**Extended Data Fig. 8i**), while GFP neurons in the substantia nigra were found only in after primary infection of magnOT neurons (**Extended Data Fig. 8j**). In line with the IMARIS analysis, the total number of neurons projecting to parvOT and magnOT neurons was 1963.6 ± 710 and 694.8 ± 121 neurons, respectively ($p=0.02$, **Fig. 5g**). Although we did not find between-groups differences in the proportion of inputs coming from hypothalamic and extrahypothalamic areas (**Fig. 5h**), PAG and SFO showed preferential innervation of parvOT and magnOT, respectively (**Fig. 5i**). This indicates that parvOT neurons receive at least partially distinct, and more pronounced neuronal inputs than magnOT neurons.

ParvOT neurons modulate social behavior

To test whether this small population of parvOT neurons can modulate social behavior by their effects on the activity of the much more abundant magnOT neurons, we used the previously described chemogenetic approach to silence or activate them during behavioral tests (**Fig. 6a**). Three weeks after viral injection, rats were injected i.p. with either CNO (3 mg/kg) or saline 60 min

before social interaction tests (**Fig. 6b**). Selectively inhibiting the parvOT neurons resulted in less social interaction: in the FSI test, the time spent with a conspecific was reduced by 37 ± 6 s (over 5-min sessions, $p < 0.001$; **Supplementary Video 2**). By contrast, in the CSI test, where no physical contact is allowed, the time spent by the experimental rat approaching the stimulus rat was unchanged (**Fig. 6c-e**, n = 15 rats). Conversely, CNO-induced activation of parvOT neurons led to more social interaction: in the FSI test, the time spent with a conspecific increased by 10 ± 6 s ($p = 0.04$). In the CSI test, no significant difference in approaching time was measured between saline- and CNO-injected rats (**Fig. 6f-h**, n = 9 rats).

Inhibition and activation of parvOT neurons also had opposite effects on crawling behavior (**Fig. 6e, h**). Moreover, after inhibiting parvocellular OT neurons, rats often actively avoided the stimulus rat, a behavior never observed in the control group (**Extended Data Fig. 9c**). Control rats injected with control virus rAAV-OTp-DIO-GFP receiving saline or CNO showed no behavioral differences (**Extended Data Fig. 9a**).

To control that alterations of social behaviors induced by DREADD-based manipulation of parvOT neurons activity was indeed an effect mediated by central OT release, the parvOT activation (Gq) experiment was repeated while applying an OTR antagonist (OTR-a)[29], by intracerebroventricular (i.c.v.) infusion (0.75 μg/5 μl)[30]. As compared to saline-infused control animals, OTR-a-infused animals showed a strong reduction in social interactions (37 ± 18% reduction, $p = 0.007$, n = 12 rats), regardless of CNO administration, while without OTR-a, CNO application caused increased social interactions (16 ± 3% increase, $p = 0.04$, n = 12; **Fig. 6i, Extended Data Fig. 9h**). We did not observe a CNO- or OTR-a-induced effect on locomotor activity (**Extended Data Fig. 9b,d-e**). This result confirms that the downstream effect on CNO-induced activation of parvOT neurons on social behavior is indeed mediated by OT and its receptors. In a second group of rats (n = 10), expressing GFP in parvOT neurons, administration of OTR-a also had a comparable effect in

reducing social behavior; as expected, CNO itself did not have any effect on social interaction of animals (**Fig 6j, Extended Data Fig. 9i**).

DISCUSSION

Here, we provide the first evidence that somatosensory stimulation in female rats activates parvOT neurons, which subsequently drive the activation of the much larger population of magnOT neurons. Using *ex vivo* and *in vivo* approaches, we demonstrated that parvOT neurons synapse onto magnOT neurons to elicit a central effect of OT to promote inter-female communication.

Social touch evokes OT neuronal activity

The use of single unit *in vivo* recording precludes discrimination between parvOT and magnOT neurons. However, considering limited number of parvOT neurons (~ 30 parvOT cells[13] vs. ~ 1200 magnOT cells[31] in the PVN of each hemisphere) it is highly likely that we exclusively recorded from magnOT cells. In support, we found that non-aggressive social interactions of female rats and, in particular, physical contacts, elicited a coordinated, clustered spiking activity of PVN OT neurons - a pattern that strongly facilitates activity-dependent secretion of OT from nerve terminals of magnOT cells in the pituitary[17] (**Extended Data Fig. 2h-j**). This activity is near-synchronous across recorded OT neurons, and it is highly correlated with theta rhythmicity of PVN local field potentials. These coordinated changes in OT neuronal electrical activity occurred only during free social interaction, allowing physical contacts between conspecifics, but not during chambered social interaction, where physical touch between animals was prevented by a barrier. Moreover, detailed analysis of PVN OT neurons activity during social behaviors revealed that the highest increase in neuronal firing occurred immediately after (0-10 s) *crawling on top* or *being crawled* behaviors (**Fig. 1**), i.e. social contacts that involved activation of cutaneous sensory nerves.

To test whether non-noxious repetitive somatosensory stimulations directly influence PVN OT neurons activity, even in the absence of other stimuli, we applied 'airpuff' stimulations onto the skin of the dorsal area of the rat, in lightly anesthetized conditions, while measuring action potentials of PVN neurons. Notably, 'airpuffs' induced a significant increase in spiking activity of most (83%) recorded putative magnOT neurons but had little or no effect on the activity of non-OT PVN neurons, reinforcing the idea that somatosensory inputs selectively activate magnOT neurons. This finding is in line with previous studies[32] that reported increased OT plasma levels in rats after 10 minutes of massage-like stroking. Furthermore, the stimulation of low-threshold mechanoreceptors, particularly the touch-sensitive nerve fibers C-tactile afferents is known to trigger OT release and has been associated with increased social motivation in rodents and human[33].

ParvOT neurons control PVN magnOT neuron activity

To shed light on the causal link between somatosensory stimulation and social behavior, we focused our research on a specific subtype of 'parvocellular' OT neurons. These neurons communicate with various autonomic centers in the brain stem and spinal cord[20], and are involved in analgesia during acute pain[13].

When we applied low-intensity, non-noxious cutaneous stimulation (airpuff) in awake rats, we observed a sustained increase of *c-fos* expression in parvOT neurons in the PVN (**Fig. 2**). As of note, we found that airpuff induced *c-fos* expression in parvOT, but not in magnOT neurons. However, the absence of *c-fos* expression in magnOT cells does not necessarily indicate the absence of their increasing activity[34–36]. Indeed, only dramatic physiological challenges such as hemorrhage, salt loading, or fear evoke *c-fos* expression in magnOT neurons[34,37]. Importantly, during lactation magnOT neurons release a large amount of OT into peripheral circulation while an increase in *c-fos* expression was never found. In analogy, our findings demonstrate increased OT plasma concentrations after chemogenetic activation of parvOT neurons (**Fig. 4**) *via* a demonstrated

parvOT→magnOT connectivity, although without detectable *c-fos* immunosignal in magnOT neurons releasing the neuropeptide into the blood.

Further, chemogenetic activation or inhibition of parvOT neurons via DREADDs resulted, respectively, in an increase or decrease in OT neuron activity in response to the air puff stimulation (**Fig. 2**). This suggests that parvOT neurons can be activated by both nociceptive[13] and non-nociceptive stimuli (present study) and subsequently promoting analgesia as well as social behavior. Such pleotropic effects of OT originating from the same parvOT neurons require further investigation.

To provide additional evidence that parvOT neurons modulate magnOT neuron activity within the PVN, we employed a combination of immunohistochemistry and three-dimensional anatomical reconstruction. We found 1.5-4-fold more synaptic-likes contacts on ParvOT somas and dendrites compared to respective compartments of MagnOT neurons (**Fig. 5**). This finding is supported by retrograde tracing data, which demonstrate substantially more inputs to parvOT neurons than to magnOT neurons (**Fig. 5**).

Do parvOT neurons control social behavior?

To investigate how parvOT neurons modulate social behavior, we performed chemogenetic manipulation of parvOT neurons by viral means. We found that targeted activation or inhibition of parvOT neurons increased or decreased the total time of social interaction with a conspecific, respectively. Further, the i.c.v. application of an OTR antagonist prevented CNO-induced social interaction after chemogenetic activation of parvOT neurons (**Fig. 6**). This suggests that the excitation of parvOT neurons is transmitted to magnOT cells, which , in turn, project axonal collaterals to numerous forebrain brain regions[5,7]. Given that parvOT neurons exclusively project to the brainstem and spinal cord[38], our results allow to hypothesize that the OTR antagonist blocks the

action of OT released from magnOT axons in socially-relevant brain regions, resulting in the attenuation of social communication between female conspecifics.

A stable OT-mediated social interaction throughout a female life?

While we exclusively used virgin females in our current study, it will be important to investigate how pregnancy and lactation changes the OT-dependent response to somatosensory stimulation. Given the drastic activation of the OT system and close physical contact with the offspring peripartum[39–41], it is plausible that the reward of tactile stimulation changes as well. Moreover, due to the interaction of OT and prolactin during the milk letdown reflex[42,43], nipples might become more sensitive to the suckling of pups, which might translate into a more rewarding experience for mothers. Further studies are needed to assess the intricate relationship between social touch, social behavior and social motivation, which requires concomitant actions of OT, serotonin, and dopamine within the nucleus accumbens and ventral tegmental area[22,44]. Accordingly, we found that parvOT, but not magnOT neurons, are innervated by neurons of the insular cortex, which is critical region processing social touch[45], and could thus be potentially involved in the recruitment of the OT-ergic system during social tactile stimulation.

Taken together, our data extend the current knowledge of the relationship between intracerebral OT release, social touch and its behavioral correlates. Our results suggest that parvOT neurons translate mechanosensory information from the periphery into social behavior (**Extended Data Fig. 10**), but the precise ascending pathways from cutaneous nerves – via the parvOT → magnOT circuit – to forebrain regions controlling social behaviors await further investigation.

While intranasal OT application has improved clinical outcomes of schizophrenia, posttraumatic stress disorders and autism spectrum disorders, there is still an ongoing debate about the validity of these findings[46], suggesting that evoking endogenous OT release might be a more reliable way to

443 exploit the benefits of this neuropeptide. Thus, a combination of gentle touch, social interaction
444 and/or intranasal OT application might be a powerful tool to treat human mental diseases, in which
445 the OT system is compromised[47,48].
446
447 **References**

448 1. Lee, H.-J., Macbeth, A. H., Pagani, J. & Scott Young 3rd, W. Oxytocin : the great facilitator
449 of life. *Prog. Neurobiol* **88**, 127–151 (2010).
450 2. Jurek, B. & Neumann, I. D. The oxytocin receptor: from intracellular signaling to behavior.
451 *Physiol. Rev.* **98**, 1805–1908 (2018).
452 3. Walum, H. & Young, L. J. The neural mechanisms and circuitry of the pair bond. *Nat. Rev.*
453 *Neurosci.* **19**, 643–654 (2018).
454 4. Russell, J. A., Leng, G. & Douglas, A. J. The magnocellular oxytocin system, the fount of
455 maternity: adaptations in pregnancy. *Front. Neuroendocrinol.* **24**, 27–61 (2003).
456 5. Knobloch, H. S. *et al.* Evoked axonal oxytocin release in the central amygdala attenuates fear
457 response. *Neuron* **73**, 553–566 (2012).
458 6. Marlin, B. J. & Froemke, R. C. Oxytocin modulation of neural circuits for social behavior.
459 *Dev. Neurobiol.* **77**, 169–189 (2017).
460 7. Grinevich, V. & Stoop, R. Interplay between oxytocin and sensory systems in the
461 orchestration of socio-emotional behaviors. *Neuron* **99**, 887–904 (2018).
462 8. Dumais, K. M., Alonso, A. G., Immormino, M. A., Bredewold, R. & Veenema, A. H.
463 Involvement of the oxytocin system in the bed nucleus of the stria terminalis in the sex-
464 specific regulation of social recognition. *Psychoneuroendocrinology* **64**, 79–88 (2016).
465 9. Dumais, K. M., Alonso, A. G., Bredewold, R. & Veenema, A. H. Role of the oxytocin
466 system in amygdala subregions in the regulation of social interest in male and female rats.
467 *Neuroscience* **330**, 138–149 (2016).
468 10. Resendez, S. L. *et al.* Social stimuli induce activation of oxytocin neurons within the

paraventricular nucleus of the hypothalamus to promote social behavior in male mice. *J. Neurosci.* **40**, 2282–2295 (2020).

11. Bobrov, E., Wolfe, J., Rao, R. P. & Brecht, M. The representation of social facial touch in rat barrel cortex. *Curr. Biol.* **24**, 109–115 (2014).

12. Chen, P. & Hong, W. Neural circuit mechanisms of social behavior. *Neuron* **98**, 16–30 (2018).

13. Eliava, M. *et al.* A new population of parvocellular oxytocin neurons controlling magnocellular neuron activity and inflammatory pain processing. *Neuron* **89**, 1291–1304 (2016).

14. Lima, S. Q., Hromádka, T., Znamenskiy, P. & Zador, A. M. PINP: a new method of tagging neuronal populations for identification during in vivo electrophysiological recording. *PLoS One* **4**, e6099 (2009).

15. Leng, T., Leng, G. & MacGregor, D. J. Spike patterning in oxytocin neurons: Capturing physiological behaviour with Hodgkin-Huxley and integrate-and-fire models. *PLoS One* **12**, e0180368 (2017).

16. Netser, S., Haskal, S., Magalnik, H. & Wagner, S. A novel system for tracking social preference dynamics in mice reveals sex- and strain-specific characteristics. *Mol. Autism* **8**, 53 (2017).

17. Maícas-Royo, J., Leng, G. & MacGregor, D. J. A predictive, quantitative model of spiking activity and stimulus-secretion coupling in oxytocin neurons. *Endocrinology* **159**, 1433–1452 (2018).

18. Portfors, C. V. Types and functions of ultrasonic vocalizations in laboratory rats and mice. *J. Am. Assoc. Lab. Anim. Sci.* **46**, 28–34 (2007).

19. Lenschow, C. *et al.* Sexually monomorphic maps and dimorphic responses in rat genital cortex. *Curr. Biol.* **26**, 106–113 (2016).

20. Althammer, F. & Grinevich, V. Diversity of oxytocin neurones: Beyond magno- and

parvocellular cell types? *J. Neuroendocrinol.* **30**, e12549 (2018).

21. Johnson, Z. V. *et al.* Central oxytocin receptors mediate mating-induced partner preferences and enhance correlated activation across forebrain nuclei in male prairie voles. *Horm. Behav.* **79**, 8–17 (2016).

22. Hung, L. W. *et al.* Gating of social reward by oxytocin in the ventral tegmental area. *Science (80-.).* **357**, 1406–1411 (2017).

23. Okabe, S., Yoshida, M., Takayanagi, Y. & Onaka, T. Activation of hypothalamic oxytocin neurons following tactile stimuli in rats. *Neurosci. Lett.* **600**, 22–27 (2015).

24. Bru, T., Salinas, S. & Kremer, E. J. An Update on Canine Adenovirus Type 2 and Its Vectors. *Viruses* **2**, 2134–2153 (2010).

25. Gunaydin, L. A. *et al.* Natural neural projection dynamics underlying social behavior. *Cell* **157**, 1535–1551 (2014).

26. VanRyzin, J. W. *et al.* Microglial phagocytosis of newborn cells is induced by endocannabinoids and sculpts sex differences in juvenile rat social play. *Neuron* **102**, 435-449.e6 (2019).

27. Erny, D. *et al.* Host microbiota constantly control maturation and function of microglia in the CNS. *Nat. Neurosci.* **18**, 965–977 (2015).

28. Wickersham, I. R. *et al.* Monosynaptic restriction of transsynaptic tracing from single, genetically targeted neurons. *Neuron* **53**, 639–647 (2007).

29. Manning, M., Stoev, S., Cheng, L. L., Ching Wo, N. & Chan, W. Y. Design of oxytocin antagonists, which are more selective than Atosiban. *J. Pept. Sci.* **7**, 449–465 (2001).

30. Grund, T. *et al.* Neuropeptide S activates paraventricular oxytocin neurons to induce anxiolysis. *J. Neurosci.* **37**, 12214–12225 (2017).

31. Rhodes, C. H., Morriell, J. I. & Pfaff, D. W. Immunohistochemical analysis of magnocellular elements in rat hypothalamus: Distribution and numbers of cells containing neurophysin, oxytocin, and vasopressin. *J. Comp. Neurol.* **198**, 45–64 (1981).

32. Uvnäs-Moberg, K., Handlin, L. & Petersson, M. Self-soothing behaviors with particular reference to oxytocin release induced by non-noxious sensory stimulation. *Front. Psychol.* **5**, 1529 (2015).

33. Walker, S. C., Trotter, P. D., Swaney, W. T., Marshall, A. & Mcglone, F. P. C-tactile afferents: Cutaneous mediators of oxytocin release during affiliative tactile interactions? *Neuropeptides* **64**, 27–38 (2017).

34. Brown, C. H., Bains, J. S., Ludwig, M. & Stern, J. E. Physiological regulation of magnocellular neurosecretory cell activity: integration of intrinsic, local and afferent mechanisms. *J. Neuroendocrinol.* **25**, 678–710 (2013).

35. Hoffman, G. E. & Lyo, D. Anatomical markers of activity in neuroendocrine systems: are we all 'Fos-ed out'? *J. Neuroendocrinol.* **14**, 259–268 (2002).

36. Hoffman, G. E., Smith, M. S. & Verbalis, J. G. c-Fos and related Immediate Early Gene products as markers of activity in neuroendocrine systems. *Front. Neuroendocrinol.* **14**, 173–213 (1993).

37. Hasan, M. T. *et al.* A fear memory engram and its plasticity in the hypothalamic oxytocin system. *Neuron* **103**, 133-146.e8 (2019).

38. Stern, J. E. Electrophysiological and morphological properties of pre-autonomic neurones in the rat hypothalamic paraventricular nucleus. *J. Physiol.* **537**, 161–177 (2001).

39. Bosch, O. J. Brain Oxytocin Correlates with Maternal Aggression: Link to Anxiety. *J. Neurosci.* **25**, 6807–6815 (2005).

40. Fenelon, V. S., Poulain, D. A. & Theodosis, D. T. Fos synthesis and neuronal activation: analysis of Fos immunoreactivity in identified magnocellular neurons during lactation. *Ann. N. Y. Acad. Sci.* **689**, 508–511 (1993).

41. Neumann, I., Douglas, A. J., Pittman, Q. J., Russell, J. A. & Landgraf, R. Oxytocin released within the supraoptic nucleus of the rat brain by positive feedback action is involved in parturition-related events. *J. Neuroendocrinol.* **8**, 227–233 (1996).

42. Augustine, R. A. *et al.* Prolactin regulation of oxytocin neurone activity in pregnancy and lactation. *J. Physiol.* **595**, 3591–3605 (2017).

43. Kennett, J. E. & McKee, D. T. Oxytocin: an emerging regulator of prolactin secretion in the female rat. *J. Neuroendocrinol.* **24**, 403–412 (2012).

44. Dölen, G., Darvishzadeh, A., Huang, K. W. & Malenka, R. C. Social reward requires coordinated activity of nucleus accumbens oxytocin and serotonin. *Nature* **501**, 179–184 (2013).

45. McGlone, F., Wessberg, J. & Olausson, H. Discriminative and affective touch: sensing and feeling. *Neuron* **82**, 737–755 (2014).

46. Leng, G. & Ludwig, M. Reply to: Improving research standards to restore trust in intranasal oxytocin. *Biol. Psychiatry* **79**, e55–e56 (2016).

47. Meyer-Lindenberg, A., Domes, G., Kirsch, P. & Heinrichs, M. Oxytocin and vasopressin in the human brain: social neuropeptides for translational medicine. *Nat. Rev. Neurosci.* **12**, 524–538 (2011).

48. Grinevich, V. & Neumann, I. D. How puzzle stones from animal studies translate into psychiatry. *Mol. Psychiatry* (2020). doi:10.1038/s41380-020-0802-9

ACKNOWLEDGEMENTS

The authors thank Thomas Grund and Xinying Liu for initial contribution to this study, Ron Stoop for valuable comments on the manuscript, Judith Müller for packaging viral vectors, Eric Kremer for the canine virus, Jorge Maicos-Roya for contributing to the modeling of OT release, Shai Netser for his comments on the manuscript, Claudia Pitzer and the Interdisciplinary Neurobehavioral Core Facility of Heidelberg University for some of behavioral experiments performed there, and Thomas Splettstoesser (www.scistyle.com) for composing Figure 7. The work was supported by German Research Foundation (DFG) within the Collaborative Research Center (SFB) 1158 seed grant for

young researchers (to AL), DFG postdoctoral fellowship AL 2466/1-1 (to FA), Alexander von Humboldt research fellowship (to DH), Human Frontier Science Program RGP0019/2015 (to VG and SW), Israel Science Foundation grants #1350/12, 1361/17, Milgrom Foundation and the Ministry of Science, Technology and Space of Israel grant #3-12068 (to SW), NIH grant R01NS094640 (to JES), BBSRC grant BB/S000224/1 (to GL), DFG grants NE 465/27, NE 465/31, and NE 465/34 (to IDN), ANR-DFG grant GR 3619/701 (to AC and VG), NARSAD Young Investigator Grant 24821 and ANR JCJC grant (to AC), DFG grant GR 3619/4-1, SFB 1158, SNSF-DFG grant GR 3619/8-1, and Fritz Thyssen Foundation grant 10.16.2.018 MN (to VG).

AUTHORS CONTRIBUTIONS

Design and project conception (YT, DB, AL, AC, VG), *ex vivo* electrophysiology (LH, PD), *ex vivo* calcium imaging (LH, ABa), *in vivo* electrophysiology (YT, DB, SW), fiber photometry (YT, AL), behavioral experiments and analyses (YT, DB, SW), immunohistochemistry and confocal microscopy (DB, ME, DH, FA), trans-synaptic labelling of OT neurons inputs (AL, JS), assistance with viruses design for trans-synaptic labelling (MS, MO, KKC), three-dimensional reconstruction and analysis (FA, MKK, RKR, JES), plasma OT dosages (ABl, IDN), modeling (GL), manuscript preparation (YT, DB, AL, LH, FA, IDN, AC, VG), supervision, project administration, and funding acquisition (IDN, AC, VG).

CONFLICT OF INTEREST

The authors declare no competing interests.

599 **FIGURE LEGENDS**

600

601 **Figure 1.** ***In vivo*** **recording of individual OT neurons in the PVN**

602 **a**, Setup for recordings of behavior, ultrasonic vocalizations, and neural activity.

603 **b,** Video-tracking and electrophysiological recording from a rat alone in the OF arena (top) and
604 during FSI (bottom): animal movement path (blue line), location of prominent OT cell activity
605 (colored dots), heatmap of time spent by the rat in different locations.

606 **c**, Example firing rate of four identified OT neurons recorded simultaneously during FSI. Red bars
607 indicate periods of social interaction.

608 **d**, Average firing rate of 15 OT neurons from five rats: OF baseline 1.1 ± 0.4 Hz, not socially
609 interacting (not SI) 1.6 ± 0.3 Hz, and social interacting (SI) 2.6 ± 0.2 Hz (OF-not SI $p = 0.07$, OF-SI
610 $p = 0.001$, not SI-SI $p = 0.03$, one-way ANOVA). Average index of dispersion on 1-s time bins of
611 15 OT neurons: OF 0.9 ± 0.2, not SI 1.4 ± 0.3, SI 3.4 ± 0.4 (OF-not SI $p = 0.16$, OF-SI $p = 0.0004$,
612 not SI-SI $p = 0.001$, one-way ANOVA). Average pairwise Pearson correlation of spiking activity
613 (1-s time bins) of 17 OT neurons' pairs recorded in OF and SI ($p = 0.005$, unpaired two-sided t
614 test).

615 **e,** Frames of recorded videos (top) of experimental rats that were placed either alone (OF), or with a
616 mesh between rats (CSI) or for FSI with a stimulus rat; representative spike raster plots of an OT
617 cell in each condition (bottom).

618 **f,** Average firing rate of 15 OT neurons while rats underwent open field (OF), CSI, and FSI tests
619 (OF-CSI $p = 0.14$, OF-FSI $p = 0.004$, CSI-FSI $p = 0.006$, n = 15 cells, one-way ANOVA). Average
620 index of dispersion on 1-s time bins (OF-CSI $p = 0.21$, OF-FSI $p = 0.001$, CSI-FSI $p = 0.003$, n =15
621 cells, one-way ANOVA). Average pairwise Pearson correlation of spiking activity (1-s time bins)
622 of 17 OT neurons' pairs (OF-CSI $p = 0.39$, OF-FSI $p = 0.002$, CSI-FSI $p = 0.003$, one-way
623 ANOVA).

g, Normalized firing rates of OT neurons during each behavior; *crawling on top* and *being crawled* elicited the strongest responses (* p = 0.036, * p = 0.024, n = 8 cells, one-way ANOVA followed by Tukey's post hoc test).

h, Representative spike raster plots, averaged response, and PSTH of OT cell activity during *'crawling on top'* (increased response, p = 0.036, n = 6 cells, Wilcoxon test), and '*being crawled'* (increased response, p = 0.024, n = 6 cells, Wilcoxon test) behaviors. Data represented as mean ± SEM.

Figure 2. Gentle non-nociceptive mechanical stimuli triggers OT neurons activation

a, Head-fixed rats injected with rAAV-pOT-ChR2-mCherry were stimulated with airpuffs at anterior, central, and posterior portion of the dorsal body region, while OT neurons were recorded with an opto-electrode. Top: PSTHs example of OT neurons responses to airpuffs. Bottom: normalized PSTHs of 10 (out of 23) recorded OT neurons response to airpuffs in three dorsal body regions (1 anterior, 2 central, 3 posterior); red indicate high spiking activity.

b, (Top) Statistics of average firing rate of OT neurons response to airpuff stimulations (peak vs. baseline, *p = 0.017, *p = 0.025, *p = 0.021, n = 23 cells from 8 rats, one-way ANOVA followed by Bonferroni post hoc comparison) indicates significant increase above basal rate (dashed line). (Bottom) latency of OT neurons responses to airpuffs. All data show average ± SEM.

c, Fluorogold-injected rats received continuous airpuffs for 10 min and were killed and perfuse-fixed 90 min later. PVN slices were triple-stained with antibodies against OT (blue), fluorogold (red) and *c-fos* (green). The confocal image shows a (fluorogold-negative) parvocellular OT neuron expressing *c-fos* (one of 99 such double-labeled neurons observed in 4 rats). Scale bars = 100 and 10 (inset) μm.

d, Rats injected bilaterally with CAV2-Cre into the SON and rAAV-OTp-DIO-mCherry into the PVN, were exposed to airpuffs for 10 min and killed 90 min later. The confocal image shows *c-fos*

expression in a parvOT neuron (mCherry-positive, labeled via the retrograde CAV2-Cre, and is one of 60 such triple-labeled neurons observed in 4 rats). Scale bars = 100 and 10 (inset) μm.

e-f, Viral vectors for recording Ca^{2+} signals in GCaMP6s-expressing OTneurons during chemogenetic activation (**e**) or silencing (**f**) of parvocellular OTneurons.

g-h, Examples of fiber photometry-based Ca^{2+} signals of PVN OT neuron population during airpuff stimulation (orange bars). Top: response to airpuffs 30-60 min after saline injection (Control); bottom: response to airpuffs 30-60 min after CNO induced activation (**g**) or silencing (**h**) of parvOT neurons.

i, Average traces of Ca^{2+} responses to airpuffs 30-60 min after injection of CNO to activate (Gq) parvOT neurons, or saline (Control). Each graphic is the average of 33 airpuffs responses (11 airpuffs per animal, n = 3); area under the curve (AUC) 0-30 s after airpuffs, relative to control (* $p = 0.03$, paired two-sided t test).

j, Average traces of Ca^{2+} responses to airpuffs 30-60 min after injection of CNO to silence (Gi) parvOT neurons, or of saline (Control). Each graphic is the average of 33 airpuffs responses (11 airpuffs per animal, n = 3); area under the curve (AUC) 0-30 s after airpuffs, relative to control (** $p = 0.007$, paired two-sided t test). All data show average ± SEM.

Figure 3. Intra-PVN connectivity of parvOT and magnOT neurons

a, Images show the three-dimensional surface reconstruction of OT, GFP and SYN. Circles with dashed lines indicate the overlap of OT, GFP and SYN.

b, Confocal image shows a single magnOT neuron (purple) innervated by a parvOT fiber (green). Scale bar = 10 μm. Dot plot graph shows that the chance of innervation by parvOT neurons depends on the anatomical location of magnOT neurons within the PVN. Bar graph shows the average chance for magnOT PVN neurons to be innervated by parvOT axons (n = 214 cells from 3 rats).

c, Schema of the viral injection into the SON and the PVN plus the electrophysiological recording in the PVN (with pipette) for the recording of parvOT neurons (expressing mCherry + GFP) and magnOT neurons (expressing mCherry).

d, Comparison of average and individual points of voltage amplitude between parvOT neurons (n = 17 cells from 4 rats) and magnOT neurons (n = 7 cells from 4 rats), for different electrophysiological parameters (AP; parvOT 70.12 ± 2.87 mV vs magnOT 71.65 ± 7.414 mV; p = 0.82, unpaired two-sided t test; transient outward rectification (TOR); magnOT = 4.39 ± 0.79 mV; low threshold depolarization (LTD); parvOT 14.88 ± 0.81 mV vs magnOT 5.93 ± 1.98 mV; ** p = 0.0019, two-sided Mann-Whitney U test).

e, Example responses of 3 parvOT neurons to a hyperpolarizing current at -100 pA followed by 4 current injections starting from 0 pA to 60 pA.

f, Example responses of 3 magnOT neurons to a hyperpolarizing current at -100 pA followed by 4 current injections starting from 0 pA to 60 pA.

g, (left) Schematic representation of viral vectors injected in the PVN (OTp-DIO-ChR2-mCherry and OTp-Venus) and in the SON (CAV2-Cre) to transduce the expression of ChR2-mCherry in parvOT neurons and of Venus in PVN OT neurons; (right) image showing viral expression in the PVN in one out of 4 rats (scale bar = 100 μm).

h, Average and individual points of voltage amplitude of magnOT neurons (n = 8 cells from 4 rats), for different electrophysiological parameters: AP, TOR, and LTD.

i, Average percentage (45 %) of responding magnOT neurons (n = 9 cells) in all the magnOT neurons that have been recorded (n = 20 cells from 4 rats). MagnOT PSC frequency reversibly increases after parvOT ChR2 photostimulation (n = 9 cells). Example responses of 3 magnOT neurons in voltage clamp configuration at -70 mV before and after the ChR2 optogenetic stimulation of parvOT neurons. Baseline vs. BL ** $p < 0.001$, BL vs. wash ** $p < 0.001$, Friedman test followed by a Dunn post hoc test. All data are represented as mean + SEM.

Figure 4. Magnocellular neurons and their release of OT into blood are controlled by parvOT neurons

a, To allow the expression of hM3D(Gq) on parvOT PVN to SON projecting neurons, rats' SON have been infected with a CAV2-Cre rAAV and the PVN were infected with an AAV allowing the Cre-dependent expression of hM3D(Gq) under the control of the OT promoter. We also make PVN OT neuron express the calcium indicator GCaMP6s to monitor calcium transients in parvOT neurons.

b, Example traces of the effect of CNO (10µM, 6min) on PVN OTergic neurons calcium activity.

c-d, CNO application increase the number of calcium transients by 5 ± 1 fold (solid line: average, shaded area: SEM, p = 0.0019, Wilcoxon test) and the AUC by 15 ± 9 fold (p = 0.0043, Wilcoxon test) in 40 ± 8% of recorded magnOT neurons (n = 20 slices from 7 rats, 70 cells). After CNO application, the probability of observing a calcium peak is increased during ~4 minutes but the duration of those peaks remains unchanged (ratio = 2 ± 0.7, p = 0.46, paired two-sided t test). Bar plots show mean + SEM.

e-h, Schema of viral vectors injected and implanted optic fiber for fiber photometry recording (**e**) of PVN OT neurons with concomitant DREADD-Gq activation of parvOT neurons. Example traces (**f**) of recorded GCaMP6s signal from PVN OT neurons before and after CNO-induced activation of parvOT neurons. Normalized area under the curve (AUC) of GCaMP6s signal (**g,** solid line: average, shaded area: SEM, 1 min bin size) of PVN OT neurons showing increase of cellular activity after parvOT activation mediated by CNO i.p. injection (indicated by arrow). 30-min averaged AUC (**h**) showing a gradual increase of cellular activity (baseline AUC vs 0-30 min p = 0.0606; vs 30-60 min *p = 0.0403) that last at least 120 min (baseline AUC vs 60-90min *p = 0.028; vs 90-120 min *p = 0.0325, n = 6 rats, two-way ANOVA Tukey's corrected post-hoc comparison).

i-l, Schema of viral vectors injected and implanted optic fiber for fiber photometry recording (**i**) of PVN OT neurons with concomitant DREADD-Gi inhibition of parvOT neurons. Example traces (**j**)

of recorded GCaMP6s signal from PVN OT neurons before and after CNO-induced inhibition of parvOT neurons. Normalized area under the curve (AUC) of GCaMP6s signal (**k,** solid line: average, shaded area: SEM, 1 min bin size) of PVN OT neurons showing decrease of cellular activity after parvOT inhibition mediated by i.p. CNO injection (indicated by arrow). 30-min averaged AUC (**l**) showing a gradual decrease of cellular activity (baseline AUC vs 0-30 min $p = 0.058$; vs 30-60 min ***$p = 0.00013$) that last at least 120 min (baseline AUC vs 60-90 min, 90-120 min ***$p = 0.00019$, $n = 3$ rats, two-way ANOVA Tukey's corrected post-hoc comparison).

m-o, Schema of viral vectors injected and implanted optic fiber for fiber photometry recording (**m**) of PVN OT neurons in control animals (DREADD-free) expressing GFP in parvOT neurons. Normalized area under the curve (AUC) of GCaMP6s signal (**n,** solid line: average, shaded area: SEM, 1 min bin size) of PVN OT neurons showing no significant changes in Ca^{2+} signal upon CNO injection. No significant changes are detected in 30-min averaged AUC (**o**) up to 120 min ($p = 0.109$, $n = 2$ rats, two-way ANOVA Tukey's corrected post-hoc comparison).

p, Panels of immunostained section of the PVN showing post-hoc verification of implanted optic fiber above the PVN and co-localization of immunoreactive GCaMP6s (green, top left), and DIO-hM3D(Gq)-mCherry (red, bottom left), and oxytocin (blue, right) in one out of six rats. Arrows indicate mCherry-positive parvOT neurons. Scale bar 100 μm and 10 μm (inset).

q, Schema of viral vectors injected for DREADD-Gq activation of parvOT neurons and blood sampling from jugular vein.

r, Chemogenetic activation of parvOT neurons evokes peripheral OT release. Plasma OT (pg/ml) taken under basal conditions and 45 as well as 90 min after i.p. CNO (3 mg/kg; depicted by arrow), $n = 8$ rats parvOT Gq group, $n = 6$ rats control group. At 45 min, ++ $p = 0.00093$ vs. basal (-45 min), ** $p = 0.0036$ vs. control (OTp-mCherry) and at 90 min, $p = 0.002$ vs. basal, $p = 0.0017$ vs control. Two-way ANOVA for repeated measures, Bonferroni corrected post-hoc. Data are presented as mean ± SEM.

Figure 5. ParvOT neurons receive more inputs than magnOT neurons

a, Three-dimensional reconstruction of parvOT and magnOT neurons and the quantification of SYN fluorescence. Asterisks (white) indicate the placement of the spheres (yellow) used to quantify the total amount of SYN fluorescence (red). Top panel shows the placement of a sphere around a magnOT neuron soma, bottom panel shows the placement of a sphere onto a parvOT neuron dendrite. Scale bars = 5 μm.

b, Quantification of SYN fluorescence in close proximity to parvOT (n = 56 cells from 3 rats) and magnOT (n = 48 cells from 3 rats) neurons at somatic (top graph) and dendritic locations (bottom graph) considering differences in cellular roundness and surface area (adjusted). Unpaired two-sided t test, ***$p < 0.0001$.

c, e, Virus injection strategy to retrotrace inputs from parvOT and magnOT neurons, respectively.

d, f, Schema representing the proportion of inputs (number of inputs from one brain area / total number of inputs) from each brain area to parvOT and magnOT neurons, respectively. Brain areas projecting only to parvOT or magnOT are circled in green or purple, respectively.

g, Quantification of the total number of inputs to parvOT and magnOT neurons. Two-sided t test, *$p = 0.0223$, n = 5 rats per group.

h, Proportion of inputs to parvOT and magnOT neurons located in the hypothalamus or outside the hypothalamus. Numbers indicate average number of neurons.

i, Bar graphs showing the proportion of inputs coming from brain areas showing preferential innervation of parvOT or magnOT. Two-sided t test, asterisks indicate significant difference: *$p = 0.0315$, *$p = 0.0153$, *$p = 0.0264$, *$p = 0.0299$, *$p = 0.0453$ and *$p = 0.0011$ respectively, n = 5 rats per group. Data represented as mean **+** SEM.

Figure 6. Modulation of parvocellular OTneurons alters social behavior

a, Viral vectors used to express gene of interests (hM4D(Gi)-mCherry or hM3D(Gq)-mCherry) in parvOT neurons.

775 **b**, CNO or saline was injected i.p. 60 min before the behavioral tests.

776 **c,** Silencing parvOT neurons (Parvo-Gi group): percentage of time spent by an experimental rat
777 injected with saline or CNO socially interacting with a conspecific in CSI ($p = 0.41$) and FSI ($n =$
778 15 rats, *** $p = 0.0001$, paired two-sided t test), calculated over the 5-min session.

779 **d**, Temporal dynamics of time spent in social interaction in 1-min bins (2^{nd} minute, **$p = 0.01$, 3^{rd}
780 minute *$p = 0.03$, 5^{th} minute *$p = 0.04$, n = 15 rats, two-way ANOVA time x treatment).

781 **e**, Parvo-Gi group: time spent in different social behaviors in rats injected with saline or CNO:
782 crawling on top (** $p = 0.008$), sniffing (* $p = 0.012$), chasing ($p = 0.13$), head-to-head ($p = 0.31$), n
783 =15 rats, one-way ANOVA Tukey's corrected post-hoc comparison.

784 **f**, Activation of parvOT neurons (Parvo-Gq group): average time spent in social interaction with
785 conspecific stimulus in CSI ($p = 0.32$) and FSI ($n = 9$ rats, * $p = 0.04$, paired two-sided t test) after
786 CNO or saline injection.

787 **g**, Temporal dynamics of time spent in social interaction in 1-min bins for rats injected with CNO
788 or saline (4^{th} minute, $p = 0.03$, 5^{th} minute, $n = 9$ rats, $p = 0.05$, two-way ANOVA time x treatment).

789 **h**, Parvo-Gq group: time spent in different social behaviors in rats injected with saline or CNO:
790 mounting (** $p = 0.006$), sniffing ($p = 0.44$), chasing ($p = 0.27$), head-to-head ($p = 0.11$), $n = 9$ rats,
791 one-way ANOVA Tukey's corrected post-hoc comparison.

792 **i**, OTR-antagonist i.c.v. infusion decreases social interaction even in presence of pharmacological
793 activation (hM3D-Gq) of parvOT neurons. Percentage of social interaction time in different
794 conditions: saline (control), CNO, OTR-antagonist, or CNO + OTR-antagonist administration.
795 Time spent social interacting over 5-minute sessions. Saline i.p. and i.c.v.: 90 ± 19 s, CNO i.p. and
796 saline i.c.v.: 105 ± 15 s, * $p = 0.04$, $n = 6$ rats, saline i.p. and OTR-a i.c.v.: 54 ± 17 s, ** $p = 0.007$,
797 CNO i.p. and OTR-a i.c.v.: 56 ± 16 s, ** $p = 0.009$, $n = 6$ rats, one-way ANOVA Tukey's corrected
798 post-hoc comparison.

799 **j**, Control group in which parvOT neurons express GFP. Saline i.p. and i.c.v.: 88 ± 18 s, CNO i.p.
800 and saline i.c.v.: 89 ± 14 s, $n = 5$ rats, saline i.p. and OTR-a i.c.v.: 53 ± 14 s, ** $p = 0.008$, CNO i.p.

and OTR-a i.c.v.: 57 ± 15 s, ** p = 0.001, n = 5 rats, one-way ANOVA Tukey's corrected post-hoc comparison. All data represented as mean ± SEM.

METHODS

Animals

Four to eight-week old female Wistar rats purchased from Janvier, France and were housed under standard laboratory conditions (12-h light/dark cycle, lights on at 07:00, 22-24 °C, 50±5% humidity, free access to food and water). All experiments were conducted under license G-102/17 (authorized by the German Animal Ethics Committee of the Baden Württemberg, Regierungspräsidium Karlsruhe) and in accordance with the German law, under license 3668-2016011815445431 from the French Ministry, and EU regulations. In total, 194 rats were used, of which 15 were excluded due to mistargeting or insufficient expression of viral vectors (**Supplementary Table 3**).

Viruses

Recombinant adeno-associated viruses (rAAVs, serotype 1/2) used in this study (carrying conserved region of the oxytocin (OT) promoter and genes of interest in direct or "floxed" orientations) were cloned and produced as reported previously [5,13,30,49]. HEK293T cells (#240073, Addgene, USA) were used for the virus production. rAAVs produced included: rAAV-OTp-mCherry/Venus, rAAV-OTp-ChR2-mCherry, rAAV-OTp-DIO-ChR2-mCherry, rAAV-OTp-DIO-hM3D(Gq)-mCherry, rAAV-OTp-DIO-hM4D(Gi)-mCherry, rAAV-OTp-DIO-GFP, rAAV-OTp-DIO-ChR2-EYFP, rAAV-OTp-GCaMP6s, rAAV-OTp-TCB (TVA fused mCherry), rAAV-Ef1A-DIO-oG. The canine adenovirus serotype 2 (CAV2-CMV-Cre) was purchased from the Institute of Molecular Genetics in Montpellier CNRS, France[24]. The retrograde AAV (rAAVretro-Ef1A-Cre)

was purchased from the Salk Institute Viral Vector Core, CA, USA. Modified rabies virus was produced at the Gene Center rabies laboratory, Ludwig Maximillian University, Munich, Germany.

Stereotactic injections of viral vectors

For stereotactic injections of viruses, rats were anesthetized with a mixture of ketamine (65 mg/kg b.w.) and xylazine (14 mg/kg b.w.). rAAV genomic titers were determined with QuickTiter AAV Quantitation Kit (Cell Biolabs, Inc., San Diego, California, USA) and RT-PCR using the ABI 7700 cycler (Applied Biosystems, California, USA). rAAVs titers were between 10^9 - 10^{10} genomic copies/µl. We injected 300 nl per PVN. CAV2-Cre was purchased from the Institute of Molecular Genetics, Montpellier (diluted to 10^9 genomic copies/µl, 300 nl per SON). Viruses were injected via a glass pipette into the target regions at 150 nl/min using a syringe pump as described in[50]. Coordinates were chosen in accordance to a rat brain atlas [51] for PVN (A/P: - 1.8 mm, M/L: ±0.3 mm, D/V: -8 mm), for SON (A/P: - 1.8 mm, M/L: ±1.2 mm, D/V -9.25 mm), and for posterior pituitary (A/P: - 5.6 mm, M/L: ±0.1 mm, D/V: -10.5 mm). Verification of injection and implantation sites and expression of genes of interest were confirmed in all rats *post-hoc* in 50-µm sections containing the PVN and SON (see "Histology" section).

***Ex vivo* experiments**

Slices preparation

4-8 weeks after injection of viruses into the PVN and SON of 5 weeks old virgin female rats, animals were anesthetized using ketamine (Imalgene 90 mg/kg) and xylazine (Rompun, 10 mg/kg) administered intraperitoneally. Then, intracardiac perfusion were performed with an ice-cold NMDG based artificial cerebro spinal fluid (aCSF) was used containing (in mM): NMDG (93), KCl (2.5), NaH_2PO_4 (1.25), $NaHCO_3$ (30), $MgSO_4$ (10), $CaCl_2$ (0.5), HEPES (20), D-Glucose (25), L-ascorbic acid (5), Thiourea (2), Sodium pyruvate (3), N-acetyl-L-cysteine (10), Kynurenic acid (2).

pH was adjusted to 7.4 using either NaOH or HCl, this after bubbling in 95% O_2-5% CO_2 gas. Rats were then decapited, brains were removed, 350 µm thick coronal slices containing the hypothalamus was obtained using a Leica VT1000s vibratome. Slices were warmed 10 minutes in 35°C NMDG aCSF and placed for minimum 1 hour in a room tempered holding chamber, containing normal aCSFs. Normal aCSF, also used during all *ex vivo* experiments, is composed of (in mM): NaCl (124), KCl (2.5), NaH_2PO_4 (1.25), $NaHCO_3$ (26), $MgSO_4$ (2), $CaCl_2$ (2), D-Glucose (15), adjusted for pH values of 7.4 with HCL or NaOH and continuously bubbled in 95% O_2-5% CO_2 gas. All aCSFs were checked for osmolality and kept for values between 305-310 mOsm. In electrophysiology or calcium imaging experiments, slices were transferred from the holding chamber to an immersion recording chamber and superfused at a rate of 2 ml/min. CNO containing solution (10µM) were bath applied through a 6 min long pumping, corresponding to several times the volume of the recording chamber (2 applications per slice maximum). All *ex vivo* experiments were conducted at room temperature.

Patch clamp recording

Whole-cell patch-clamp recordings were visually guided by infrared oblique light videomicroscopy (DM-LFS; Leica), using 4–9 MΩ borosilicate pipettes filled with a $KMeSO_4$ based intrapipette solution composed of containing (in mM): $KMeSO_4$ (135), NaCl (8), HEPES (10), $ATPNa_2$ (2), GTPNa (0.3). The pH was adjusted to 7.3 with KOH and osmolality checked to be 300 mOsm/l, adjusted with sucrose if needed. Data were acquired with an Axopatch 200B (Axon Instruments) amplifier and digitized with a Digidata 1440A (Molecular Devices, CA, USA). Series capacitances and resistances were compensated electronically. Data sampled at 20 kHz and lowpass filtered at 5 kHz using the pClamp10 software (Axon Instruments). Further analysis was performed using Clampfit 10.7 (Molecular Devices; CA, USA) and Mini analysis 6 software (Synaptosoft, NJ, USA)

874 in a semi-automated fashion (automatic detection of events with chosen parameters followed by a
875 visual validation).
876
877 **Evoked activity.** To test effects of CNO on neuronal excitability *ex vivo*, we used a current step
878 method. To this purpose, we make PVN→SON projecting neurons express the DREADD receptors
879 by injecting rats' SON with a CAV2-Cre virus (rAAV-CAV-Cre) and PVN with an OT specific
880 Cre-inducible DREADD construct (rAAV-OTp-DIO-hM4D(Gi)-mCherry or OTp-DIO-hM3D(Gq)-
881 mCherry). 6-8 weeks after infection, coronal slices were prepared and fluorescent neurons
882 (indicative of the viral expression) were selected for whole cell patch-clamp recordings. After
883 establishing the clamp, neurons were recorded in current clamp mode with 0pA injected. To test the
884 effect of the effects of DREADD activation - hM4D(Gi) or hM3D(Gq) - neurons were subjected to
885 the following current steps. For hM4D(Gi), neurons received an injection of an -100 pA negative
886 current to hyperpolarize the neuron membrane (reaching -100 mV) before each step. These steps
887 start at -80 pA and increased by 20 pA, reaching +120 pA. For hM3D(Gq), steps start at -20 pA and
888 increased by 10 pA, reaching 80 pA. To quantify the effects of DREADD activation, the number of
889 action potentials triggered by these steps were evaluated.

890 **Spontaneous activity.** To evaluate the effect of DREADD activation on neuronal activity, neurons
891 were also recorded 2 minutes before and after CNO exposure in voltage or current clamp mode. In
892 these cases, the frequency of post-synaptic current (PSC) or action potentials (AP) were quantified.

893 **Identification of parvOT and magnOT.** The identity of PVN's OT neurons was verified through
894 a current step protocol [52], this method has been used in several other studies in order to allow
895 discrimination between parvocellular and the magnocellular neurons[13,53–56]. Neurons received an
896 injection of an -100 pA current to hyperpolarize the neuron membrane (reaching -100 mV) before
897 each step. These steps start at 0 pA and increased by 20 pA, reaching +60 pA. To discriminate

between parvOT and magnOT, we have measured the hyperpolarising notch and the T outward rectification.

ChR2 Stimulation of SON's ParvOT neurons. In order to decipher the connexion between SON parvOT neurons and PVN magnOT neurons, we have used an optogenetic strategy. First, we have identified PVN OT neurons by injecting rats' PVN with an rAAV containing the coding sequence of the fluorescent marker Venus under the control of the OT promoter (OTp-Venus). Then, we aimed to specifically activate SON→PVN projection by using a combination of two rAAV : the first one were injected in the SON and induce the expression of the Cre recombinase in SON targeting neurons, and the second one were injected in the PVN to allow the expression of the ChR2 in OT neurons after a Cre-dependant recombination (OTp-DIO-ChR2-mCherry). 6-8 weeks after infection, coronal slices containing the PVN were prepared and the Venus positive / mCherry negative neurons were selected for whole cell patch-clamp recordings. This combination of fluorescent markers allows us to select PVN OT neurons that are not directly targeting the SON.

Neurons were recorded 2 minutes in voltage clamp to establish the baseline frequency of postsynaptic currents (PSC) and then, we performed an optogenetic stimulation of ChR2-expressing OTergic neurons by applying light pulses (10ms at 30Hz for 20s) using light source X-Cite® 110LED from Excelitas Technologies through a GFP filter, controlled with a Clampex-driven TTL. Neurons were also recorded during the ChR2 stimulation in order to observed that the neurons are not expressing ChR2 itself. Finally, we continue to recorded 10 minutes after the stimulation to observed the effect of the SON parvOT neurons stimulation on the PSC frequency of the recorded neurons. PSC were detected using Mini analysis 6 software (Synaptosoft, NJ, USA).

Calcium Imaging

To test whether the chemogenetic activation of PVN→SON projecting OTergic neurons can modify the intra PVN microcircuits activity, we have used an *ex vivo* calcium imaging approach. To this

goal, rats' SON have been infected with a CAV2-Cre and the PVN were infected with a virus allowing the expression of hM3D(Gq) under the control of OT promoter after a Cre-dependant recombination (OTp-DIO-hM3D(Gq)-mCherry). We also make PVN OT neuron express the calcium indicator GCaMP6s using a third viral vector (rAAV-OTp-GCaMP6s). 6-8 weeks after infection, coronal slices containing the PVN were prepared and neurons which were positive for GCaMP but negative for mCherry were recorded. To perform this fluorescence microscopy, we have used a Zeiss Axio examiner microscope with a 40x water immersion objective (numerical aperture of 1.0), mounted with a X-Light Confocal unit – CRESTOPT spinning disk. Images were acquired at 5Hz with an optiMOS sCMOS camera (Qimaging, BC, Canada). Neurons within a confocal plane were illuminated for 100 ms at λ = 475 nm using a Spectra 7 LUMENCOR. The different hardware elements were synchronized through the MetaFluor software (Molecular Devices, LLC, Ca, USA). Neurons calcium levels were measured in hand drawn region on interest (ROI). In all recordings, the Fiji rolling ball algorithm was used to increase signal/noise ratio. Recordings in which movements / drifts were visible were discarded.

Off-line data analysis was performed using a custom written python-based script.

First, a linear regression and a median filter was applied to each trace. Peaks were then detected using the 'find_peaks' function of the SciPy library. More precisely, fluorescence variation was identified as a calcium peak if its prominence exceeds two times the standard deviation and if the maximum peak value surpasses 3 fluorescence units. ROI with zero calcium variations were excluded from the analysis. The remaining ROI were considered as living neurons and the number of peaks was quantified before and after the drug application. The AUC was estimated as the sum of the local area of each peak to avoid biased AUC estimation due to baseline drift. All these data were normalized according to the duration of the recording and neurons were labelled as "responsive" when their AUC or their number of peaks were increased by at least 20% after drug application. Because the time post-stimulation is longer than the baseline, the probability of observing a spontaneous calcium peak is stronger post-stimulation. To avoid this bias, neurons with

only one calcium peak during the whole recording were removed from responsive neurons. The response probability was calculated as the number of responsive neurons with a least 1 calcium event per time bin (30s) divide per the number of responsive neurons in each recording. Finally, all data were normalized per slice and this result was used as statistical unit. All data were compared using paired statistical analysis (before vs after drug application) and the results are expressed in ratio (baseline/drug effect), so a ratio of 1 meaning neither an increase or a decrease of the measured parameter.

***In vivo* optoelectrode recordings**

Implantation of opto-electrodes

Silicon probes (A1x32-Poly3-10mm, NeuroNexus) containing a 32-channel single shank combined with an optic fiber (diameter: 100 µm, Thorlabs) (opto-electrodes) were used in acute (anaesthetized and head-fixed) recordings. For freely moving recordings, thirty-two channel chronic optoelectrodes were hand-made, consisting of eight tetrodes and one specially designed microdrive. The microdrives and tetrodes were manually assembled as described previously[57]. The tetrodes were made with 0.0005-inch Tungsen wires (Stablohm 675, California Fine Wire Company, CA, USA). Eight tetrodes and an optic fiber (200 µm, Thorlabs) were loaded into the micro-drive via a guiding tube and were arranged in parallel order. Assembled opto-electrodes were gold plated and impedance of each channel was measured between 250 and 350 kOhm. For implantation, rats were anesthetized with 2% isoflurane and placed in a stereotaxic frame. Bregma position and horizontal level were aligned during the implantation. Opto-electrode tips were implanted into the target location and the microdrive was fixed on the skull by six micro screws (Knupfer, Germany) and dental cement (Paladur, Heraeus Kulzer, Germany).

Optogenetic identification of oxytocin neurons

974 Electrophysiological signals were acquired by Open-Ephys acquisition board (Open Ephys, USA)
975 and sampled at 30 kHz. To identify ChR2-positive oxytocin neurons in the PVN, pulses of blue
976 light (wavelength λ=473 nm, DreamLasers) were delivered by the optic fiber while recording
977 extracellular electrical activity of the neurons. The pulse train was controlled by a pulse generator
978 (Master9, A.M.P.I.), pulses had a duration of 10 ms and were applied at stimulation frequencies of
979 1, 5, and 10 Hz. In each session, the laser output at the optic fiber terminal was measured as 20
980 mW/mm^2. Neurons with a clear time-locked response to light pulses (spikes within 2-8 ms from
981 onset of pulses) were classified as oxytocin neurons (**Extended Data Fig. 1e**).
982
983 **Analysis of spike waveforms**
984 Spike sorting was done manually in Plexon Offline Sorter 4.0 (Plexon, Inc., TX, USA), with
985 tetrodes mode. The raw data were filtered at 250 Hz with a butterworth high-pass filter, and
986 waveform detection thresholds were placed at -0.5-0.8% of ADC range (or -0.32 ~ -0.51 mV),
987 depending on the signal-to-noise ratio. Magnocellular neurons have spikes with a width at half
988 amplitude of about 0.5 ms, an absolute refractory period of about 2.5 ms and a long relative
989 refractory period reflecting a prominent hyperpolarizing afterpotential[17]. Therefore, the sample
990 length in waveform detection was set to 1.4 ms (400 μs pre-threshold period, at the 30 kHz
991 sampling rate, a single waveform consists of 42 data points, and in the tetrodes waveform, each unit
992 detected 168 data points), and dead time was set to 1.2 ms. Next, the detected waveforms were
993 aligned at the valley point, when the neurons were depolarized at their maximum, and Principle
994 Component Analysis (PCA) and Slice features of waveform were plotted and projected into 3D
995 space for visual separation of clusters into presumptive single-units. The timestamp feature was
996 used to exclude mechanical noise recorded at same time across 4 channels among the tetrodes. In
997 different recording sessions (e.g., open field and social interaction), we analyzed whether the
998 features of spike waveforms remain consistent with the 3D plot results. After clustering, units with
999 a minimum inter-event interval exceeding 2500 μs were accepted as single hypothalamic neurons.

1000 Units displaying minimum inter-event intervals between 1200-2500 μs were recognized as arising
1001 from multiple neurons and were excluded from the statistics of the study.
1002
1003 **Statistical analyses of spike patterning**
1004 From segments of stationary activity recorded in open field conditions, inter-spike interval
1005 distributions were constructed to verify that these were consistent with distributions characteristic
1006 of oxytocin neurons under basal conditions recorded in anesthetized rats[58]. To quantify the
1007 regularity of spike firing, we calculated the index of dispersion (IoD) of firing rate in 1-s bins as the
1008 ratio of the variance to the mean. For events that arise as a result of a random process that is
1009 invariant in time, the index will be equal to 1 independently of the mean rate, and independently of
1010 the binwidth. If events arise more regularly than chance, the index will be less than 1, and if they
1011 are more variable than expected by chance – as when spikes occur in clusters or bursts, the index
1012 will be greater than 1.
1013 In oxytocin neurons, spikes cannot arise purely randomly because of the refractory period, and the
1014 IoD reduces slightly with increasing firing rate because at higher rates the relative refractory period
1015 is larger as a proportion of the mean interspike interval. The IoD also reduces with increasing
1016 binwidth because oxytocin neurons also display a prolonged activity-dependent
1017 afterhyperpolarization that acts to stabilize mean firing rates over a timescale of seconds.
1018 Collectively the known intrinsic membrane properties of rat oxytocin neurons, as tested through
1019 computational models, imply that if spikes arise as a result of a purely random and time-invariant
1020 process, then the IoD of firing rate in 1-s bins will be in the range 0.3-1 for neurons firing at up to 6
1021 spikes/s, depending on firing rate and on individual variability in membrane properties[17,58].
1022
1023 **Local field potentials in the PVN**
1024 Local field potentials (LFPs) were sampled at 1 kHz with low-pass filter. Subsequent analysis was
1025 done using custom MATLAB (MathWorks, USA) scripts. We estimated power spectrum density

(PSD) of LFP signal using multi-tapper approach based on Thomson's method ('pmtm' function). Spectrograms were computed for each recording using standard 'spectrogram' function. Power of theta oscillations was calculated as average of PSD in the range 5-10 Hz. Phase-lock analysis was performed to investigate the relation between theta oscillations in the PVN and the timing of spikes in oxytocin neurons. The phase of the oscillatory activity was extracted with Hilbert transformation ('Hilbert' function) and converted into angle degrees. Then, we used Rayleigh's tests for circular uniformity, which indicates whether there is a significant correlation between the timing of spikes and a specific phase of the theta cycle (**Extended Data Fig. 1h-j**).

***In vivo* fiber photometry**

Optic guided implantation of optic fibers

We injected a modified adenovirus (AAV-OTp-GCaMP6s) bilaterally into the PVN or SON to transduce expression of the Ca^{2+} indicator GCaMP6s in oxytocin neurons, and verified that this was expressed cell-specifically (87±4 % of oxytocin neurons, n = 1371 neurons, n=4 rats, **Fig. 4p**). Optic fibers (M127L01 Ø 400µm, 0.50 NA, 10 mm, Thorlabs) were implanted ~100 µm above the dorsal border of the PVN (A/P: -1.8 mm, M/L: 0.35 mm, D/V: -7.85 mm) or SON (A/P: -1.25 mm, M/L: 1.90 mm, D/V: -9.0 mm) under 1.5% isoflurane anesthesia. Four 1 mm screws (Knupfer, Germany) and a metal implant guide (OGL, Thorlabs) were attached to skull with OptiBond FL (Kerr, Germany) and fixed by dental cement (Paladur, Heraeus Kulzer, Germany).

During implantation, the implantable cannula was fixed in an adaptor (ADAL3, Thorlabs) attached to stereotactic holder; while the other end of the cannula was connected through a pre-bleached Patch cord (FP400URT, Thorlabs) to the photodetector and LED of fiber photometry system (FOM, NPI Electronic, Germany). The digitalized photometry signal was monitored and recorded via digital input/output (DIO) board (OpenEphys, USA) to the DAQ system. (OpenEphys, USA) with 0.1-20 Hz bandpass filter and 20 s time scale set in to visualize the Ca^{2+} signal online, while the cannula tip was gradually lowered into the PVN at 1 mm/min. When the optic fiber tip was close to

the PVN where GCaMP6s was expressed, a slight increase in the signal baseline and a minor spontaneous fluctuation could be visually detected. During implantation, rats were under 1.5% isoflurane anesthesia and body temperature was kept stable at 37° C by a heating plate (RWD, China). The LED power in fiber photometry system was set at a constant value between 5-10 mW/mm^2. The fiber photometry recordings were conducted after one week of recovery from the implantation. Fiber photometry raw data were sampled at 30 kHz in OpenEphys GUI and analyzed with custom written MATLAB scripts.

Fiber photometry data analysis

Digitalized optical signal acquired from the fiber photometry system was first downsampled at 3000 Hz and then low-pass filtered (MATLAB 'butteworth' function) at 10 Hz to exclude noise at higher frequency. Secondly, to correct the baseline drifting due to photo-bleaching of fluorophores we fitted the signal with a polynomial curve (MATLAB 'polyfit' function) and subtracted it to the signal. Next, we smoothed the signal with a Savitzky-Golay filter (MATLAB 'smooth' function, option 'sgolay'). For each experiment, the signal F was converted to $\Delta F/F_0$ by

$$\Delta F/F(t) = \frac{F(t) - F_0}{F_0}$$

where F_0 was calculated as the average value of F of a 600 second recording at the beginning of the experiment. The data was subdivided in 1 min bins and the mean $\Delta F/F_0$ was calculated for each bin. We detected calcium transients similar to those reported by our previous study[59]. Finally, we calculated the area under the curve (AUC) of the Ca^{2+} signal (MATLAB 'trapz' function) to estimate the cumulative fluorescence for each bin and normalized the AUC to values from 0 to 1. Values of normalized AUC was displayed in 1 min bin and averaged in 30 min bins. The ratios of AUCs between experimental and control conditions were used for quantitative analysis and called "relative AUC increase".

Application of airpuffs and OT neurons response

Airpuffs from a pressured air can (Toolcraft 20793T 400 ml, Germany) were applied through a stiff micropipette tip with a 2-mm opening positioned 10–15 mm above the skin in the area of ~ 2 cm^2. A plastic cover with 2-cm holes was placed above the rat's body to restrict the area of stimulation. The controlled air pressure was 1.139 g/cm^3. During *in vivo* electrophysiology recordings, in each stimulation point, 5 airpuffs (duration 0.2 s, interval between puffs 1 s) were delivered in sequence with intervals of 1 min between sequences (**Fig. 2a and Extended Data Fig. 4**). During fiber photometry recordings, one airpuff (duration 1 s) was applied every 1 min (**Fig. 2e-j**).

OT neurons response to airpuff stimulations

We applied airpuffs to the skin of three regions of the rat's dorsal body area (anterior, central, and posterior part), two regions of the rat's ventral area (abdomen and anogenital area), and to the whiskers on both sides. We considered a recorded neuron as responsive to airpuff stimulations if the average firing rate after (from 0 to 2 s) stimuli onset increased of at least 2 times the standard deviation (SD) of the baseline activity (2 s prior to stimuli onset). Onset of the response was calculated as the time at which the firing rate of a responsive neurons increased of 1 time the SD of the baseline activity. We recorded the activity of n = 23 oxytocin neurons in response to airpuffs applied on the rat's dorsal body area which showed variable response latencies up to 30 s (**Extended Data Fig. 4a-b**); 10 of those neurons exhibited a response within 1 s after stimuli onset and are shown in **Fig. 2a-b.**

Blood sampling and plasma OT measurements

To monitor neurohypophysial OT release after chemogenetic activation of hypothalamic parvOT neurons, we performed blood sampling from the jugular vein in urethane-anesthetized rats. After surgery, rats were placed on a heating pad for the rest of the experiment to maintain constant body temperature. The jugular vein catheter was connected to a 1-ml syringe containing sterile

heparinized saline (30 IU/ml). 45 min before, and 45 min as well as 90 min after ip CNO, 500 µl of blood was drawn (**Fig. 4q-r**), which was replaced by 500 µl sterile saline. After each sample, the catheter was filled with heparinized saline to avoid blood clotting. Blood samples were collected in EDTA-tubes (Bayer, Germany) on ice, centrifuged (5000 x g, 10 min, 4 °C), and 200-µl plasma samples were stored at -80°C prior to extraction and OT quantification by radioimmunoassay. OT content in extracted plasma was analyzed by a highly sensitive radioimmunoassay with a detection limit of 0.1 pg and cross-reactivity < 0.7 % (RIAgnosis, Germany)[60,61].

Behavior

Starting from 14 days prior to behavioral tests, vaginal smears were collected to monitor ovarian cycle. Rats in metestrus, proestrus and estrus phases were excluded from experiments and reintroduced once they reached diestrus.

Behavioral tests were conducted in an arena (material non-absorbent to odors) with dimensions 60x60x60 cm under dim light condition (< 20 lux; lux-meter SO 200K, Sauter, Germany). On the day before the test, the experimental rat was exposed to the arena for 15 min for habituation. The arena was cleaned with 70% ethanol after each session to eliminate residual odors. Experimental and stimuli rats were housed in separate cages and had not previous encountered each other before the social interaction tests. The same rat was exposed to social interaction tests twice on separate days, each time with a different social stimulus rat so that the experimental paradigm always represented interaction with a novel, unfamiliar conspecific.

Open field test:

The experimental rat was placed in a corner of the arena and was allowed to freely explore the environment. These tests served as a “baseline” for social interaction tests.

Free social interaction (FSI) test:

The experimental and the stimulus rats were placed in opposite corners of the arena at the same time and were allowed to freely interact with each other and/or explore the environment.

Chambered social interaction (CSI) test:

For this test, two plexiglas transparent meshes (dimensions 20x30x1 cm) provided with three opening/holes (dimensions 15 x 0.75 cm) were placed in two opposite corners of the arena. The mesh separated a little triangular area (14 x 14 x 20 cm, corresponding to ~3% of the total area of the arena) to the rest of the arena (central compartment). The experimental rat was placed in the central compartment while the stimulus rat was placed in one of the two little compartments. The two rats were able to see, hear, and smell each other through the openings, but they were not able to touch one another.

Chemogenetic inhibition or activation of parvocellular oxytocin neurons by DREADD

To selectively activate or inhibit parvocellular oxytocin neurons, rats were injected with rAAV-OTp-DIO-hM3D(Gq)-mCherry (Parvo-Gq group), rAAV-OTp-DIO-hM4D(Gi)-mCherry (Parvo-Gi group), or rAAV-OTp-DIO-GFP (Parvo-GFP control group) into the PVN and CAV2-Cre into the SON, as previously described [13].

All groups (Parvo-Gq, Parvo-Gi, and Parvo-GFP) were subjected to the same protocol. On day 1 experimental rats were exposed to the open field arena for 15 min for habituation. On day 2, the experimental rat was injected i.p. with either CNO or saline solution 60 min before beginning the tests and then was subjected to one CSI and one FSI session for 5 min each.

Intracerebroventricular administration of OT-receptor antagonist

Guide cannulas were implanted above the lateral ventricle for intracerebroventricular (i.c.v.) infusion of OTR antagonist (OTR-a) des-Gly-NH_2,d$(CH_2)_5$[Tyr(Me)^2,Thr^4]OVT[29]. OTR-a 0.75 µg/5 µl[30,62] was infused 15 minutes prior to behavioral tests. Four groups of rats were studied, which received i.p. injection and i.c.v. infusion of Saline/Saline, CNO/Saline, Saline/OTR-a, or CNO/OTR-a respectively.

Video and audio analyses of behavior

The videos were recorded using a GigE color HD camera (Basler AG, Germany). The tracks of the experimental and stimulus rat were extracted from videos using two softwares: Ethovision XT 11.5 (Noldus) and MATLAB Toolbox idTracker (MathWorks). Results of the two softwares were compared and cross-validated. The distance moved by each rat, velocity, the time spent in different areas of the arena, and the distance between rats and time spent in close proximity were calculated automatically. Social interactions were also analyzed manually to classify social behaviors into different categories: '*sniffing*', '*chasing*', '*crawling on top*', '*being crawled*', and '*head-to-head*' approaching; time spent by experimental rat for each behavioral category was used for all analysis. Manual scoring of social behavior scoring were done by a researcher (different from the one who performed the experiment) that was blind to treatment conditions.

Ultrasonic vocalizations were recorded with an ultrasound microphone (Avisoft-Bioacustic, Germany) and analyzed with Avisoft-SASlab Pro 5.2 software. After calculation of sound spectrogram, vocalizations time, duration, and frequency were extracted. Each 'call' was classified into non-social (peak frequency ~ 22 kHz) or appetitive/social (peak frequency ~ 50 kHz) call. Social vocalizations were further classified in trills (<10 ms), single component calls (>10 ms, not modulated), and complex vocalizations (>10 ms, frequency modulated or combined)[63].

Freely moving single unit recordings – experimental groups

Open field and FSI group: experimental rats implanted with opto-electrodes for single unit recordings in the PVN were subjected to one open field session and one FSI session for 10 min each. Between the two session the rat was place in the home cage (single-housed) for 15 min.

Open field, CSI, and FSI group: experimental rats implanted with opto-electrodes for single unit recordings in the PVN were subjected to one open field, one CSI, and one FSI session for 10 min each, without pauses in between. Stimulus rats were placed in one of the little chambers separated by a plexiglas mesh at the beginning of the CSI session; the wall was then lifted up (**Fig. 6b**) at the

beginning of the FSI session allowing the stimulus rat to join the experimental rat in the central compartment.

Histology

Anesthetized rats were transcardially perfused with PBS followed by 4% PFA. Brains were dissected out and post-fixed overnight in 4% PFA at 4 °C with gentle agitation. 50-µm vibratome coronal sections containing the PVN and the SON were cut and collected. Immunohistochemistry was performed on free-floating sections with the following antibodies: anti-OT (PS38, 1:2000; mouse; kindly provided by Harold Gainer), anti-OT (T-5021, 1:50,000, Peninsula, guinea-pig), anti-synaptophysin (ab32127, 1:1,000, abcam anti-rabbit), anti-Ds-Red (#632397, 1:1000; rabbit; Clontech), anti-GFP (ab13970, 1:1000, chicken, Abcam), anti *c-fos* (#9F6, 1:500, rabbit, Cell Signaling), anti-Fluorogold (NM-101, 1:1000, guinea pig, Protos Biotech), anti-Cre (#69050, 1:2000, mouse, Novagen). Further information on validation of primary antibodies can be found in the Life Science Reporting Summary. The signals were visualized with the following secondary antibodies, CY3-conjugated (711-165-152) or CY5-conjugate (115-175-146, Jackson Immuno-Research Laboratories) or Alexa 488 (A11039) and 594 (A11012, Invitrogen) and Alexa-594 (715-585-151) and Alexa-647 (713-645-147, Jackson Immuno-Research Laboratories). All secondary antibodies were diluted 1:500.

Fluorogold treatment and visualization

To discriminate between magno- and parvocellular oxytocin neurons, rats received a single injection of Fluorogold (Santa Cruz Biotechnology, Dallas, 15 mg/kg bw i.p.) 7 days before the perfusion. Brain sections were stained with a primary antibody for Fluorogold (guinea pig anti-FG, dilution 1:1000, Protos Biotech Corp, New York) and Fluorogold immunosignal was visualized by secondary antibodies conjugated with CY3 (Goat anti-rabbit, dilution 1:500, Jackson Immuno-

Research, Newmarket Suffolk, UK). The colocalization of Fluorogold, oxytocin, and *c-fos* signals were manually quantified in the PVN (n = 4 rats; 6 sections/brain).

Images of immunostained tissue sections

All images were acquired on a Leica TCS SP5 (DKFZ Light Microscopy Facility) confocal laser-scanning microscope. Digitized images were analyzed using Fiji (NIMH, Bethesda, MD, USA) and Adobe Photoshop CS5 (Adobe, Mountain View, CA).

Confocal microscopy and 3D IMARIS analysis

For the 3D reconstruction of OT neurons, we took Z-stack images (50 µm depth, 1µm steps, 40x magnification) of PVN and SON using a Zeiss LSM 780 confocal microscope (1024x1024 pixel, 16-bit depth, pixel size 0.63-micron, zoom 0.7). Raw czi files were used for further analysis using IMARIS[26,27,64] software (Version 9.31, Oxford Instruments: https://imaris.oxinst.com). First, IMARIS was used to reconstruct the cellular surface using the following custom settings: surfaces Detail 0.700 µm (smooth); thresholding Background subtraction (Local Contrast), diameter of largest Sphere, which fits into the object: 2.00; Color: base, diffusion transparency: 65%. After surface reconstruction, we used the filter function to remove unspecific background signals: Filter: Volume max – 400 μm^3. After deletion of all background signals the 'mask all' function was used to create the final surface reconstruction. Next, the surface reconstruction was used as the template for the filament reconstruction using the following custom settings: detect new starting points: largest Diameter 7.00 µm, seed points 0.300 µm; remove seed points around starting points: diameter of sphere regions: 15 µm. Seed points were corrected for (either placed in or removed from the center of the somata) manually if the IMARIS algorithm placed them incorrectly. All surface and filament parameters were exported into separate Excel files and used for data analysis. For all quantifications, we used 6-8 40x z-stacks per animal (2 z-stacks per brain hemisphere). We used a computer suited for IMARIS analysis (Intel Core i7 8700 @3.2 GHz, 64 GB RAM, x-64-bit,

Windows 10 Enterprise). All images used for analysis were taken with the same confocal settings (pinhole, laser intensity, digital gain and digital offset). Sholl analysis was performed using IMARIS in the filament reconstruction mode and individual data sets were exported into separate Excel files for further analysis. To assess the number of SYN+/GFP-positive axons, we used a simplified version of the Sholl analysis, where we only included the first 2-8 spheres (starting in the soma center) either until we could detect SYN+/GFP intersections or were more than 2µm apart from the border of the respective soma. The total amount of immunoflourescene (synaptophysin) was calculated using the extract intensity/number of spots function. First, we created spheres that precisely engulfed the respective somata (parvOT and magnOT neurons) so that both ends of the cell soma (maximum diameter) touched the border of the respective sphere. To account for individual variability in roundness and surface area, we calculated surface area for each individual OT cell using the surface reconstruction mode. Given that cells with a larger surface area occupy more three-dimensional space within the artificially constructed sphere that could confound precise quantification of SYN fluorescence, we adjusted each calculated value (SYN+ voxels per sphere) based on the surface area. Assuming an inverse near-linear relationship between cell volume and the total amount of SYN fluorescence within a sphere, we calculated the degree of occupancy (i.e. percentage) for each somata within the respective sphere. Finally, we calculated the final SYN+ voxels using the following equation: (number of SYN+ voxels) * (degree of occupancy). For the quantification along the dendrites we used spheres with a 10µm radius along the dendrite for both parvOT and magnOT neurons.

Projection-specific trans-synaptic retrograde tracing

Input tracing experiments were performed in female Wistar rats (aged 10-12 weeks). We used EnvA-pseudotyped rabies virus G deletion-mutant EnvA ΔG-EGFP (Rb-GFP [28]) to monosynaptically retrogradely trace neurons projecting to parvOT and magnOT neurons. Rb-GFP selectively enters neurons expressing the avian sarcoma and leucosis virus receptor (TVA), and can

only spread presynaptically from neurons expressing the rabies virus glycoprotein (we used the optimized glycoprotein, oG, from[65]). We injected a 300 nL mixture of 1:1 rAAV-OTp-TCB:rAAV-Ef1A-DIO-oG into the right PVN of female rats. Then, to specifically trace inputs to parvOT neurons, we injected rats (n=5) with CAV2-CMV-Cre into the right SON (**Extended Data Fig. 8a**). In another group of rats (n=5), we employed a similar strategy to express oG only in magnOT neurons: we injected an AAV retrograde expressing Cre (rAAVretro-Ef1A-Cre) into the posterior pituitary (**Extended Data Fig. 8c**, based on[66]). This strategy makes Rb-GFP selectively enter in all OT neurons, but specifically spread retrogradely from neurons expressing oG (i.e, parvOT or magnOT neurons). After two weeks, we injected 300 nL of EnvA ΔG-EGFP into the right PVN, and seven days later, animals were perfused with 4% PFA. The number of projecting neurons was quantified from brain sections as follows: every third 50-µm section was imaged and neurons were counted, and then multiplied by three, to estimate the real number of inputs. GFP+ neurons on the injected hemisphere were counted and assigned to brain areas based on classifications of the Paxinos Mouse Brain Atlas37, using anatomical landmarks in the sections visualized by tissue autofluorescence. Very few contralateral inputs were noticed and we thus decided to neglect them. While we had good infection at injection sites for both parvOT and magnOT groups (**Extended Data Fig. 8g**), starter neurons could not be reliably counted, as rabies virus toxicity prevented us to correctly visualize mCherry in the PVN. Thus, the analysis presented here does not take into account inputs to OT neurons from within PVN. The percentage of inputs from each region was obtained by dividing the number of inputs from one region per the total number of inputs. Input regions that were detected in a subset of animals only were discarded from analysis. We used unpaired two-sided Student's t tests to compare the total number of inputs to parvOT and magnOT neurons and Chi squared tests to compare proportions of inputs between regions.

We controlled that TVA was selectively expressed in OT neurons by injecting control rats (n=2) with rAAV-OTp-TCB in the PVN, and staining for OT. This revealed that most OT neurons expressed mCherry and that no non-OT neurons expressed mCherry (**Extended Data Fig. 8e**).

Furthermore, we verified that Rb-GFP was selectively entering OT neurons by injecting control rats (n=2) with rAAV-OTp-TCB, and Rb-GFP 2 weeks later. This resulted in specific expression of GFP in PVN OT neurons (**Extended Data Fig. 8f**).

In each rat, we confirmed SON injection site by staining for Cre for the parvOT neurons tracing (**Extended Data Fig. 8a,b**) and by injecting a virus Cre-dependently expressing mCherry in the SON of magnOT neurons tracing, which led to expression of mCherry in SON magnocellular neurons (**Extended Data Fig. 8c,d**).

Oxytocin secretion model

The OT secretion model[17] simulates stimulus-secretion coupling in oxytocin neurons. The model is a continuous approximation of the stochastic release process from all neuronal compartments. It is based on extensive studies on activity-dependent hormone secretion from magnocellular neurosecretory neurons[58] and it matches experimental data closely. In the model, when spikes invade the secretory terminals, exocytosis occurs in response to fast rising Ca^{2+} concentrations (*e*). At higher frequencies, the spikes broaden, producing a larger increase of *e*. The rate of secretion is modeled as the product of: *e* raised to the power of φ (which accounts for the cooperativeness of the Ca^{2+} activation), of the pool of releasable OT *p*, and a secretion scaling factor α, and is calculated as:

$$s = e^{\varphi} \cdot \alpha \cdot p$$

where $\varphi = 2$, $\alpha = 0.003$ pg/s.

The non-linear dependence of the secretion rate gives high secretion probability upon short spike intervals. To infer OT secretion arising from the spike trains observed in the present study, the recorded event timings were used to drive the secretion model described fully elsewhere[17]. The published model is scaled to quantitatively match secretion from the pituitary nerve terminals of a single oxytocin neuron. The scaling factor α cannot be used for absolute quantitative estimates of

release within the brain, but the relative efficacy of two firing patterns can be compared using the model, as α is eliminated in the ratio.

Statistics

Statistical analyses were performed using SigmaPlot 11 (Systat, USA) and GraphPad Prism 7.05 (GraphPad Software, San Diego, California, USA). Two-sided Wilcoxon signed-rank W test was used to compare the variation of spike frequencies measured for the same neuron in different conditions. Two-sided Mann-Whitney U test was used to compare low threshold depolarization in different cells. Two-sided Student's t tests were used to compare average values in two conditions when the data satisfied assumptions of normality. One-way ANOVA, followed by multiple comparison post-hoc test, was used to compare averages in three or more conditions. Two-way ANOVA, followed by multiple comparison post-hoc test, was used to analyze electrophysiological or behavioral data with repeated measures and CNO/Saline/OTR-a treatment (time x treatment). No statistical methods were used to pre-determine sample size but our sample sizes are similar to those reported in previous publications[5,13,30].

Differences were considered significant for $p < 0.05$. Asterisks were used to indicate the significance level: * $0.01 \leq p < 0.05$, ** $0.001 \leq p < 0.01$, *** $p < 0.001$. Statistical analyses of neuronal spike trains and local field potentials, such as peristimulus time histograms (PSTHs), auto- and cross-correlation, spikes burst analysis, power spectrum density, and phase-locking were performed using NeuroExplorer 3 (Nex Technologies, Colorado, USA) and custom written Matlab scripts.

Data and code availability

Python code (used for ex-vivo calcium imaging data analysis in **Fig. 4a-d**) and Matlab code (used for in-vivo fiber photometry data analysis in **Fig. 4e-o**, **Extended Data Fig. 7a-n**) can be found in Supplementary Software. All data that supporting the findings of this study, as well as Matlab codes

for the analysis of extracellular recording data, are available from the corresponding author upon reasonable request.

Methods only references

49. Menon, R. *et al.* Oxytocin signaling in the lateral septum prevents social fear during lactation. *Curr. Biol.* **28**, 1066-1078.e6 (2018).

50. Grinevich, V. *et al.* Somatic transgenesis (Viral Vectors). **3**, 243–274 (2016).

51. Paxinos, G. & Watson, C. The Rat Brain in Stereotaxic Coordinates Seventh Edition. *Elsevier Acad. Press* (2014).

52. Tasker, J. G. & Dudek, F. E. Electrophysiological properties of neurones in the region of the paraventricular nucleus in slices of rat hypothalamus. *J. Physiol.* **434**, 271–293 (1991).

53. Chu, C.-P. *et al.* Effects of Stresscopin on Rat Hypothalamic Paraventricular Nucleus Neurons In Vitro. *PLoS One* **8**, e53863 (2013).

54. Luther, J. A. & Tasker, J. G. Voltage-gated currents distinguish parvocellular from magnocellular neurones in the rat hypothalamic paraventricular nucleus. *J. Physiol.* **523**, 193–209 (2000).

55. Luther, J. A. *et al.* Neurosecretory and Non-Neurosecretory Parvocellular Neurones of the Hypothalamic Paraventricular Nucleus Express Distinct Electrophysiological Properties. *J. Neuroendocrinol.* **14**, 929–932 (2002).

56. Yuill, E. A., Hoyda, T. D., Ferri, C. C., Zhou, Q.-Y. & Ferguson, A. V. Prokineticin 2 depolarizes paraventricular nucleus magnocellular and parvocellular neurons. *Eur. J. Neurosci.* **25**, 425–434 (2007).

57. Tang, Y., Benusiglio, D., Grinevich, V. & Lin, L. Distinct types of feeding related neurons in mouse hypothalamus. *Front. Behav. Neurosci.* **10**, 91 (2016).

58. Maícas Royo, J., Brown, C. H., Leng, G. & MacGregor, D. J. Oxytocin neurones: intrinsic mechanisms governing the regularity of spiking activity. *J. Neuroendocrinol.* **28**, (2016).

59. Grund, T. *et al.* Chemogenetic activation of oxytocin neurons: Temporal dynamics, hormonal release, and behavioral consequences. *Psychoneuroendocrinology* **106**, 77–84 (2019).

60. Jong, T. R. de *et al.* Salivary oxytocin concentrations in response to running, sexual self-stimulation, breastfeeding and the TSST: The Regensburg Oxytocin Challenge (ROC) study. *Psychoneuroendocrinology* **62**, 381–388 (2015).

61. Landgraf, R., Neumann, I., Holsboer, F. & Pittman, Q. J. Interleukin-1β stimulates both central and peripheral release of vasopressin and oxytocin in the rat. *Eur. J. Neurosci.* **7**, 592–598 (1995).

62. Neumann, I. D., Maloumby, R., Beiderbeck, D. I., Lukas, M. & Landgraf, R. Increased brain and plasma oxytocin after nasal and peripheral administration in rats and mice. *Psychoneuroendocrinology* **38**, 1985–1993 (2013).

63. Ishiyama, S. & Brecht, M. Neural correlates of ticklishness in the rat somatosensory cortex. *Science* **354**, 757–760 (2016).

64. Althammer, F., Ferreira-Neto, H. C., Rubaharan, M., Roy, K. R. & Stern, J. E. Three-dimensional morphometric analysis reveals time-dependent structural changes in microglia and astrocytes in the central amygdala and hypothalamic paraventricular nucleus of heart failure rats. *Research square,* preprint (2020). doi:10.21203/rs.3.rs-22630/v1

65. Kim, E. J., Jacobs, M. W., Ito-Cole, T. & Callaway, E. M. Improved monosynaptic neural circuit tracing using engineered rabies virus glycoproteins. *Cell Rep.* **15**, 692–699 (2016).

66. Bin Zhang, Liyao Qiu, Wei Xiao, Hong Ni, Lunhao Chen, Fan Wang, Weihao Mai, Hui Gong, Shumin Duan, Anan Li, V. O. P. G. Reconstruction of the hypothalamo-neurohypophysial system and functional dissection of magnocellular oxytocin neurons in the brain. *bioRxiv,* preprint (2020). doi:10.1101/2020.03.26.007070

Figure 1

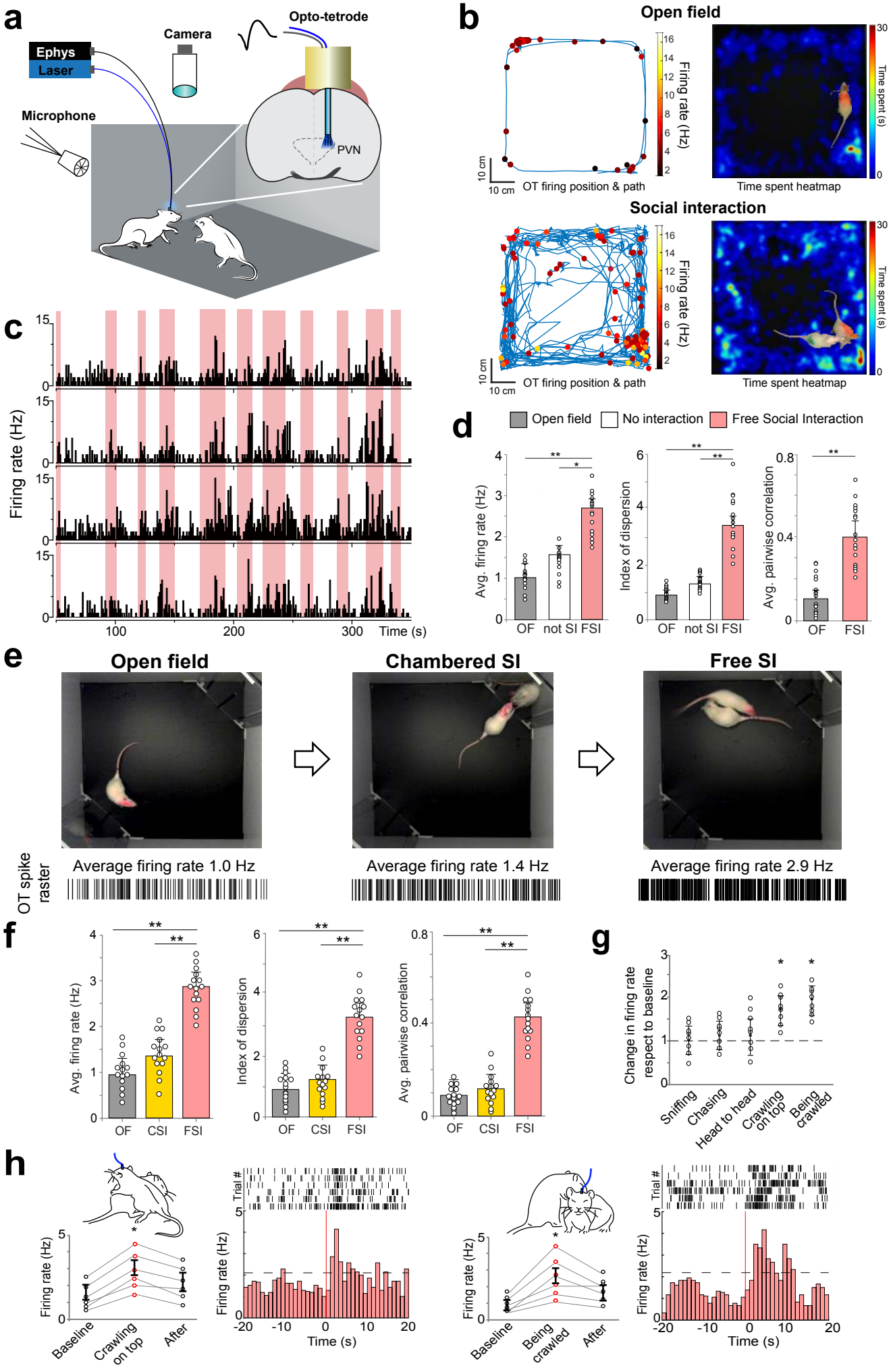
a
Ephys
Laser
Camera
Opto-tetrode
Microphone
PVN
b
Open field
Firing rate (Hz)
10 cm
10 cm
OT firing position & path
Time spent heatmap
Time spent (s)
Social interaction
c
Firing rate (Hz)
Time (s)
d
Open field
No interaction
Free Social Interaction
Avg. firing rate (Hz)
Index of dispersion
Avg. pairwise correlation
OF
not SI
FSI
e
Open field
Chambered SI
Free SI
OT spike raster
Average firing rate 1.0 Hz
Average firing rate 1.4 Hz
Average firing rate 2.9 Hz
f
Avg. firing rate (Hz)
Index of dispersion
Avg. pairwise correlation
OF
CSI
FSI
g
Change in firing rate respect to baseline
Sniffing
Chasing
Head to head
Crawling on top
Being crawled
h
Firing rate (Hz)
Baseline
Crawling on top
After
Trial #
Time (s)
Being crawled

Figure 2

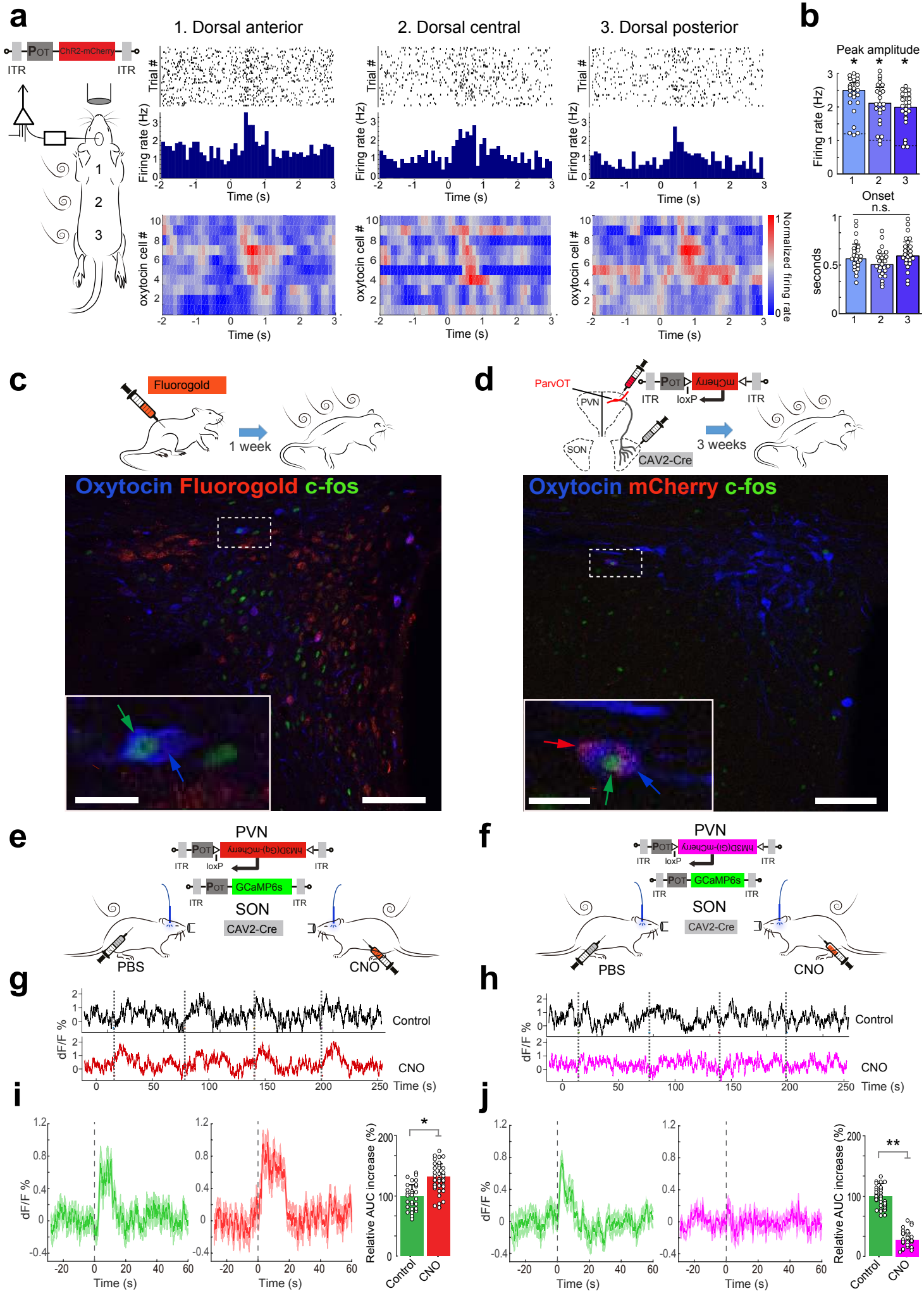
a
1. Dorsal anterior
2. Dorsal central
3. Dorsal posterior
POT
ChR2-mCherry
ITR
Trial #
Firing rate (Hz)
Time (s)
oxytocin cell #
Normalized firing rate
b
Peak amplitude
Onset
n.s.
seconds
c
Fluorogold
1 week
Oxytocin Fluorogold c-fos
d
ParvOT
PVN
SON
CAV2-Cre
3 weeks
Oxytocin mCherry c-fos
loxP
e
PVN
hM3D(Gq)-mCherry
GCaMP6s
SON
CAV2-Cre
PBS
CNO
f
hM3D(Gi)-mCherry
g
dF/F %
Control
CNO
h
i
Relative AUC increase (%)
j

Figure 3

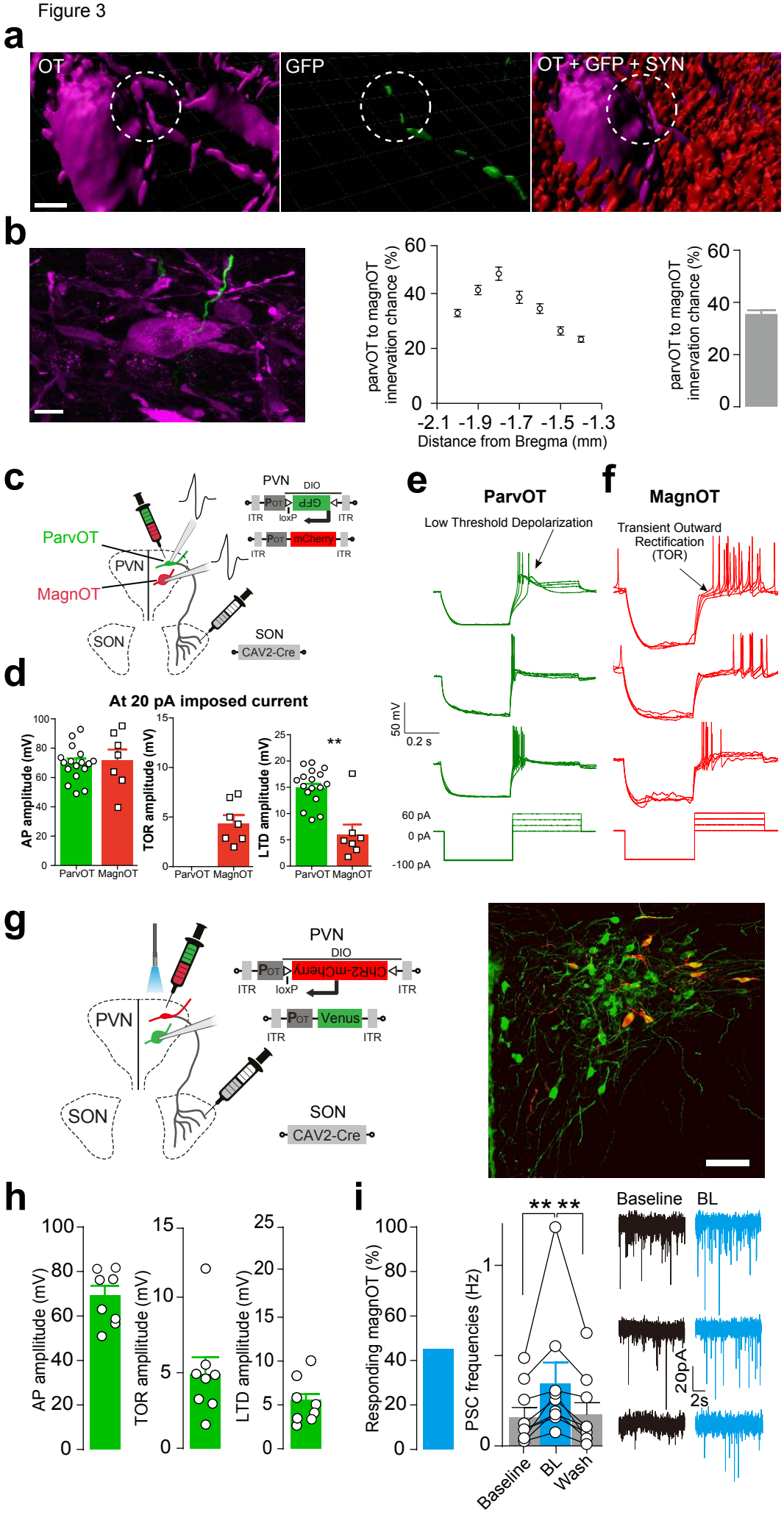
a
OT
GFP
OT + GFP + SYN
b
parvOT to magnOT innervation chance (%)
Distance from Bregma (mm)
-2.1 -1.9 -1.7 -1.5 -1.3
c
PVN
DIO
ITR
loxP
ITR
mCherry
ITR
ITR
ParvOT
PVN
MagnOT
SON
SON
CAV2-Cre
d
At 20 pA imposed current
AP amplitude (mV)
TOR amplitude (mV)
LTD amplitude (mV)
**
ParvOT MagnOT
ParvOT MagnOT
ParvOT MagnOT
e
ParvOT
Low Threshold Depolarization
50 mV
0.2 s
60 pA
0 pA
-100 pA
f
MagnOT
Transient Outward Rectification (TOR)
g
PVN
DIO
ITR
loxP
ITR
Venus
ITR
ITR
PVN
SON
SON
CAV2-Cre
h
AP amplitude (mV)
TOR amplitude (mV)
LTD amplitude (mV)
i
Responding magnOT (%)
PSC frequencies (Hz)
** **
Baseline
BL
Wash
Baseline
BL
20pA
2s

Figure 4

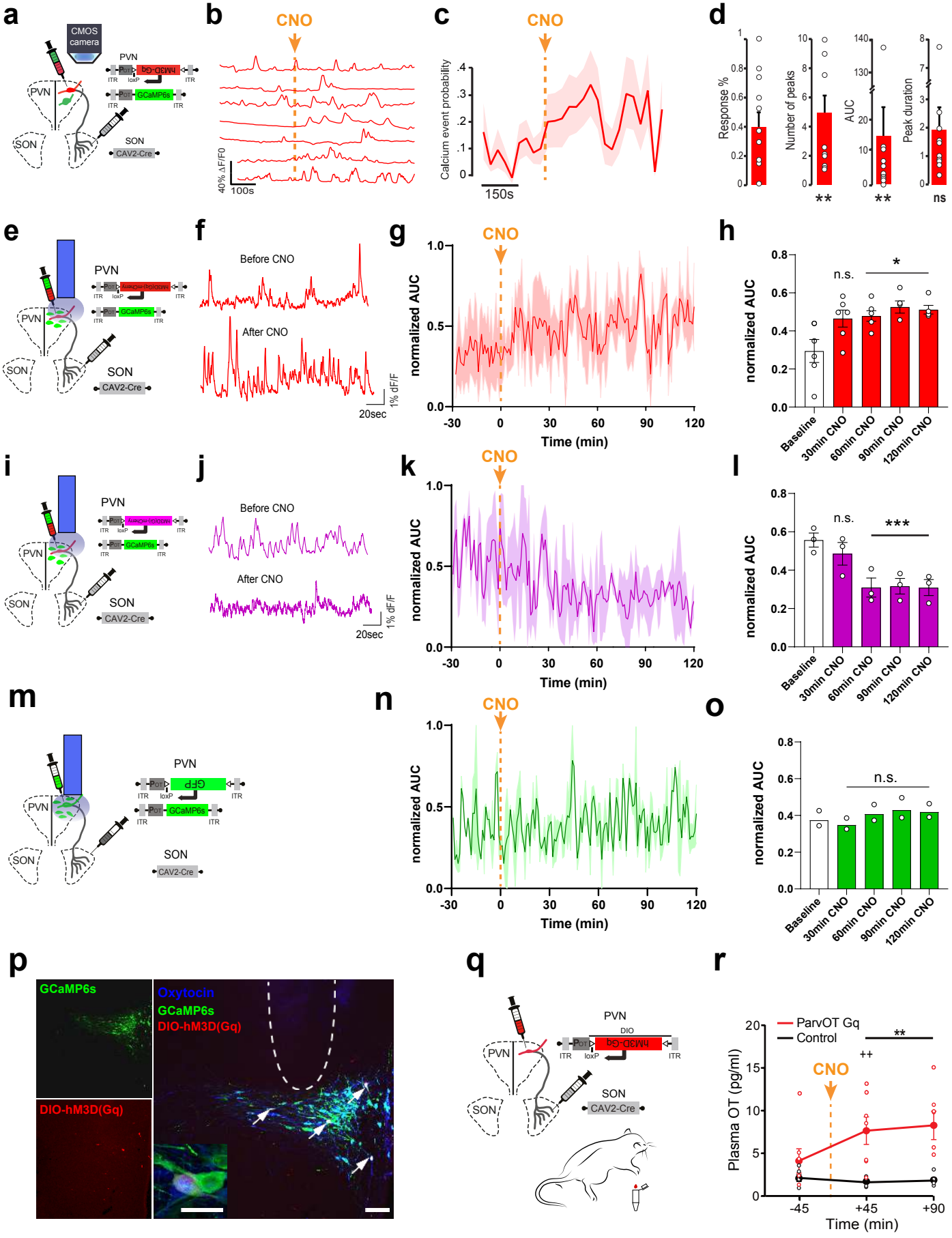
a
CMOS camera
PVN
SON
CAV2-Cre
b
CNO
40% ΔF/F0
100s
c
CNO
Calcium event probability
150s
d
Response %
Number of peaks
AUC
Peak duration
**
**
ns
e
PVN
SON
CAV2-Cre
f
Before CNO
After CNO
1% dF/F
20sec
g
CNO
normalized AUC
Time (min)
h
normalized AUC
n.s.
*
Baseline
30min CNO
60min CNO
90min CNO
120min CNO
i
PVN
SON
CAV2-Cre
j
Before CNO
After CNO
1% dF/F
20sec
k
CNO
normalized AUC
Time (min)
l
normalized AUC
n.s.
***
Baseline
30min CNO
60min CNO
90min CNO
120min CNO
m
PVN
SON
CAV2-Cre
n
CNO
normalized AUC
Time (min)
o
normalized AUC
n.s.
Baseline
30min CNO
60min CNO
90min CNO
120min CNO
p
GCaMP6s
DIO-hM3D(Gq)
Oxytocin
GCaMP6s
DIO-hM3D(Gq)
q
PVN
DIO
SON
CAV2-Cre
r
ParvOT Gq
Control
**
++
CNO
Plasma OT (pg/ml)
Time (min)

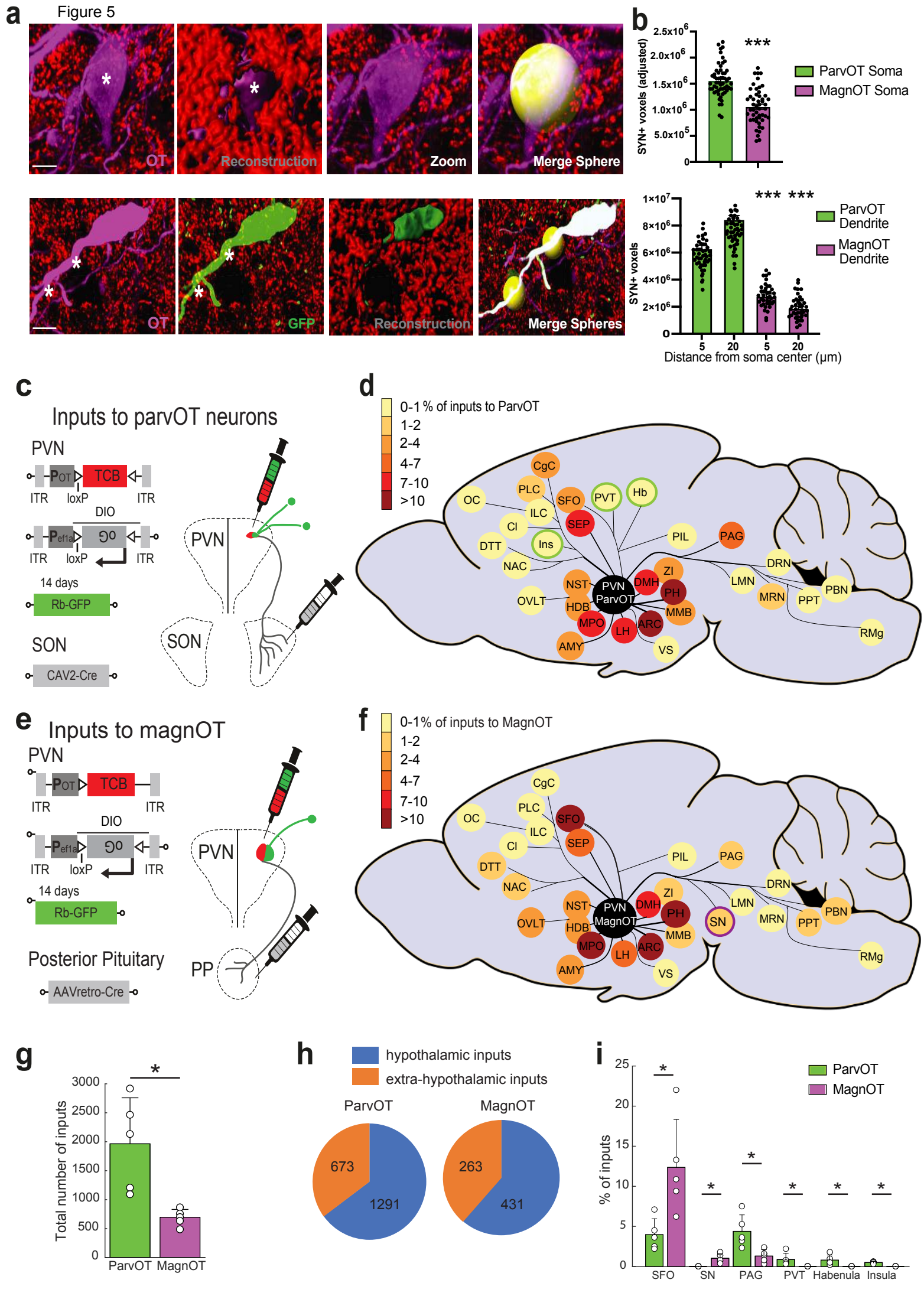
a
Figure 5
OT
Reconstruction
Zoom
Merge Sphere
OT
GFP
Reconstruction
Merge Spheres
b
SYN+ voxels (adjusted)
2.5x10^6
2.0x10^6
1.5x10^6
1.0x10^6
5.0x10^5
0
***
ParvOT Soma
MagnOT Soma
SYN+ voxels
1x10^7
8x10^6
6x10^6
4x10^6
2x10^6
0
*** ***
ParvOT Dendrite
MagnOT Dendrite
5
20
5
20
Distance from soma center (µm)
c
Inputs to parvOT neurons
PVN
POT
TCB
ITR
loxP
ITR
DIO
Pef1a
G
ITR
loxP
ITR
14 days
Rb-GFP
SON
CAV2-Cre
PVN
SON
d
0-1 % of inputs to ParvOT
1-2
2-4
4-7
7-10
>10
CgC
PLC
OC
SFO
PVT
Hb
ILC
SEP
Cl
Ins
DTT
NAC
PIL
PAG
ZI
DMH
NST
PVN
ParvOT
PH
OVLT
HDB
MMB
MPO
LH
ARC
AMY
VS
DRN
LMN
MRN
PPT
PBN
RMg
e
Inputs to magnOT
PVN
POT
TCB
ITR
ITR
DIO
Pef1a
G
ITR
loxP
ITR
14 days
Rb-GFP
Posterior Pituitary
AAVretro-Cre
PVN
PP
f
0-1% of inputs to MagnOT
1-2
2-4
4-7
7-10
>10
CgC
PLC
OC
SFO
ILC
SEP
Cl
DTT
NAC
PIL
PAG
ZI
DMH
NST
PVN
MagnOT
PH
SN
OVLT
HDB
MMB
MPO
LH
ARC
AMY
VS
DRN
LMN
MRN
PPT
PBN
RMg
g
Total number of inputs
3000
2500
2000
1500
1000
500
0
*
ParvOT
MagnOT
h
hypothalamic inputs
extra-hypothalamic inputs
ParvOT
MagnOT
673
1291
263
431
i
% of inputs
25
20
15
10
5
0
*
*
*
*
*
*
ParvOT
MagnOT
SFO
SN
PAG
PVT
Habenula
Insula

Figure 6

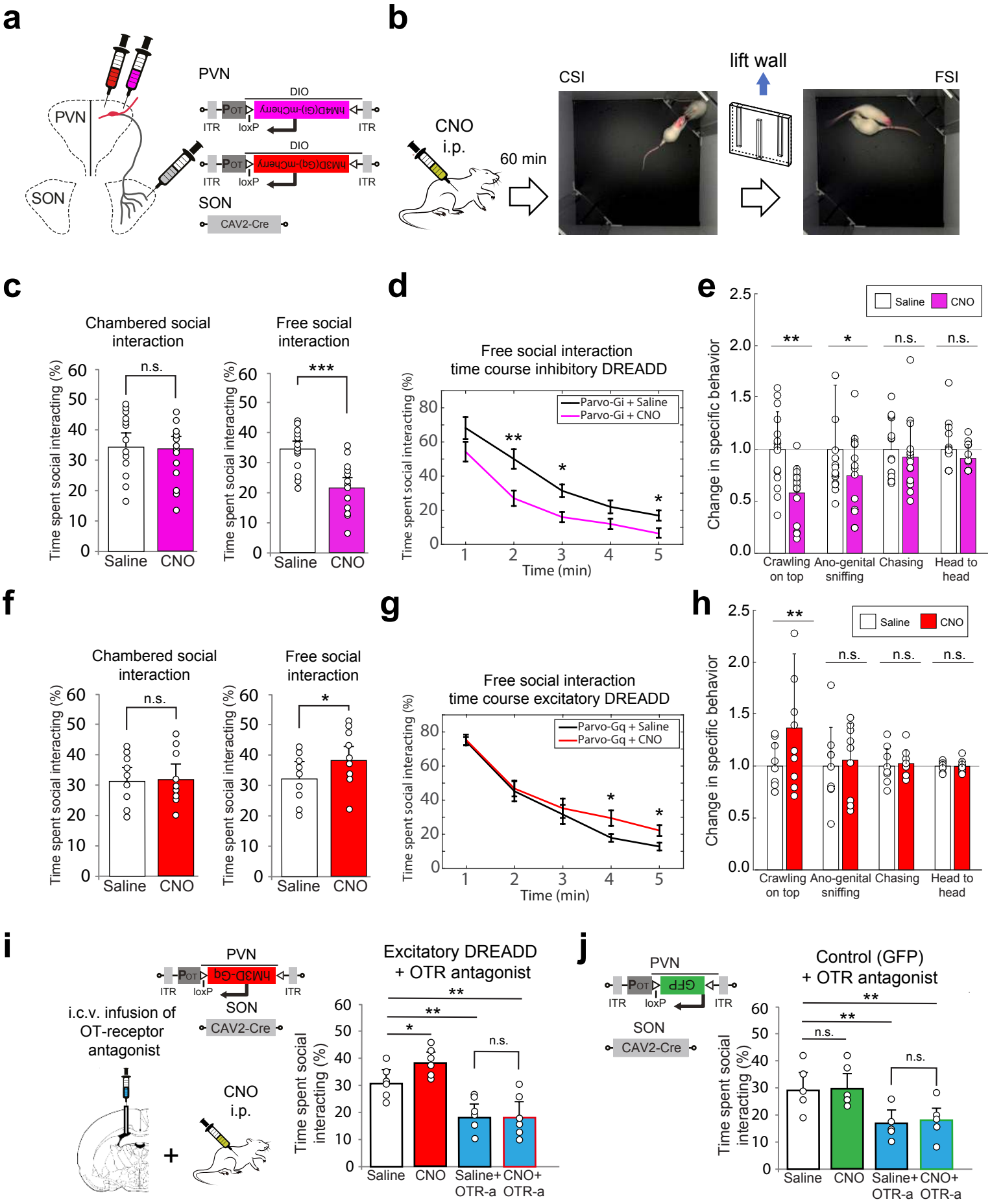
a
PVN
SON
DIO
hM4D(Gi)-mCherry
ITR
loxP
ITR
DIO
hM3D(Gq)-mCherry
ITR
loxP
ITR
SON
CAV2-Cre
b
CNO
i.p.
60 min
CSI
lift wall
FSI
c
Chambered social interaction
Free social interaction
Time spent social interacting (%)
n.s.
***
Saline
CNO
d
Free social interaction
time course inhibitory DREADD
Parvo-Gi + Saline
Parvo-Gi + CNO
Time spent social interacting (%)
Time (min)
e
Saline
CNO
Change in specific behavior
Crawling on top
Ano-genital sniffing
Chasing
Head to head
f
Chambered social interaction
Free social interaction
n.s.
*
g
Free social interaction
time course excitatory DREADD
Parvo-Gq + Saline
Parvo-Gq + CNO
h
i
PVN
hM3D-Gq
SON
CAV2-Cre
i.c.v. infusion of OT-receptor antagonist
CNO
i.p.
Excitatory DREADD
+ OTR antagonist
Saline
CNO
Saline+ OTR-a
CNO+ OTR-a
j
PVN
GFP
SON
CAV2-Cre
Control (GFP)
+ OTR antagonist

a

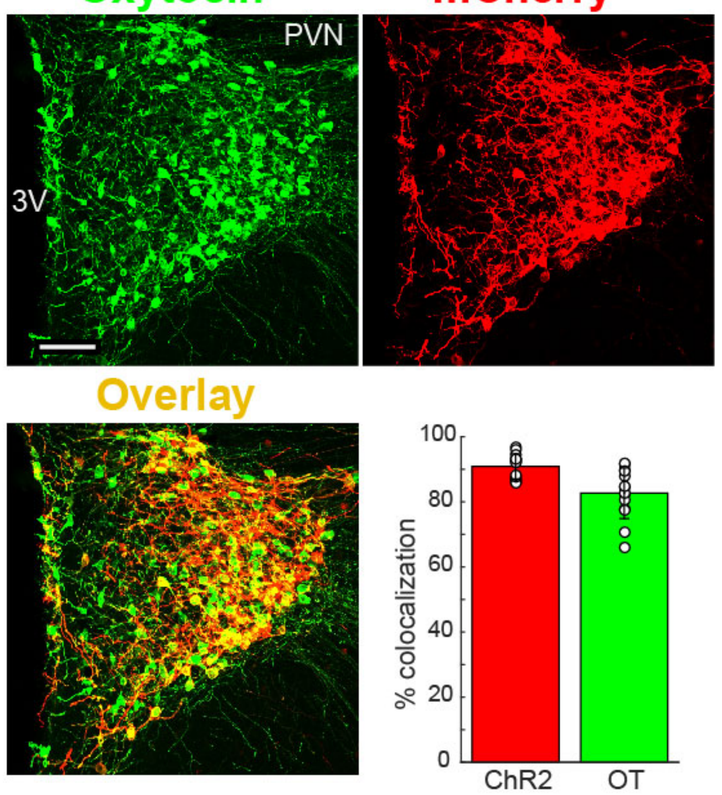

b

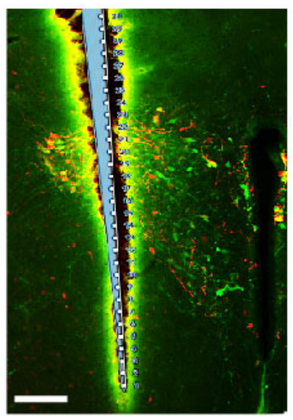

c

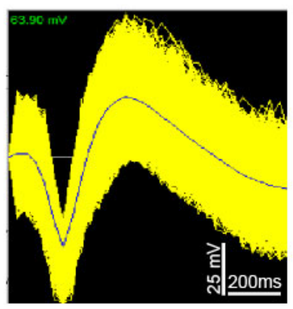

d

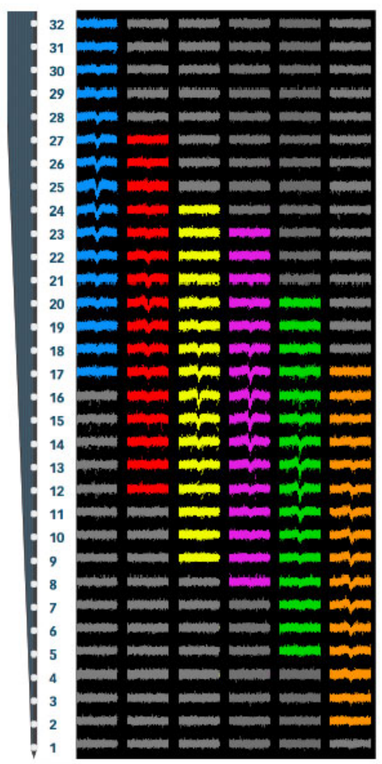

e

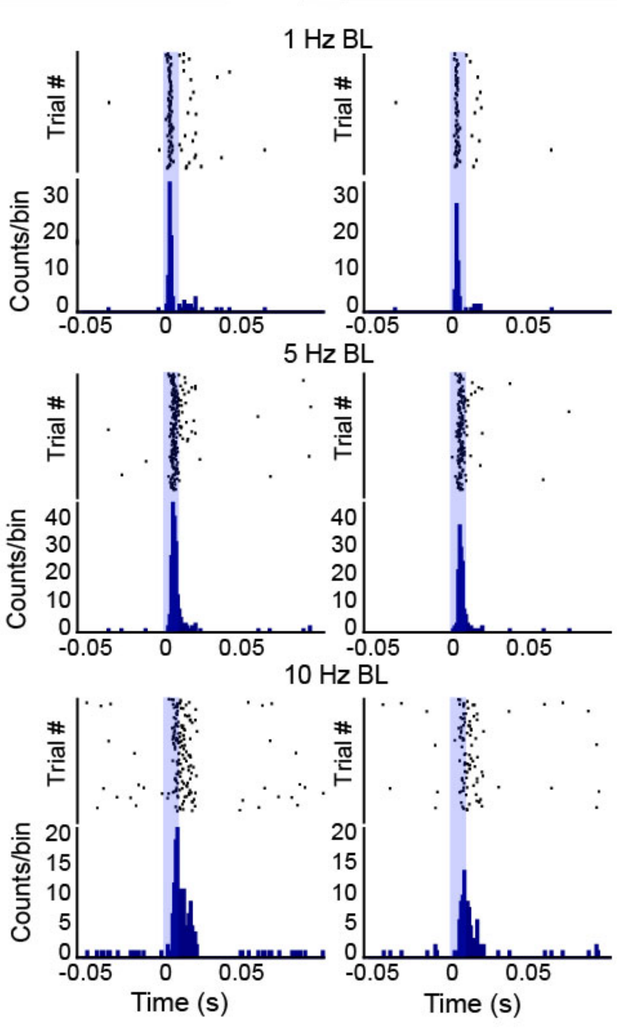

f

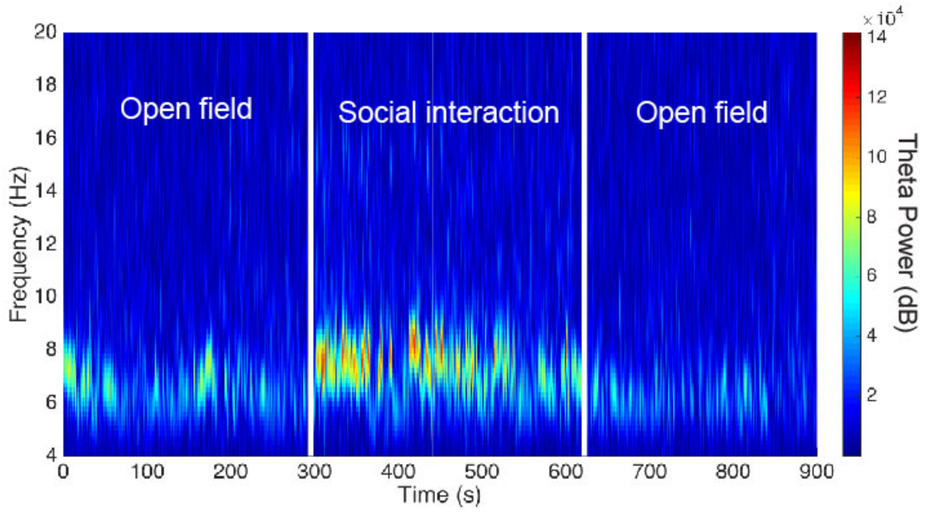

g

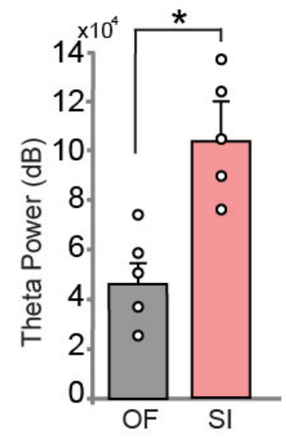

h

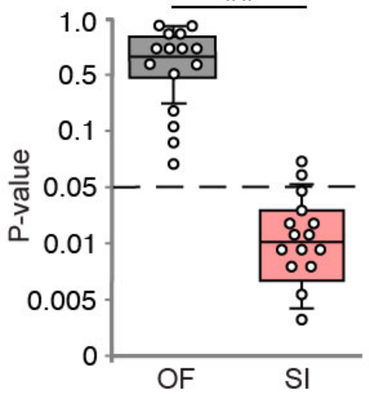

i

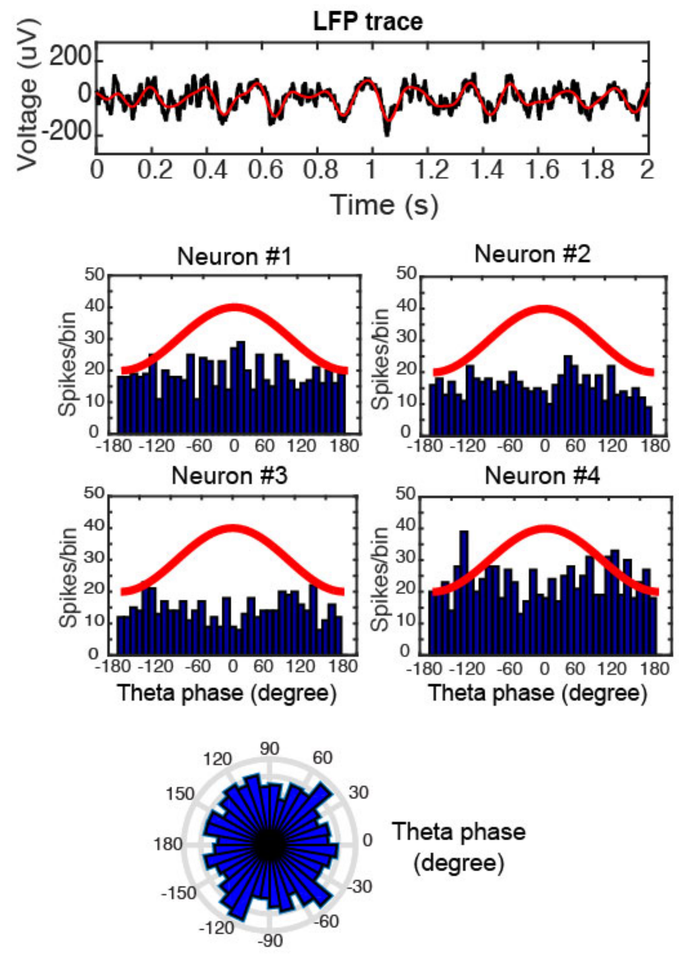

j

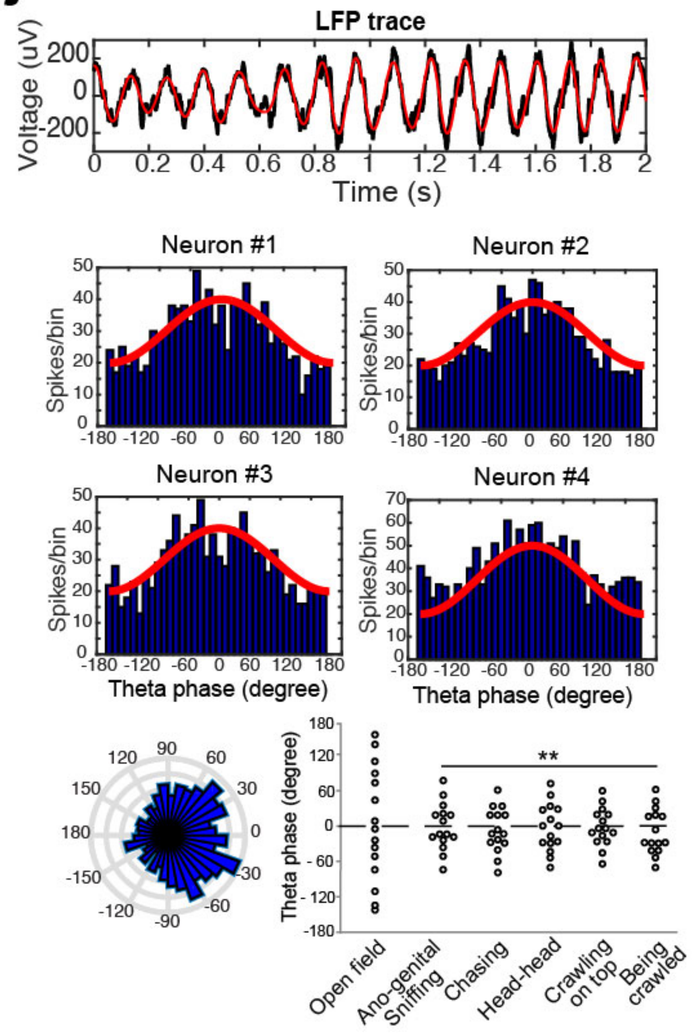

k

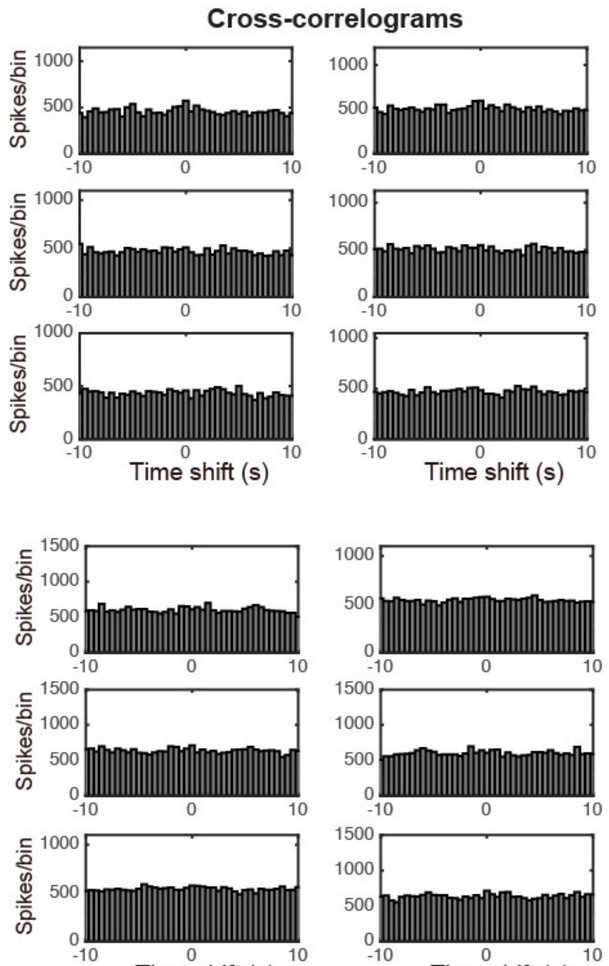

l

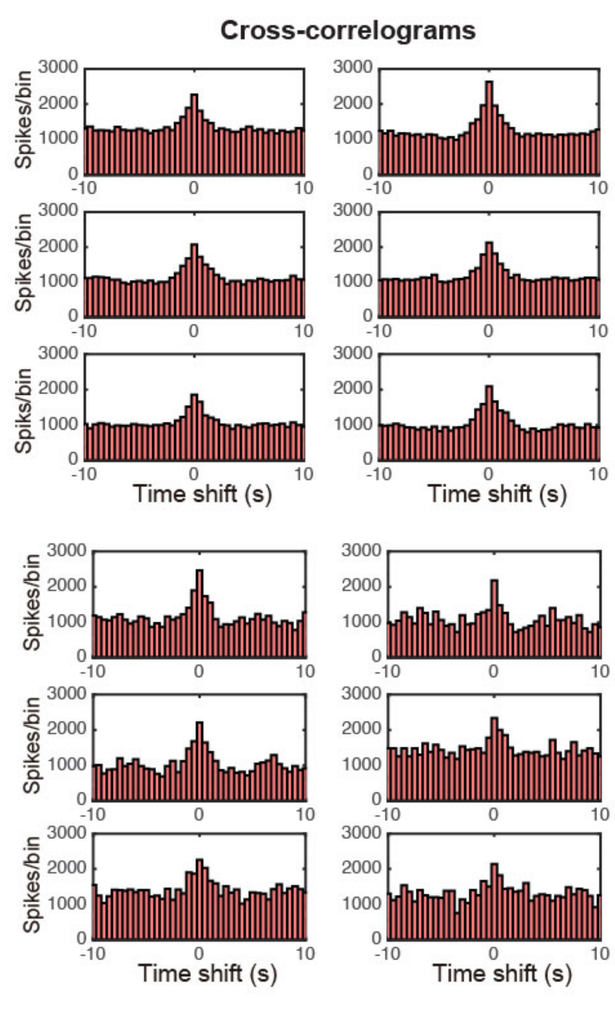

m

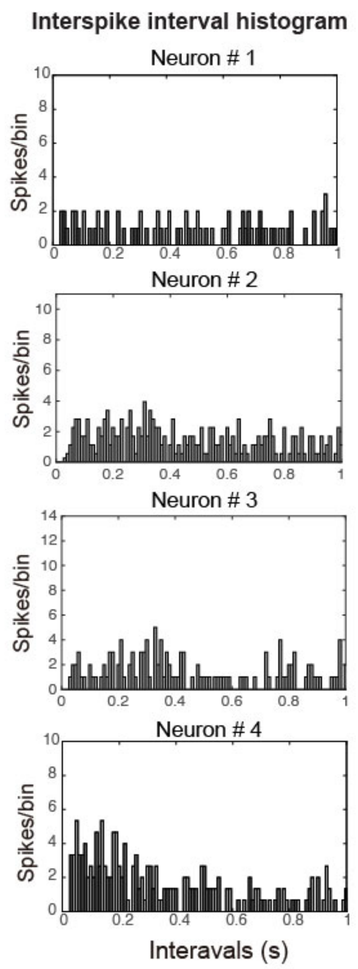

n

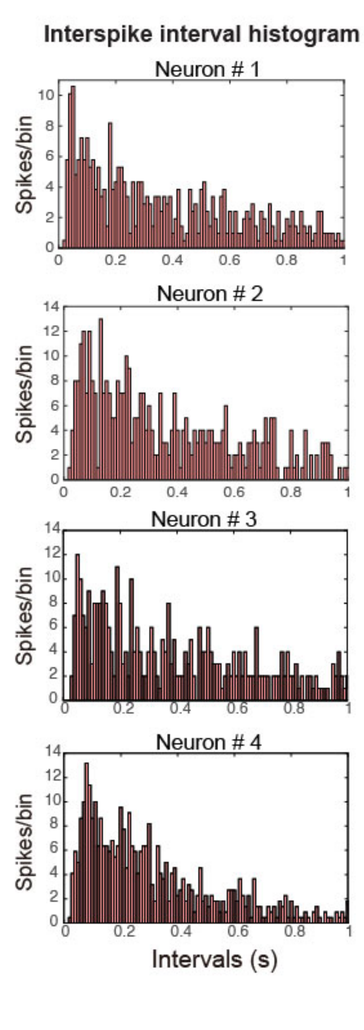

a
Ano-genital sniffing
Trial #
Firing rate (Hz)
Time (s)
n.s.
Baseline
Ano-genital sniffing
After
b
Chasing
Trial #
Firing rate (Hz)
Time (s)
n.s.
Baseline
Chasing
After
c
Head-head
Trial #
Firing rate (Hz)
Time (s)
n.s.
Baseline
Head-head
After
d
PVN OT neurons (Open Field)
Frequency (Hz)
Time (s)
e
PVN
OT neurons
PVN
non-OTneurons
Proximity
Non-proximity
r = - 0.3
r = - 0.04
Firing rate (Hz)
Rats' distance (cm)
f
PVN non-OT neurons
Open field
Not interacting
Socially interacting
n.s.
Avg. firing rate (Hz)
OF
not SI
SI
Index of dispersion
Avg. pairwise correlation
g
PVN non-OT neurons (Social Interaction)
Frequency (Hz)
Time (s)
h
Measured spike pattern
Theoretical
oxytocin secretion model
$f(x)$
Predicted OT secretion rate
MagnOT neuron
Pituitary
i
Open Field
Average firing rate 1.0 Hz
Chambered SI
Average firing rate 1.4 Hz
Free SI
Average firing rate 2.9 Hz
OT spike raster
j
Theoretical oxytocin secretion model
Predicted OT secretion rate (fg/s)*10
Time (s)
**
**
OF
CSI
FSI

a

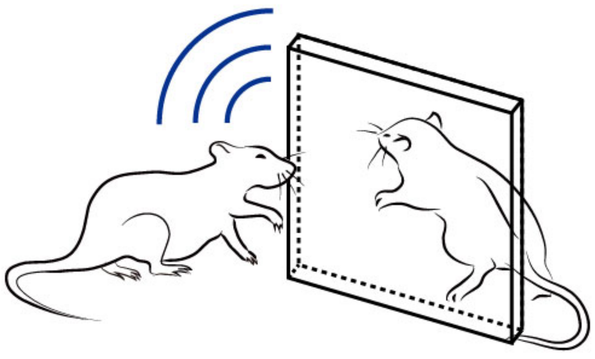

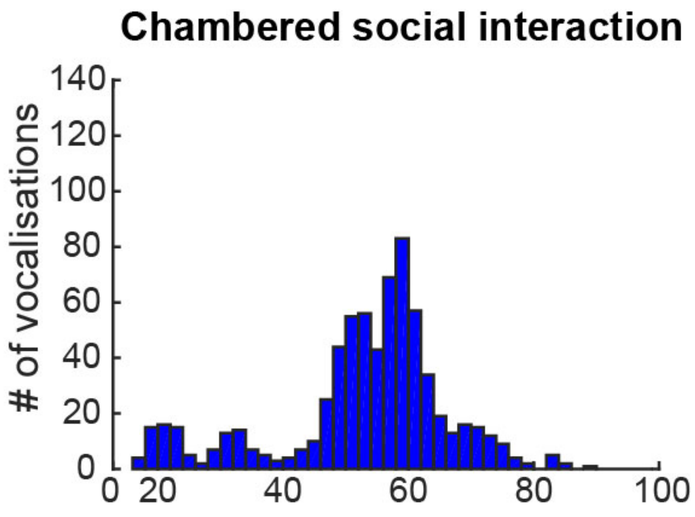
Chambered social interaction
# of vocalisations
0
20
40
60
80
100
120
140
0
20
40
60
80
100

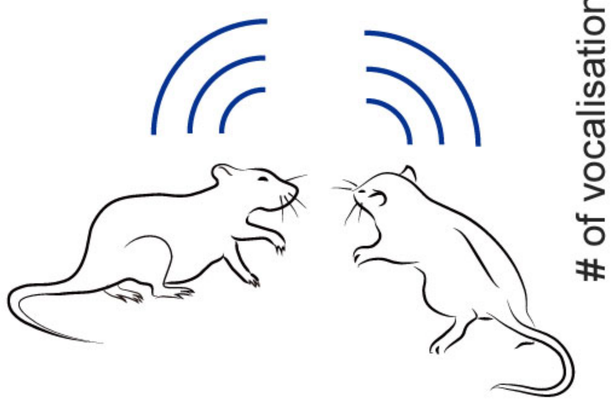

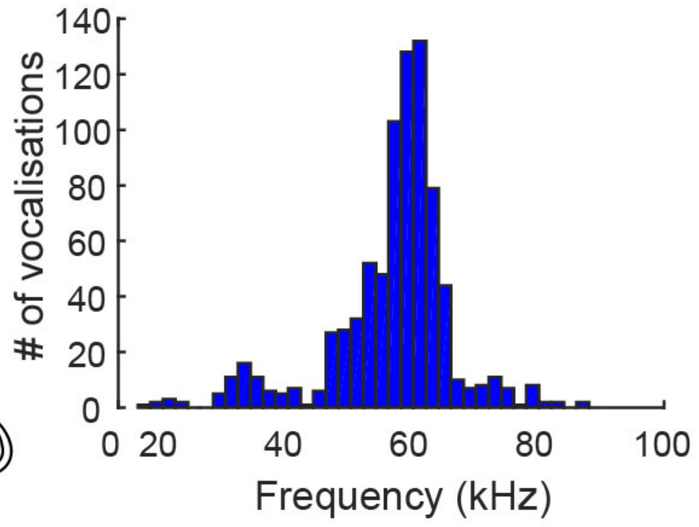
Free social interaction
# of vocalisations
0
20
40
60
80
100
120
140
0
20
40
60
80
100
Frequency (kHz)

b

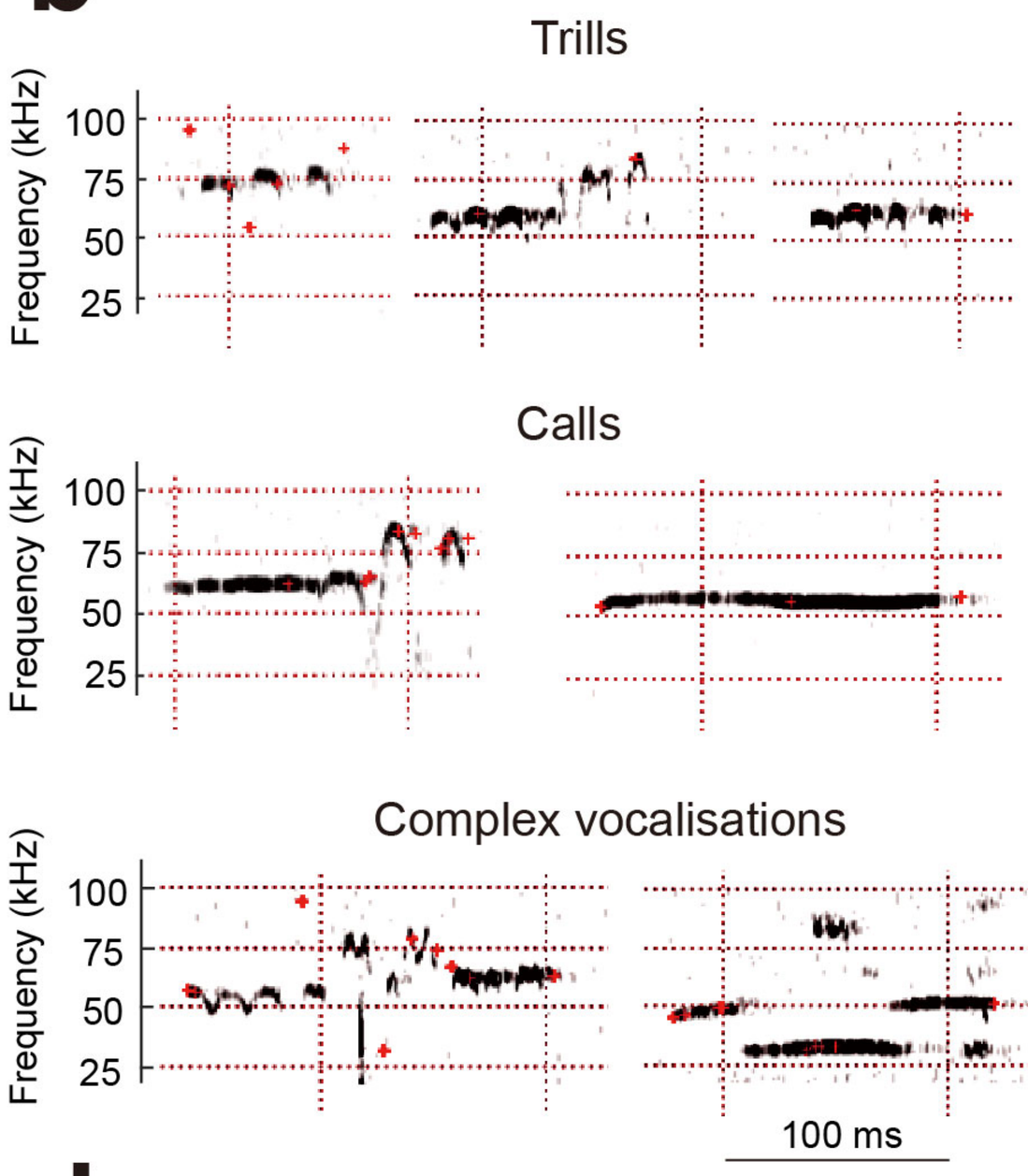
Trills
Frequency (kHz)
100
75
50
25
Calls
Frequency (kHz)
100
75
50
25
Complex vocalisations
Frequency (kHz)
100
75
50
25
100 ms

c

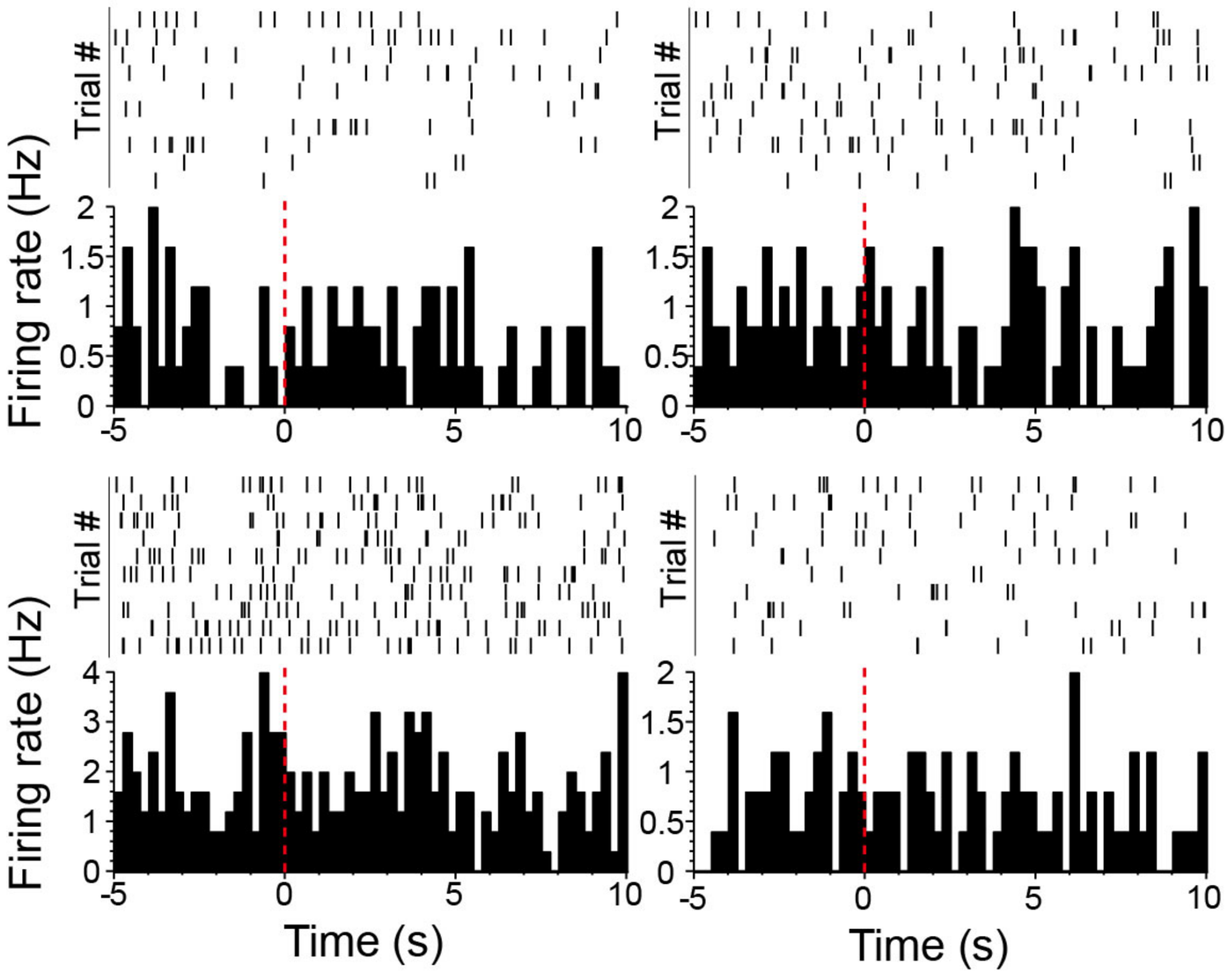
Trial #
Trial #
Trial #
Trial #
Firing rate (Hz)
Firing rate (Hz)
Time (s)
Time (s)
-5
0
5
10

d

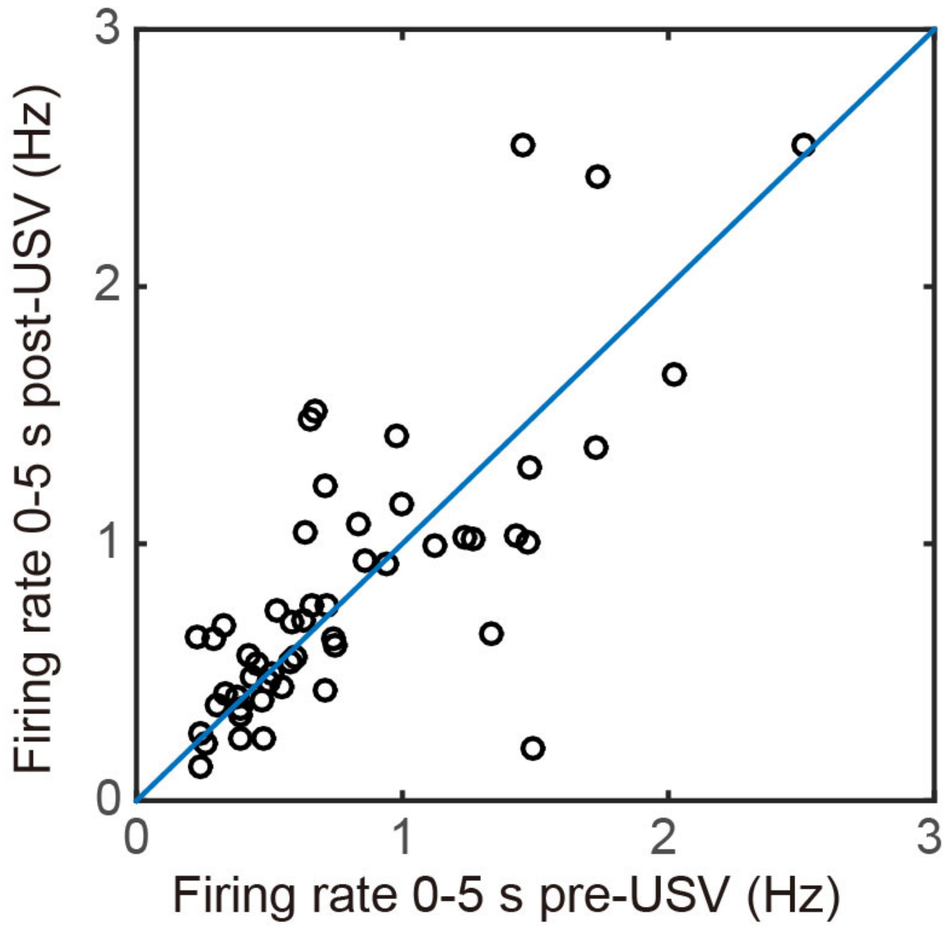
Firing rate 0-5 s post-USV (Hz)
Firing rate 0-5 s pre-USV (Hz)
0
1
2
3

e

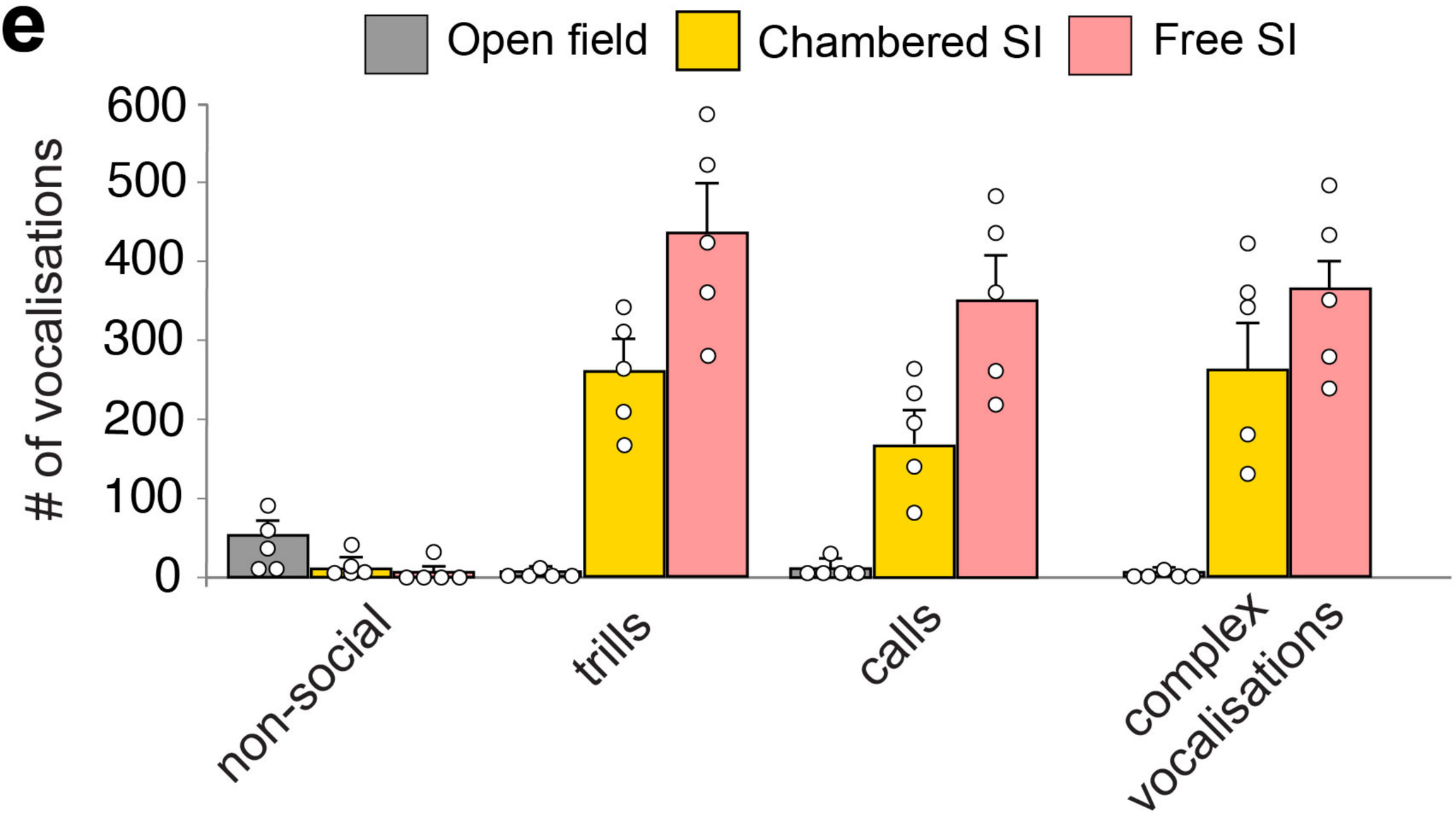
Open field
Chambered SI
Free SI
# of vocalisations
0
100
200
300
400
500
600
non-social
trills
calls
complex vocalisations

a

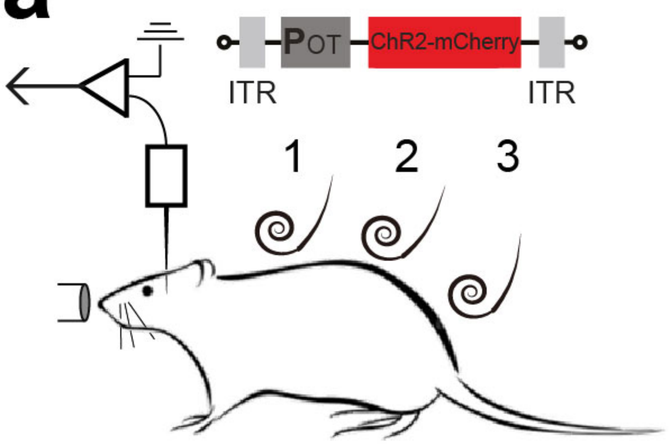

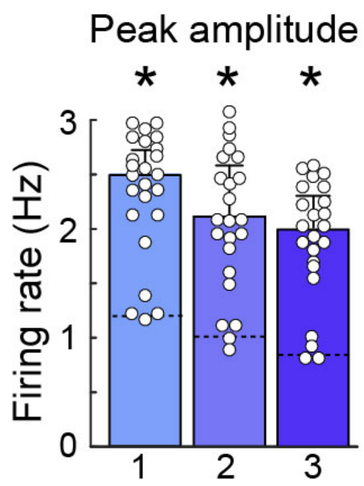

1. Dorsal anterior

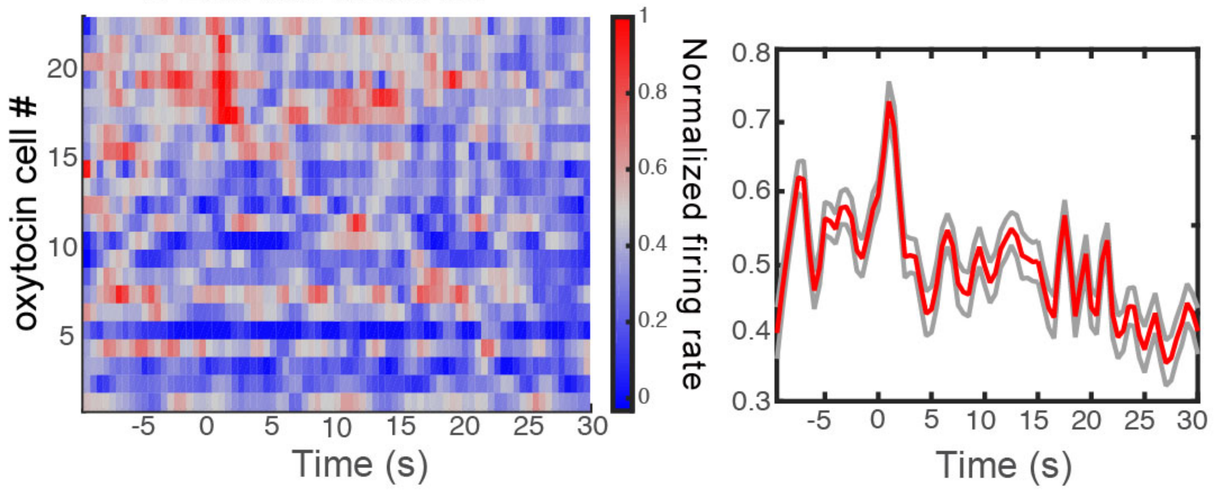

2. Dorsal central

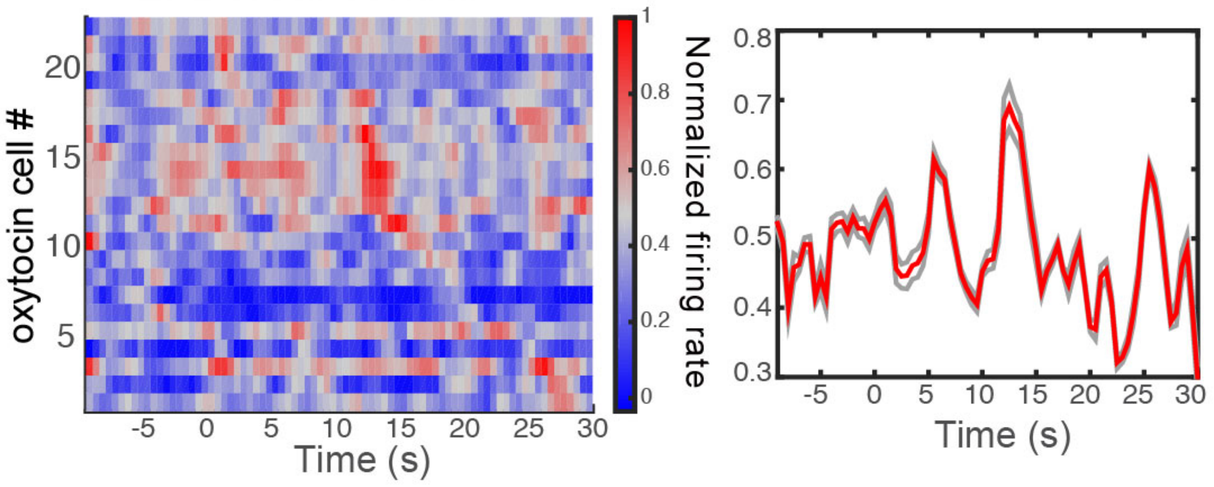

3. Dorsal posterior

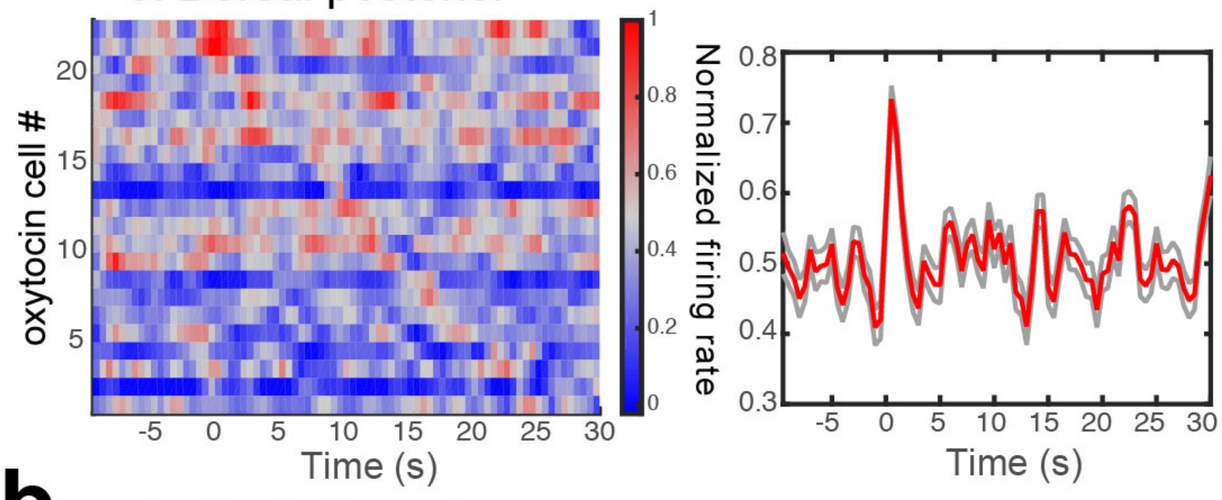

b

1.+2.+3. Dorsal

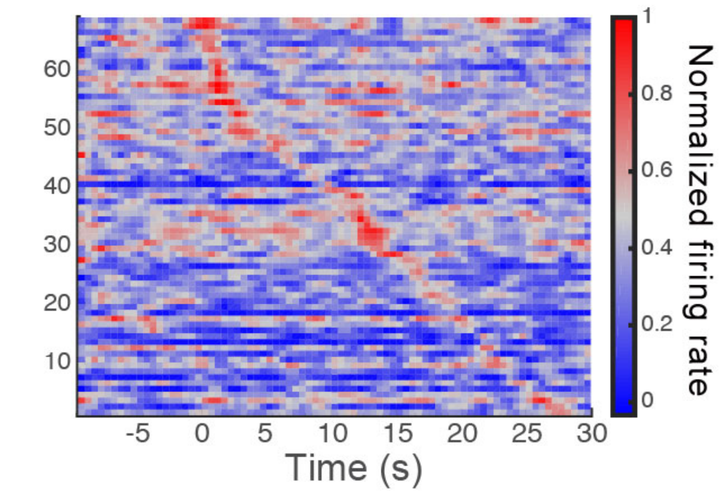

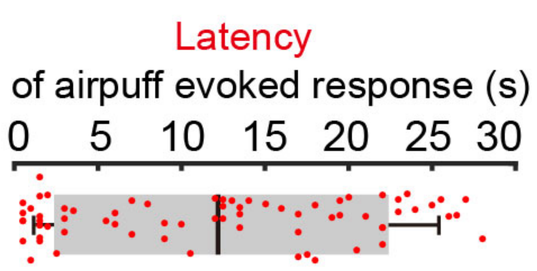

c

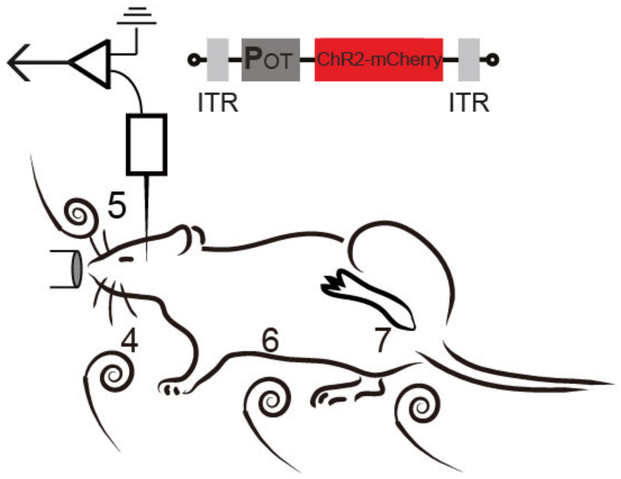

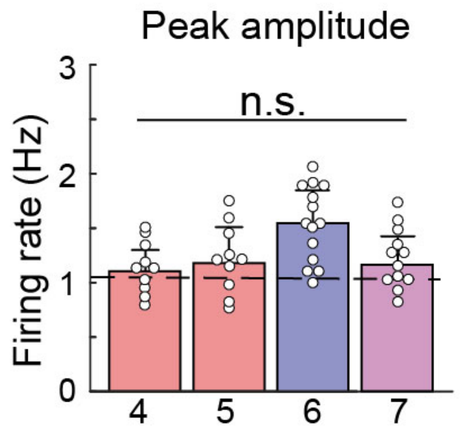

4. Wiskers contralateral

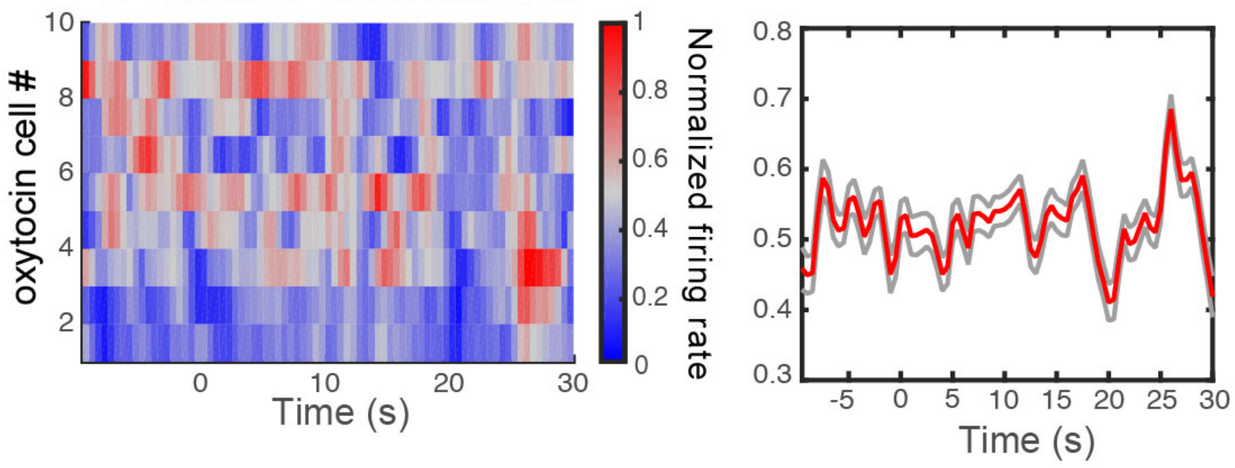

5. Wiskers ipsilateral

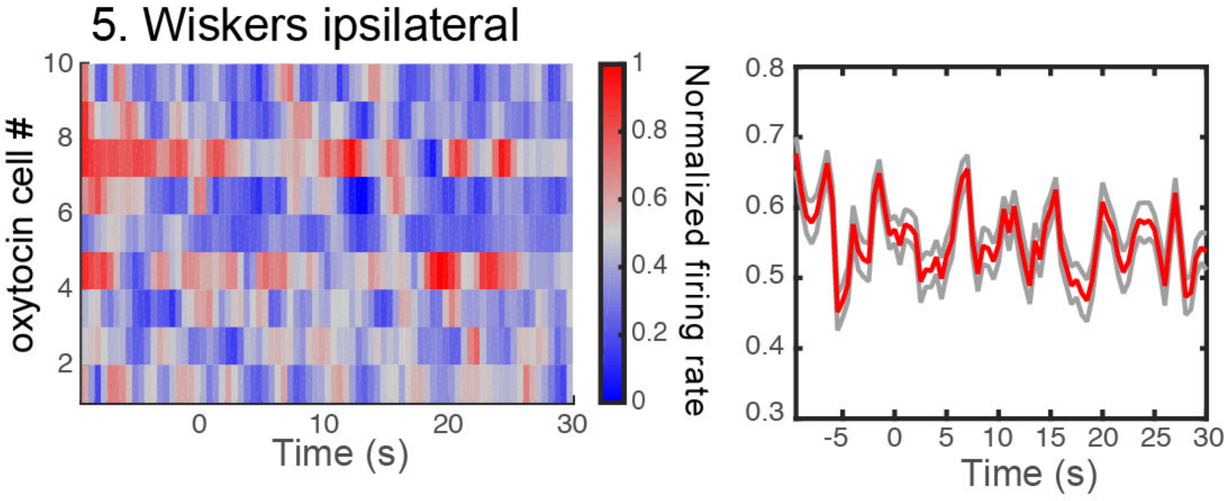

6. Abdomen

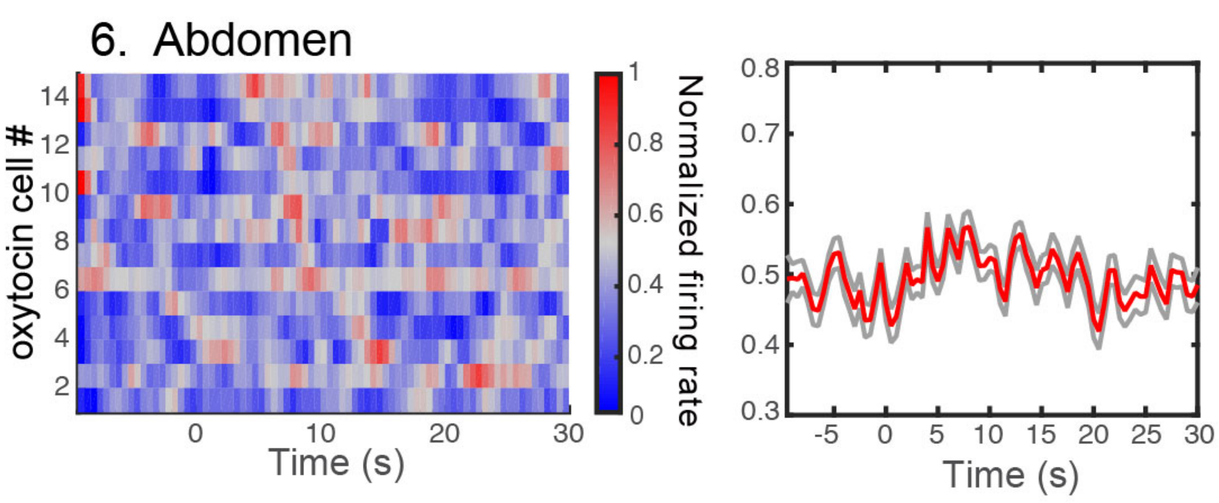

7. Ano-genital area

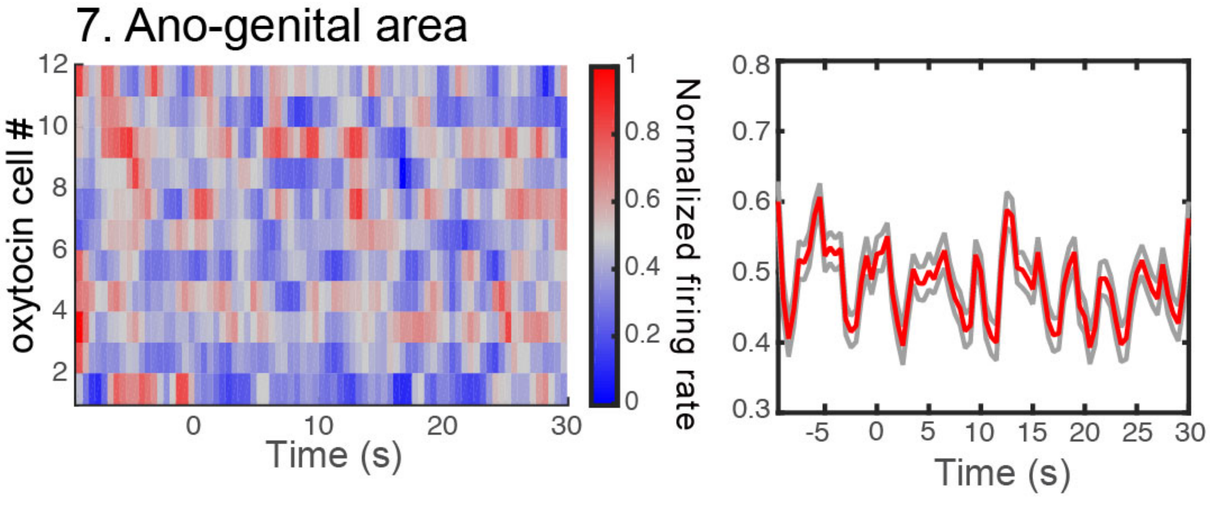

d

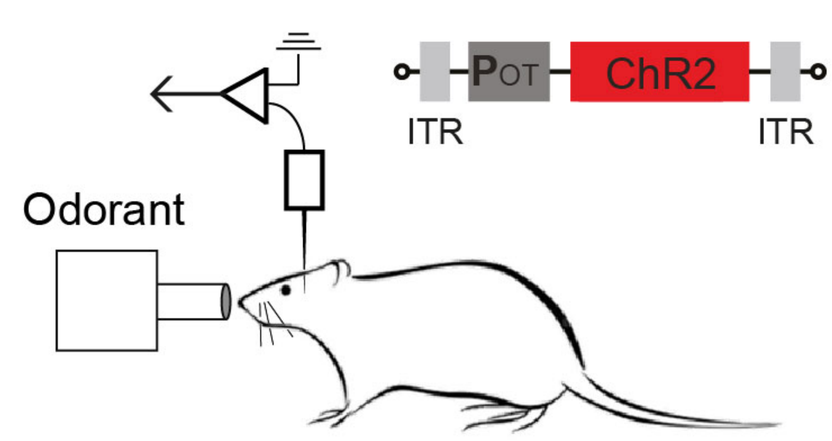

e

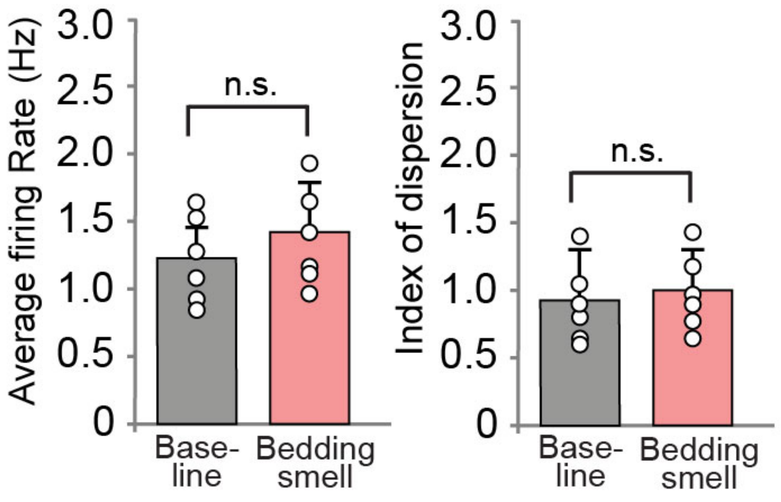

f

a

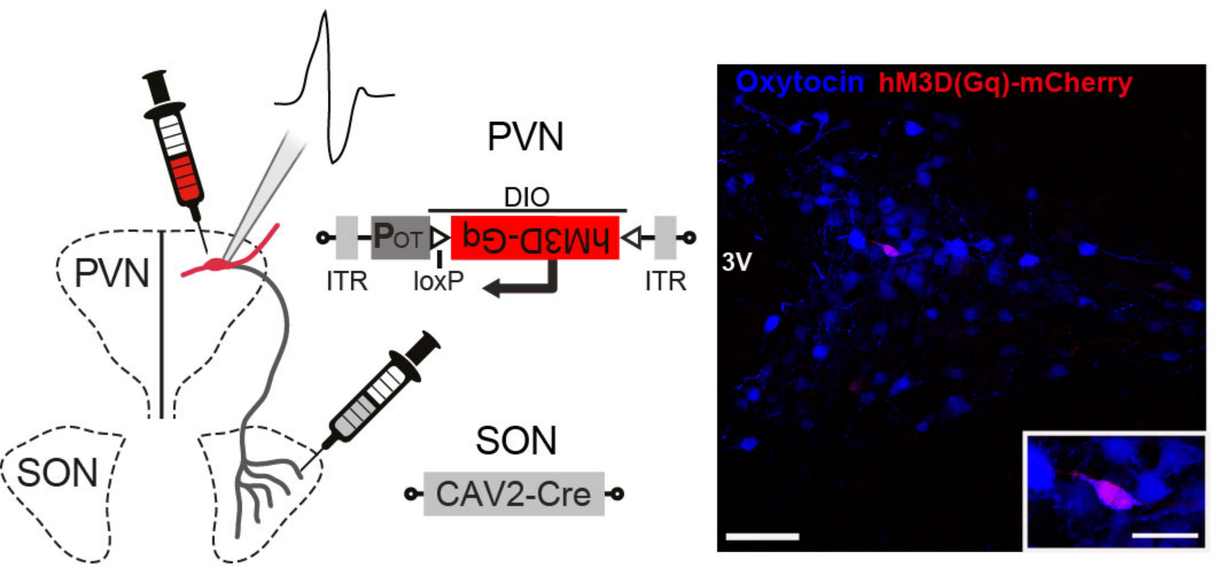

b

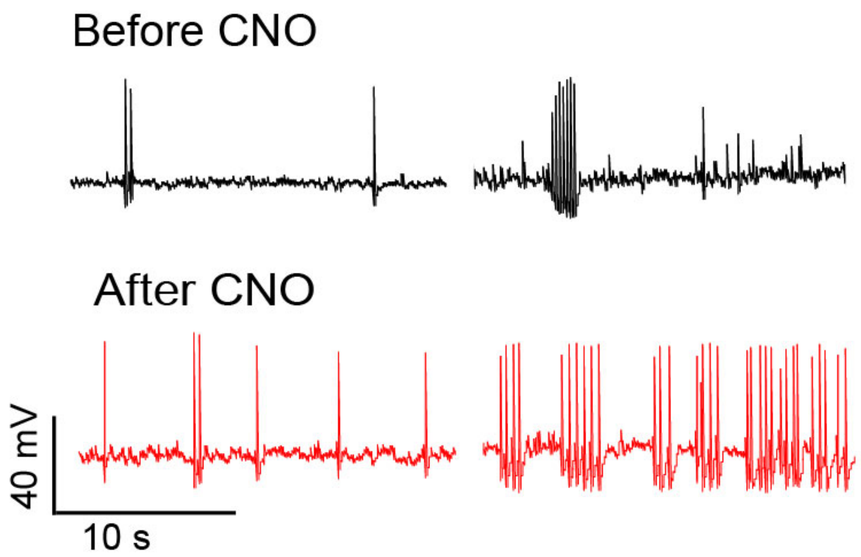

c

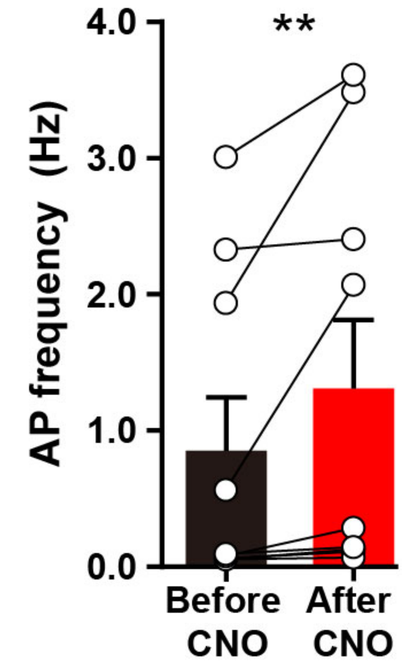

d

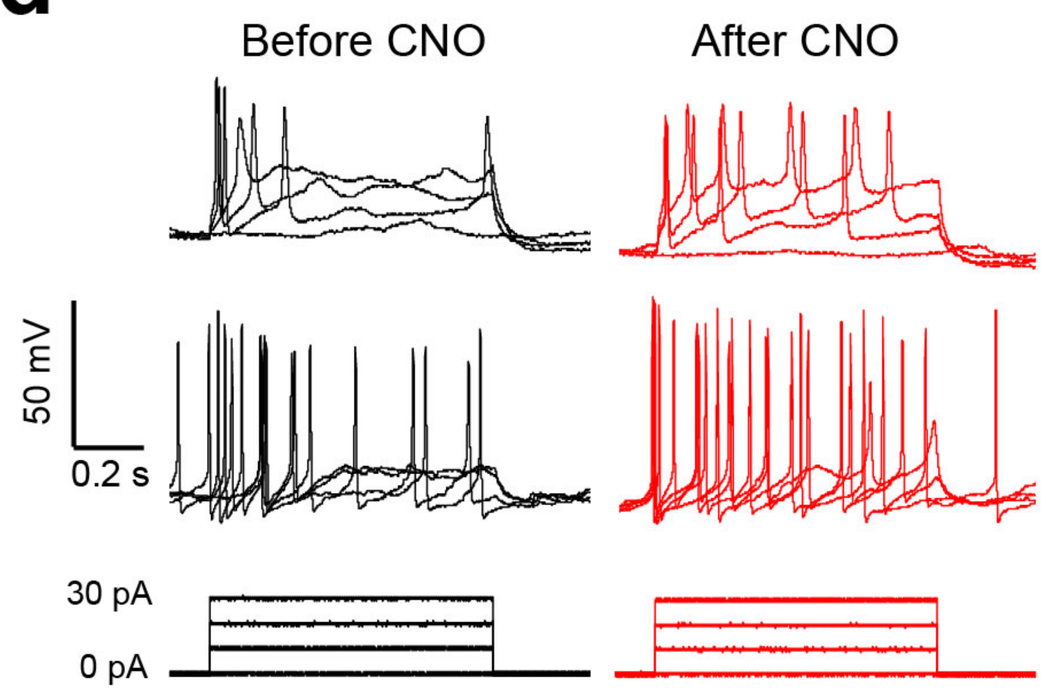

e

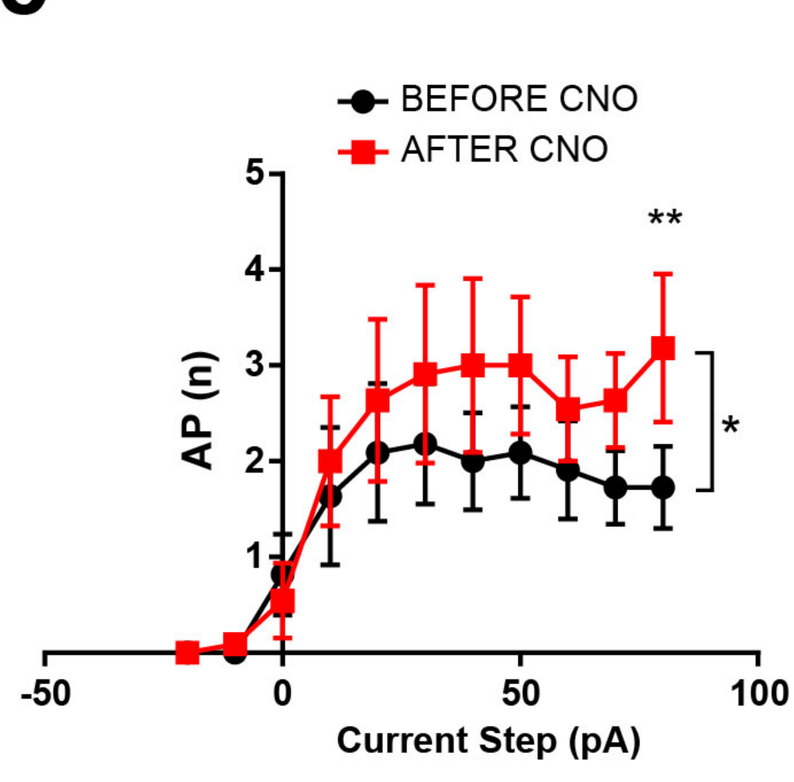

f

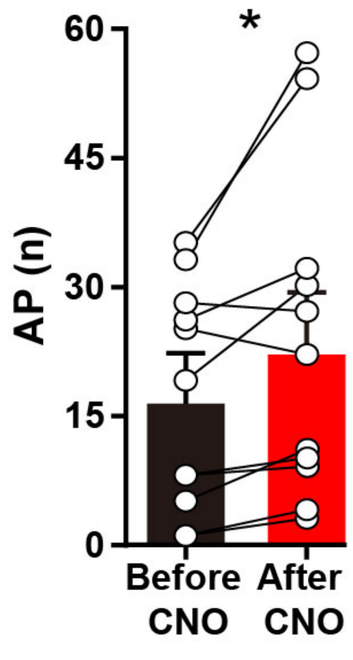

g

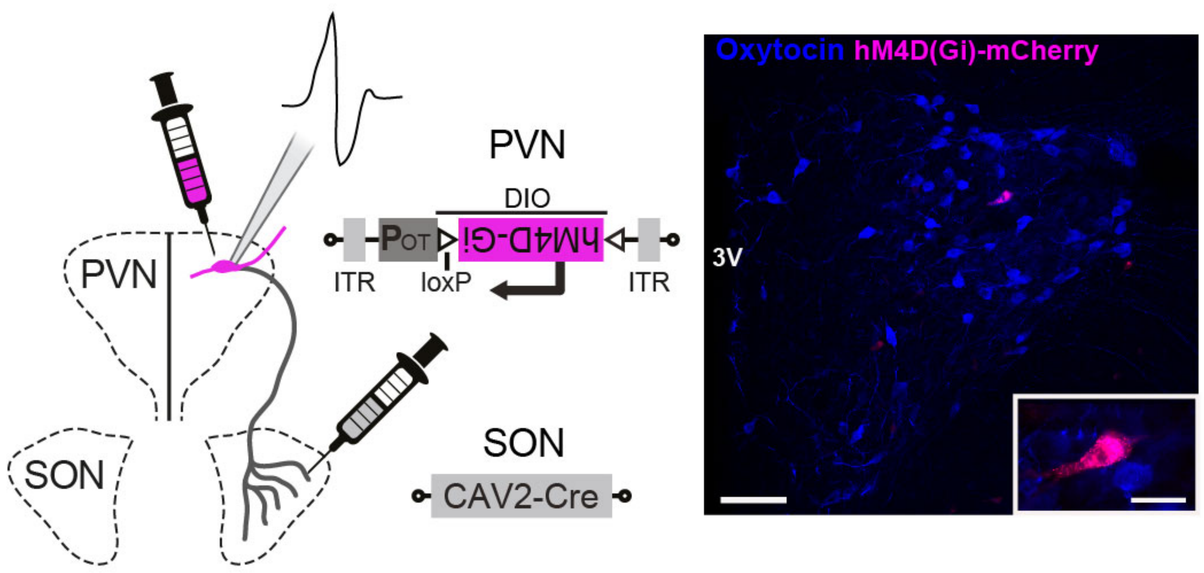

h

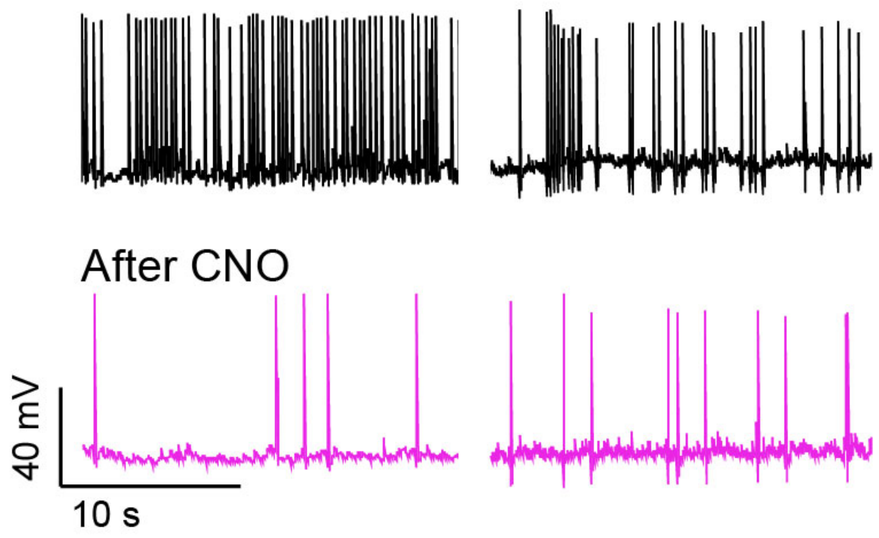

i

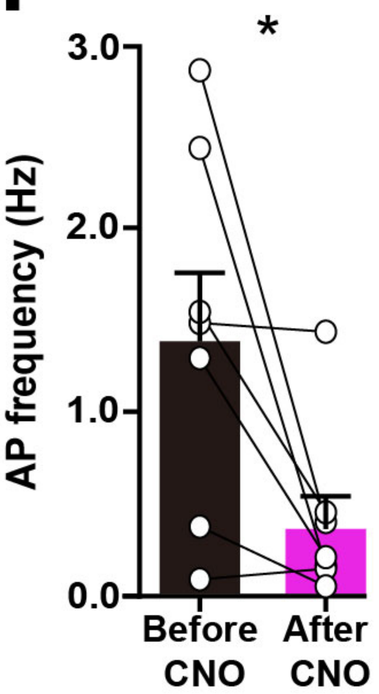

j

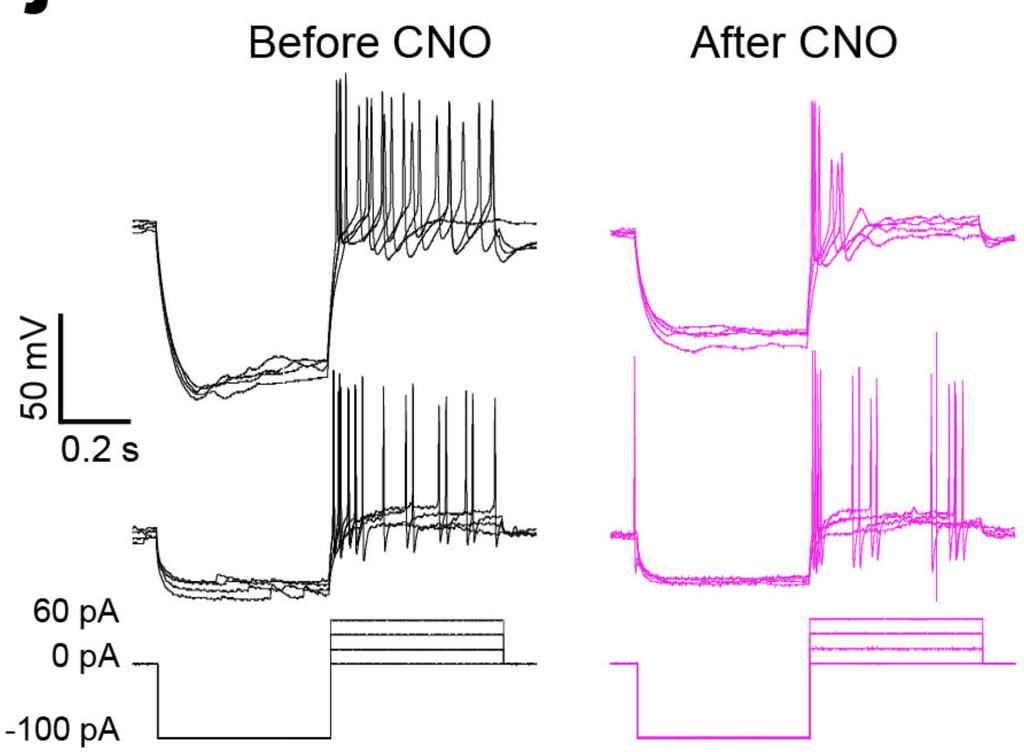

k

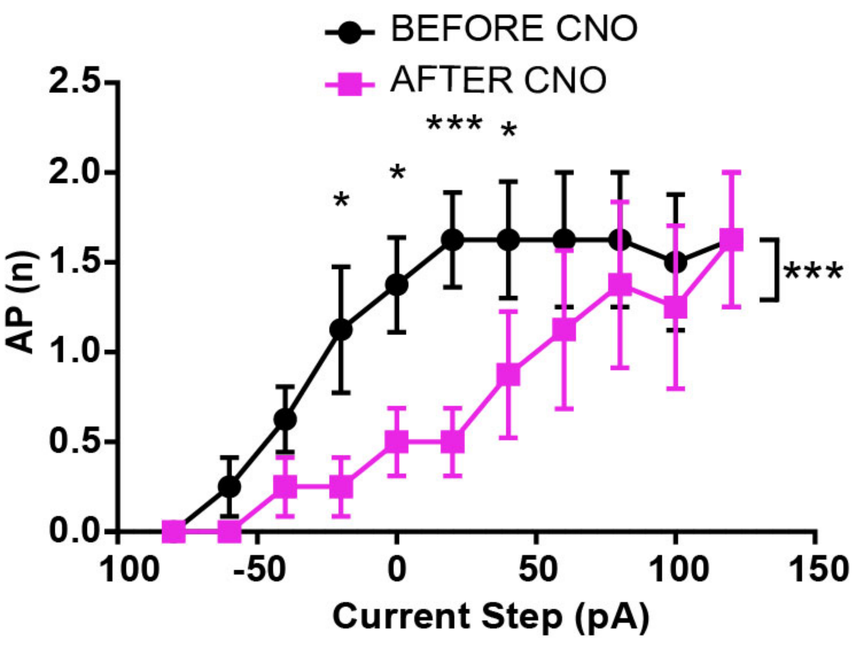

l

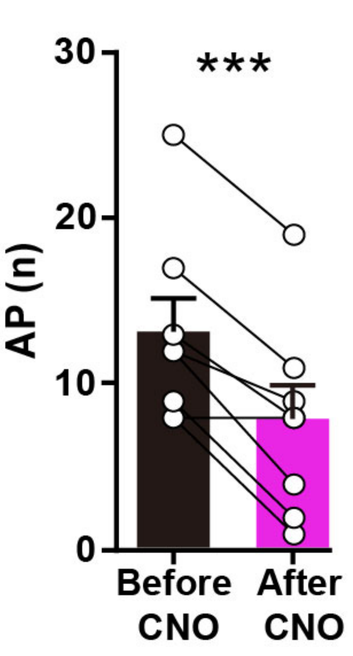

a

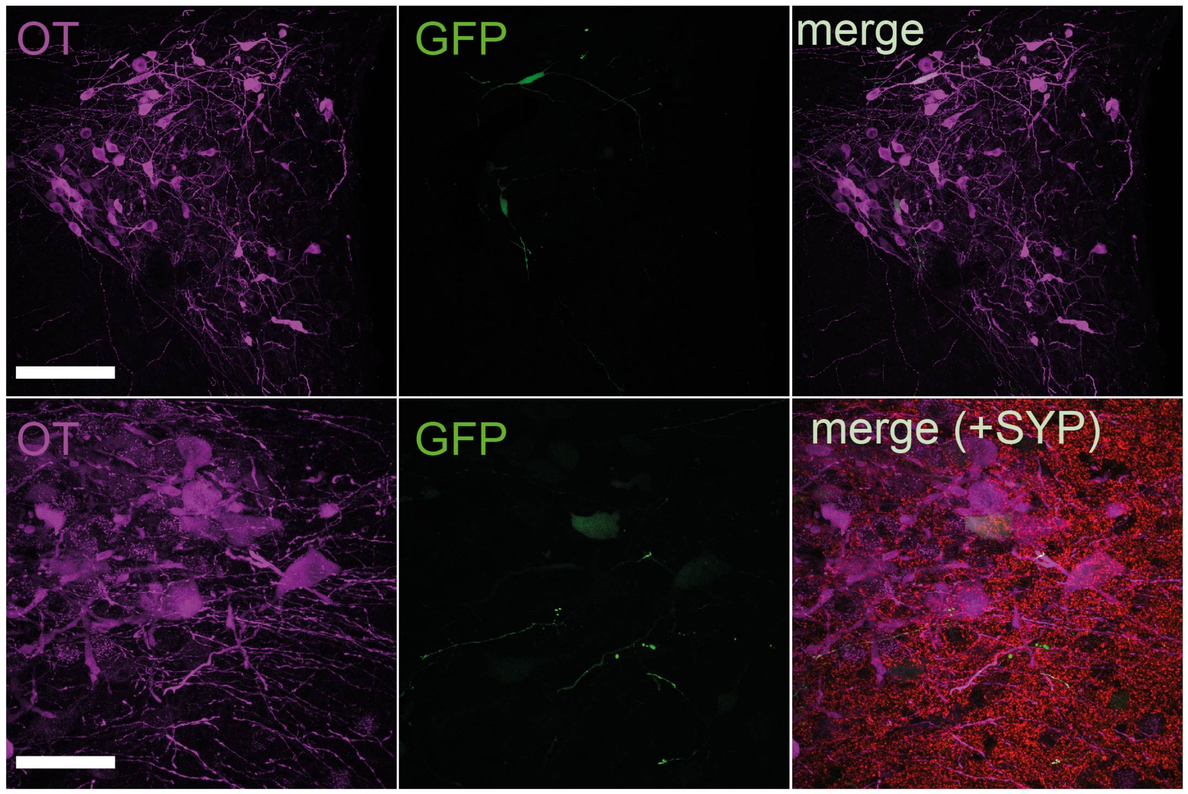
OT
GFP
merge
OT
GFP
merge (+SYP)

b

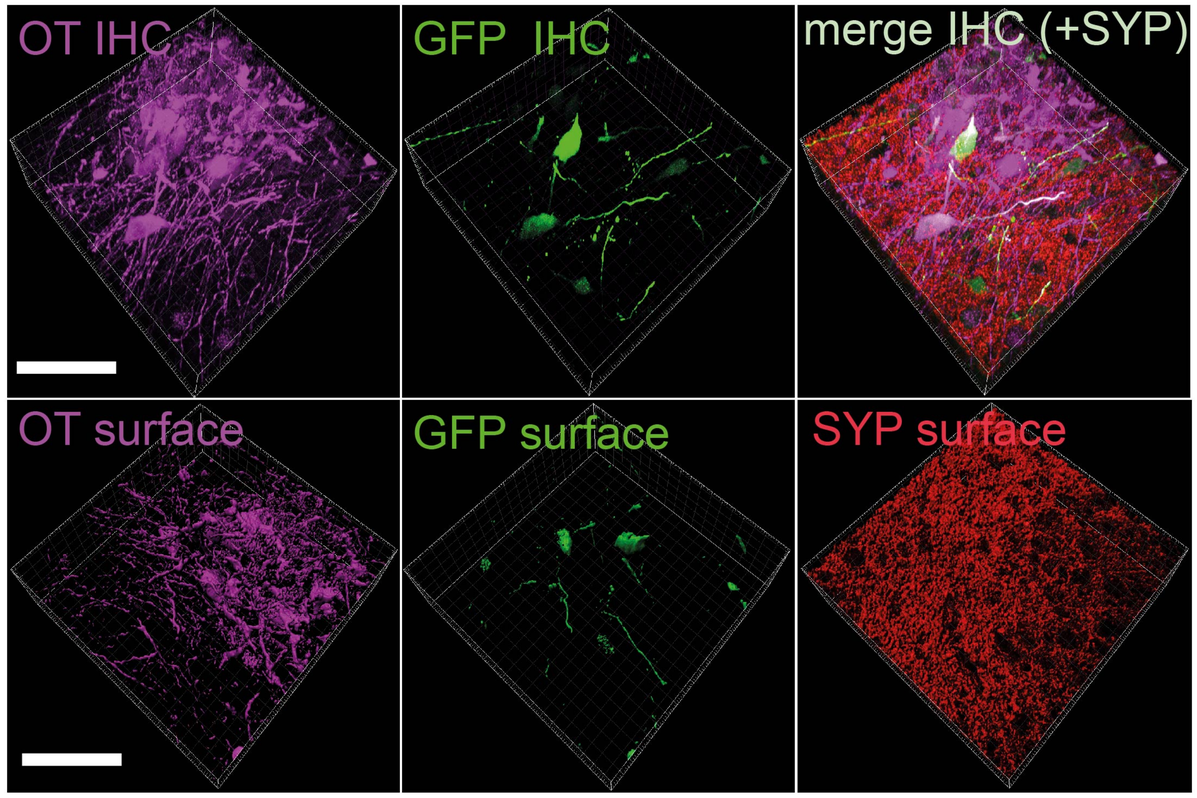
OT IHC
GFP IHC
merge IHC (+SYP)
OT surface
GFP surface
SYP surface

c

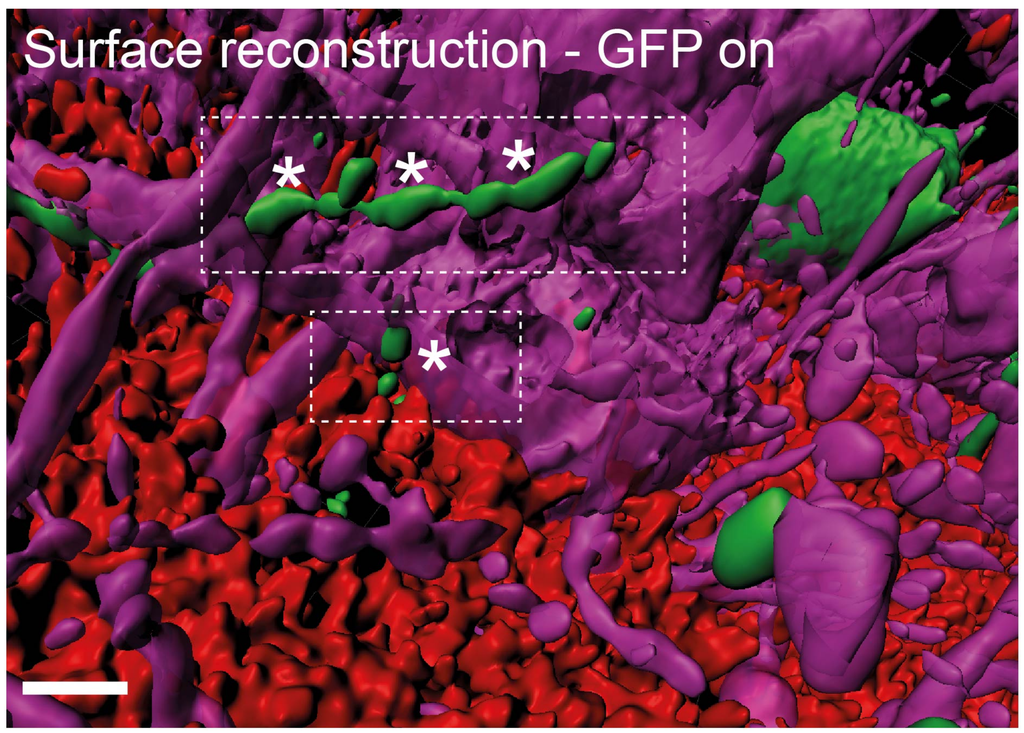
Surface reconstruction - GFP on

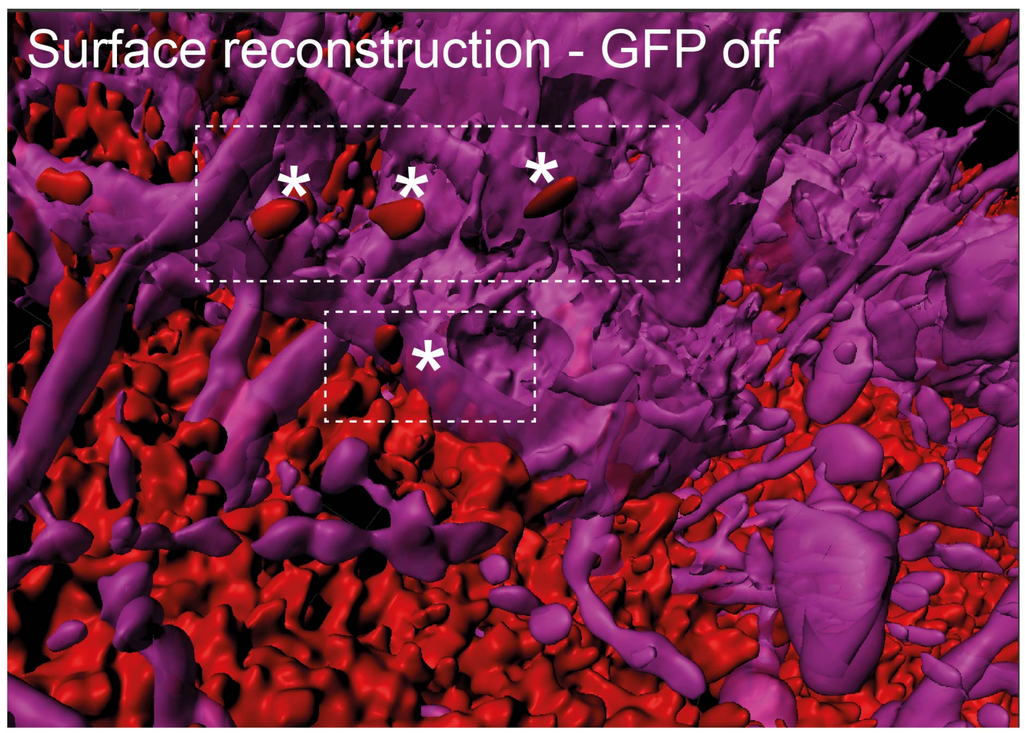
Surface reconstruction - GFP off

d

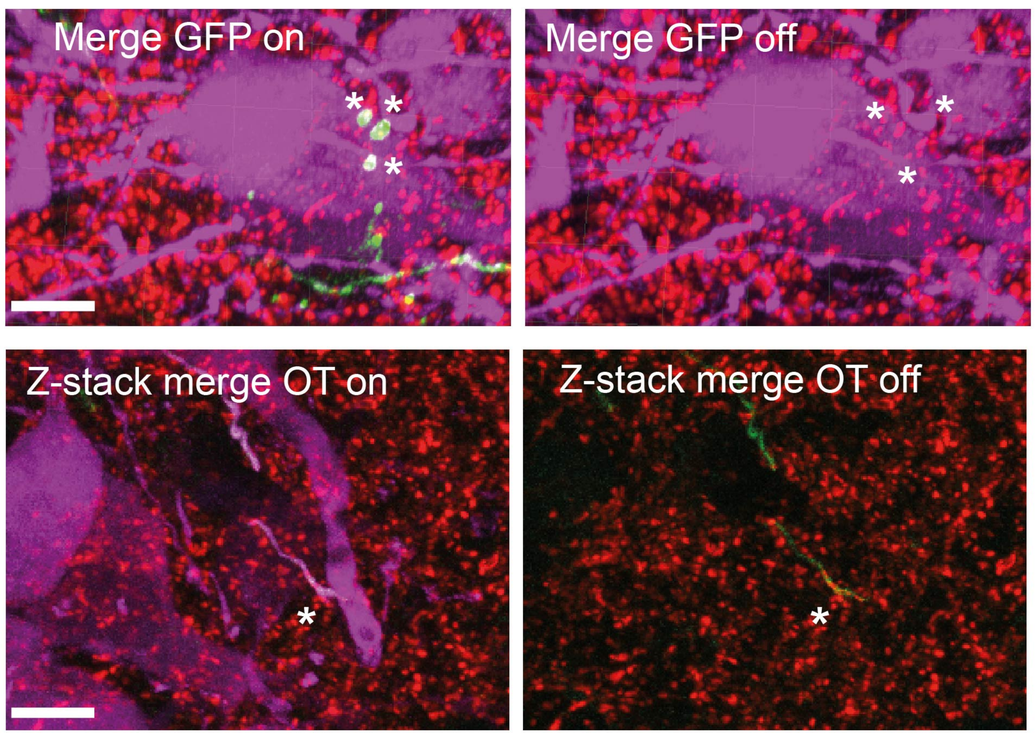
Merge GFP on
Merge GFP off
Z-stack merge OT on
Z-stack merge OT off

e

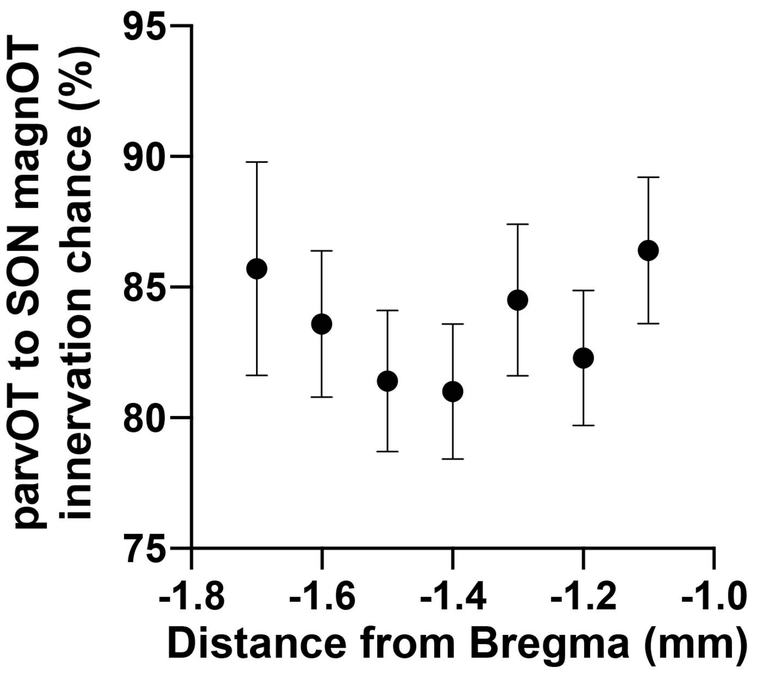
parvOT to SON magnOT innervation chance (%)
95
90
85
80
75
-1.8
-1.6
-1.4
-1.2
-1.0
Distance from Bregma (mm)

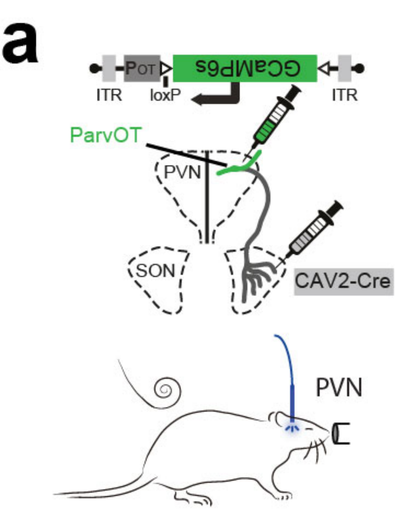
a
POT
GCaMP6s
ITR
loxP
ITR
ParvOT
PVN
SON
CAV2-Cre
PVN

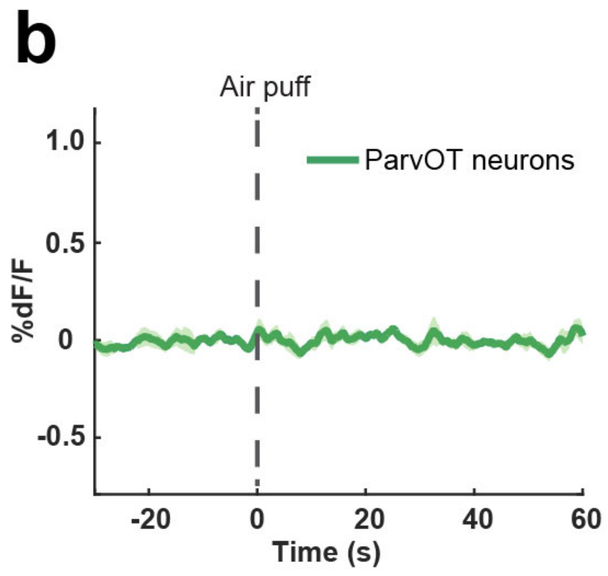
b
Air puff
ParvOT neurons
%dF/F
1.0
0.5
0
-0.5
-20
0
20
40
60
Time (s)

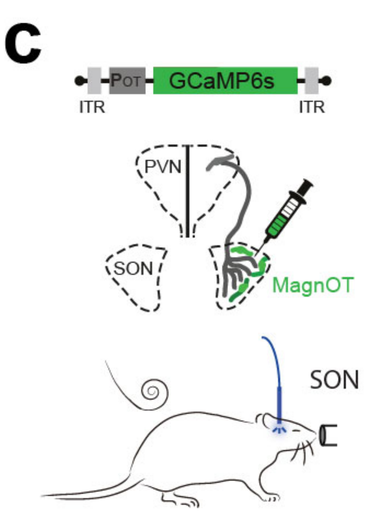
c
POT
GCaMP6s
ITR
ITR
PVN
SON
MagnOT
SON

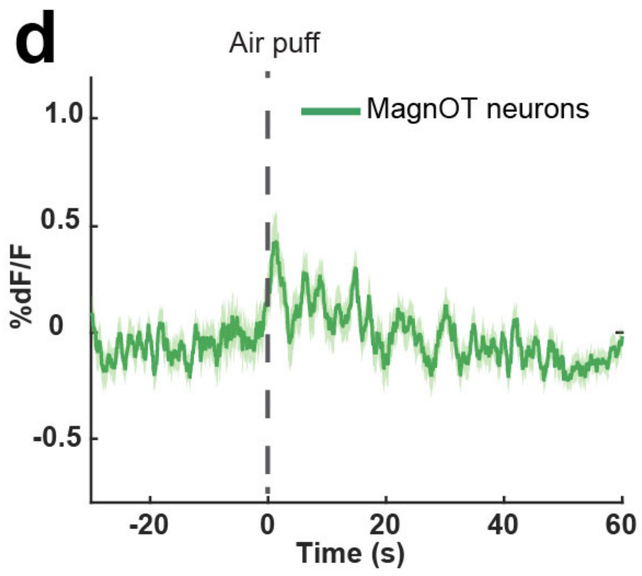
d
Air puff
MagnOT neurons
%dF/F
1.0
0.5
0
-0.5
-20
0
20
40
60
Time (s)

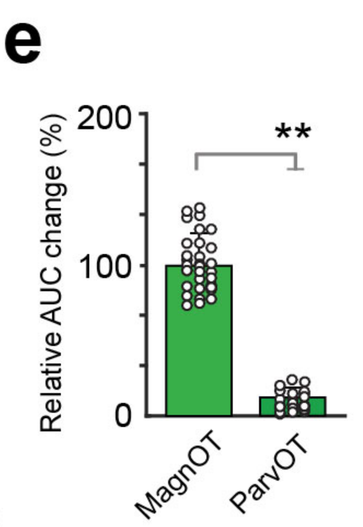
e
Relative AUC change (%)
200
100
0
**
MagnOT
ParvOT

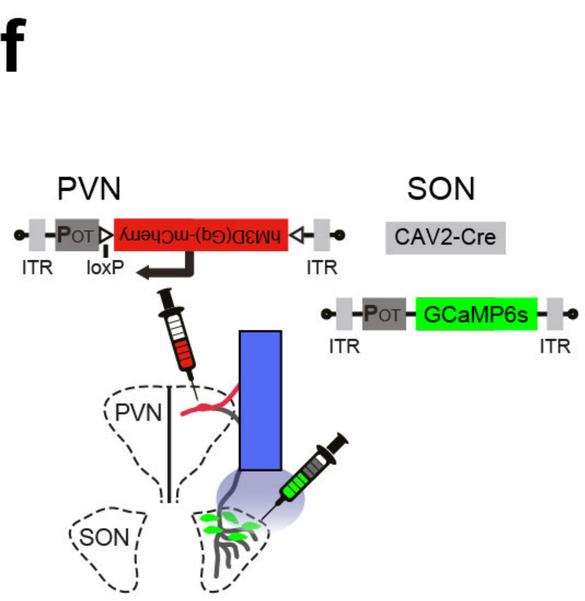
f
PVN
SON
POT
hM3D(Gq)-mCherry
ITR
loxP
ITR
CAV2-Cre
POT
GCaMP6s
ITR
ITR
PVN
SON

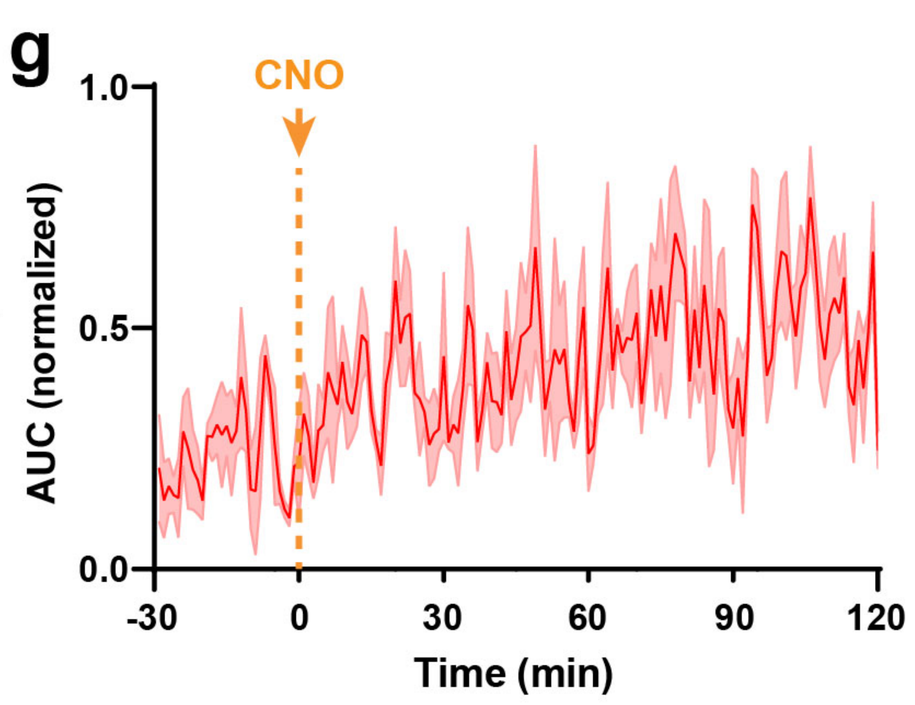
g
CNO
AUC (normalized)
1.0
0.5
0.0
-30
0
30
60
90
120
Time (min)

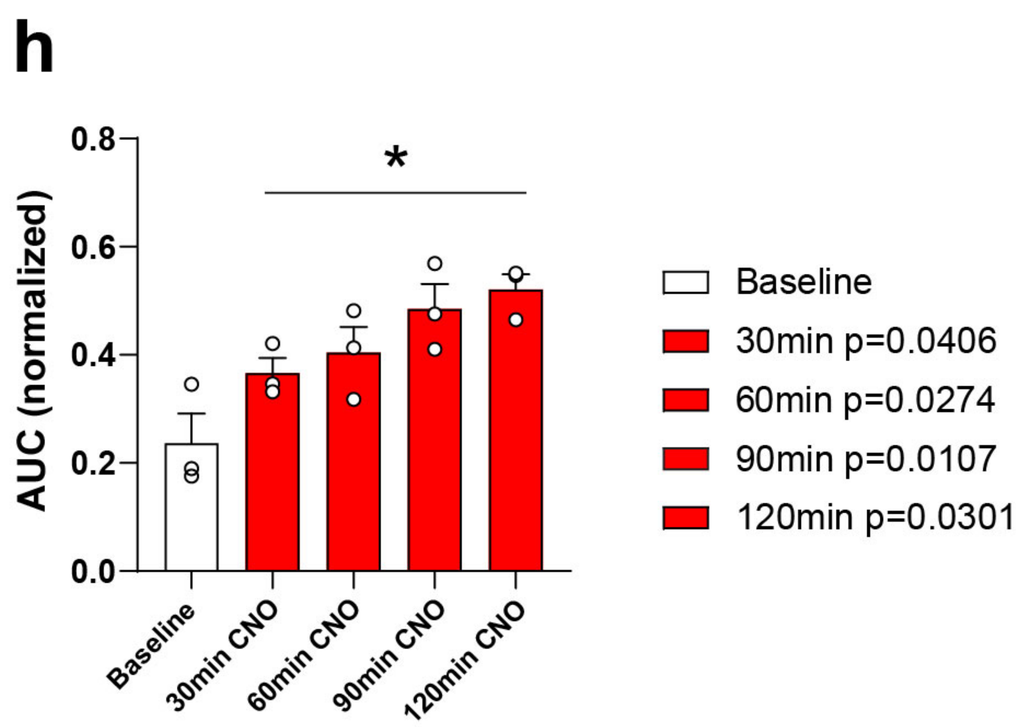
h
AUC (normalized)
0.8
0.6
0.4
0.2
0.0
*
Baseline
30min CNO
60min CNO
90min CNO
120min CNO
Baseline
30min p=0.0406
60min p=0.0274
90min p=0.0107
120min p=0.0301

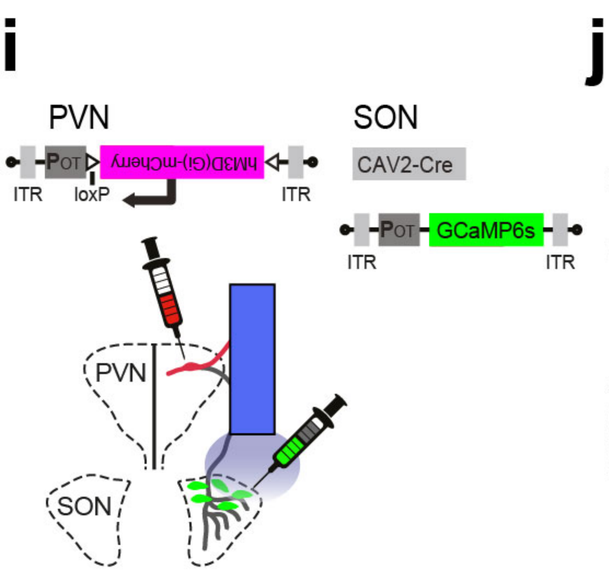
i
PVN
SON
POT
hM3D(Gi)-mCherry
ITR
loxP
ITR
CAV2-Cre
POT
GCaMP6s
ITR
ITR
PVN
SON

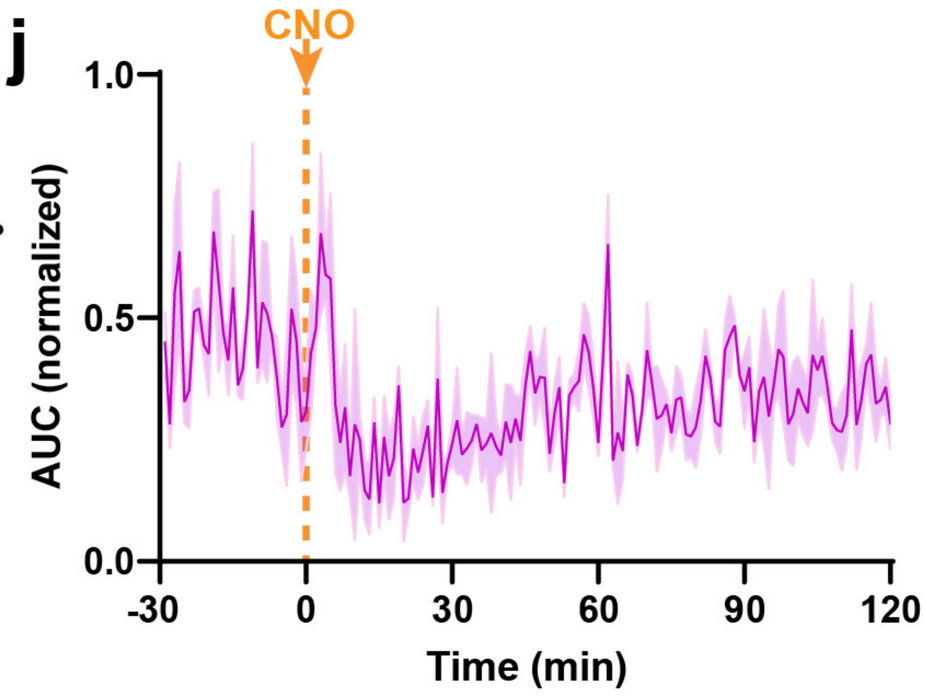
j
CNO
AUC (normalized)
1.0
0.5
0.0
-30
0
30
60
90
120
Time (min)

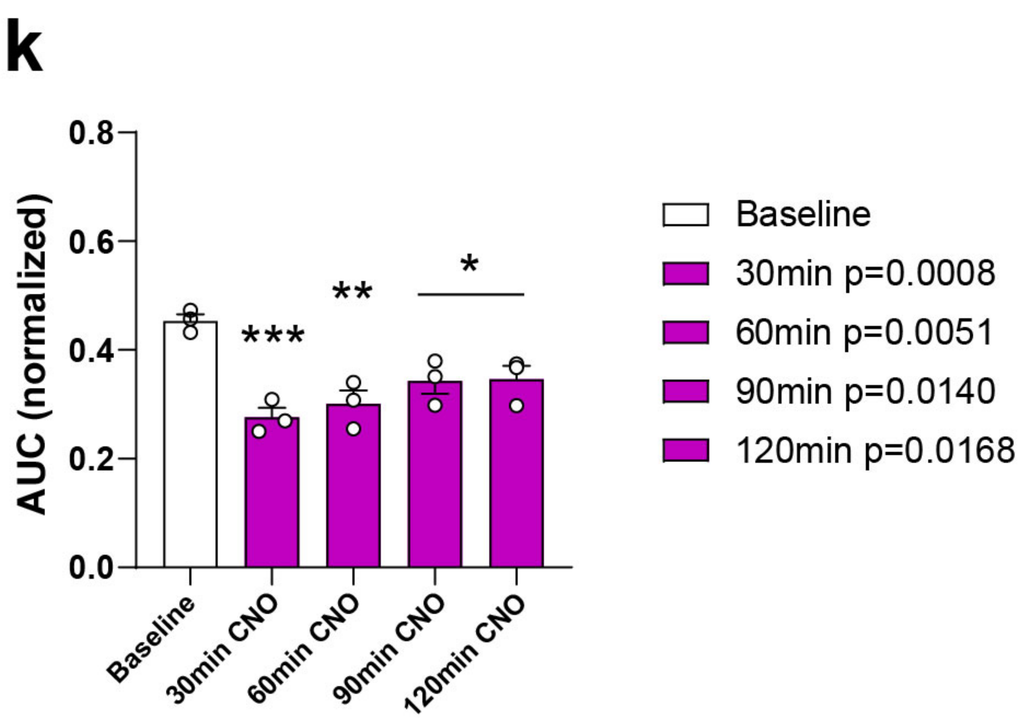
k
AUC (normalized)
0.8
0.6
0.4
0.2
0.0
***
**
*
Baseline
30min CNO
60min CNO
90min CNO
120min CNO
Baseline
30min p=0.0008
60min p=0.0051
90min p=0.0140
120min p=0.0168

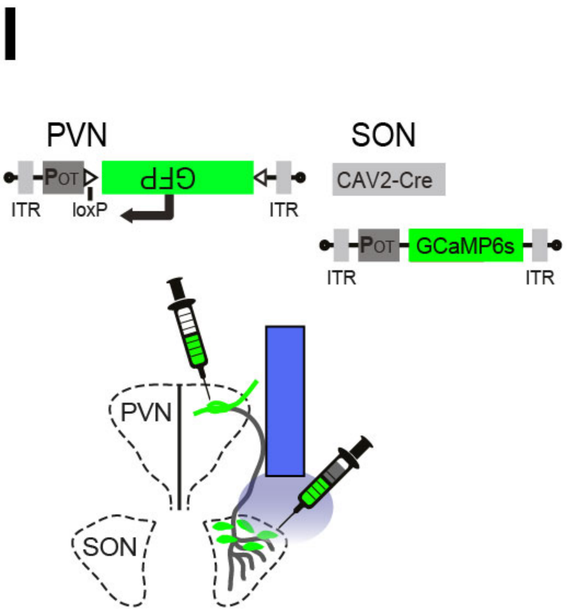
l
PVN
SON
POT
GFP
ITR
loxP
ITR
CAV2-Cre
POT
GCaMP6s
ITR
ITR
PVN
SON

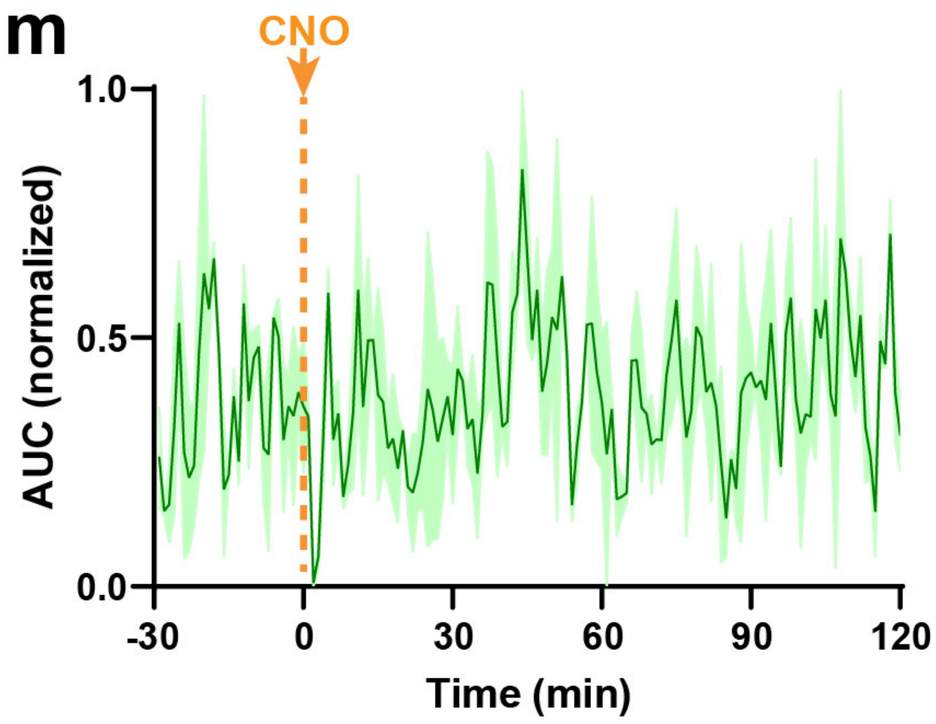
m
CNO
AUC (normalized)
1.0
0.5
0.0
-30
0
30
60
90
120
Time (min)

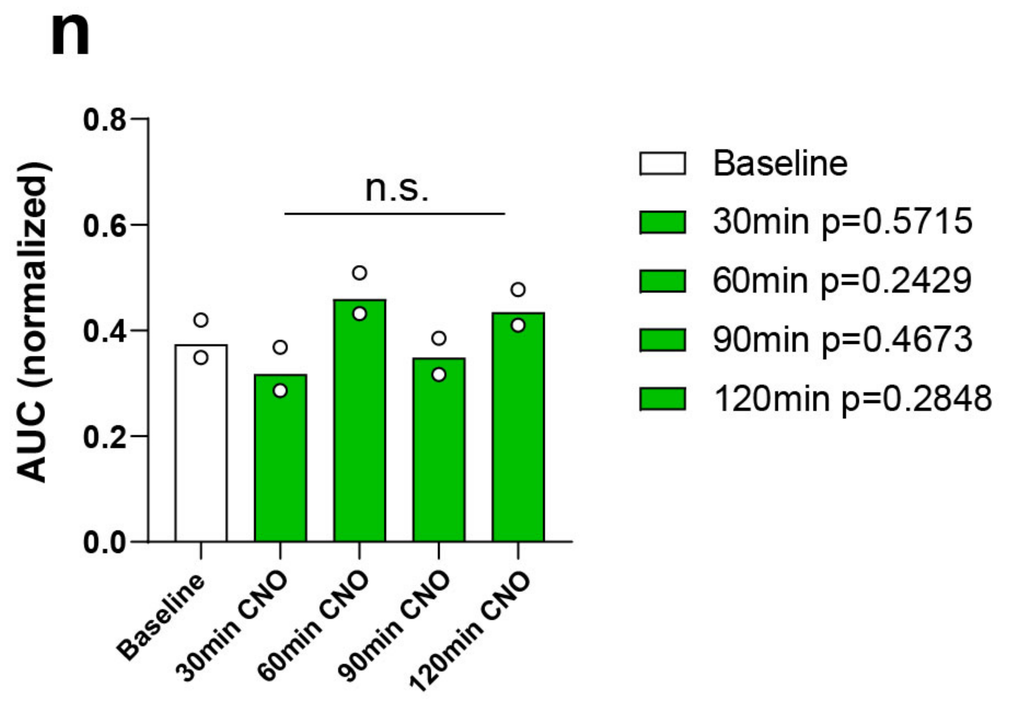
n
AUC (normalized)
0.8
0.6
0.4
0.2
0.0
n.s.
Baseline
30min CNO
60min CNO
90min CNO
120min CNO
Baseline
30min p=0.5715
60min p=0.2429
90min p=0.4673
120min p=0.2848

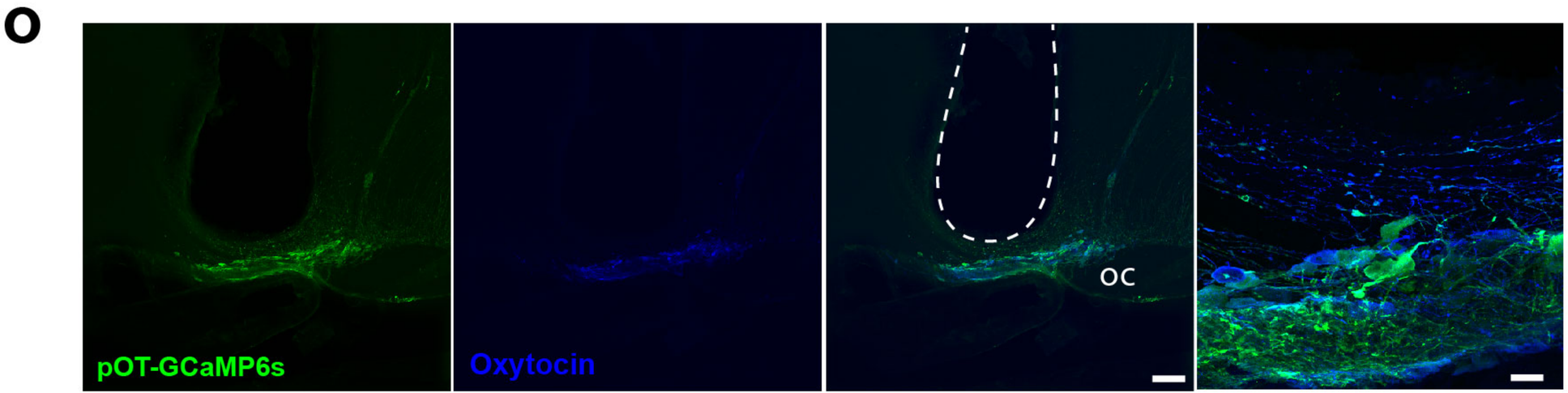
o
pOT-GCaMP6s
Oxytocin
OC

a
Inputs to parvOT neurons
PVN
POT
TCB
ITR
loxP
ITR
DIO
Pef1a
G
ITR
loxP
ITR
14 days
Rb-GFP
SON
CAV2-Cre
PVN
SON
b
Cre
Opt
c
Inputs to magnOT
PVN
POT
TCB
ITR
ITR
DIO
Pef1a
G
ITR
loxP
ITR
SON
DIO
Pef1a
mCherry
ITR
loxP
ITR
Posterior Pituitary
AAVretro-Cre
14 days
Rb-GFP
PVN
SON
PP
d
mCherry
Opt
e
TVA
3v
OT
3v
Overlay
3v
g
3V
f
OT
3v
Rb
3v
Overlay
3v
PVN
3V
h
Sep
lv
MPO
3v
SFO
3v
Arc
3v
CeA
ic
Sep
lv
MPO
3v
SFO
3v
Arc
3v
CeA
ic
i
Ins
CPu
CI
PVT
V
Hb
V
j
SN

a

SON

CAV2-Cre

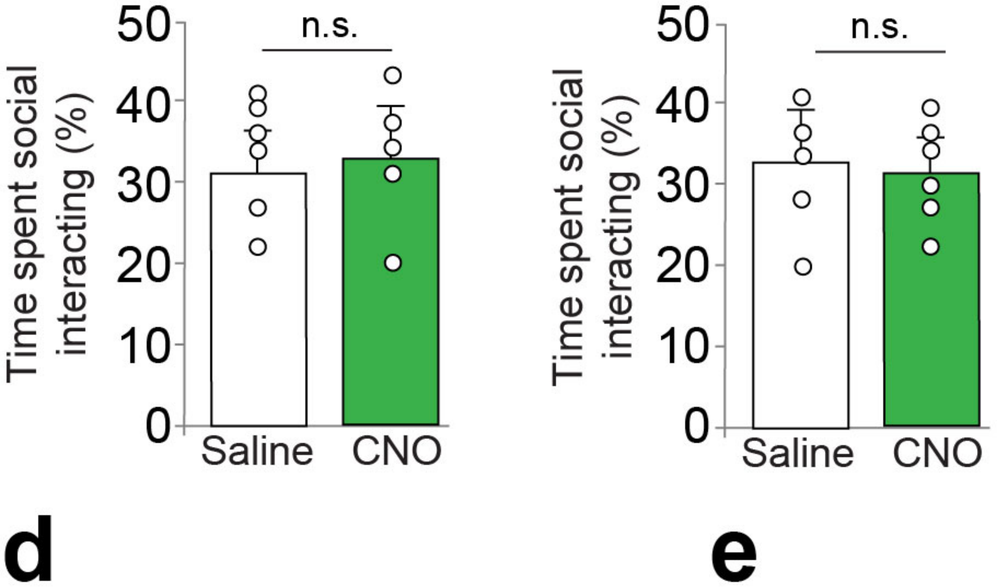

b

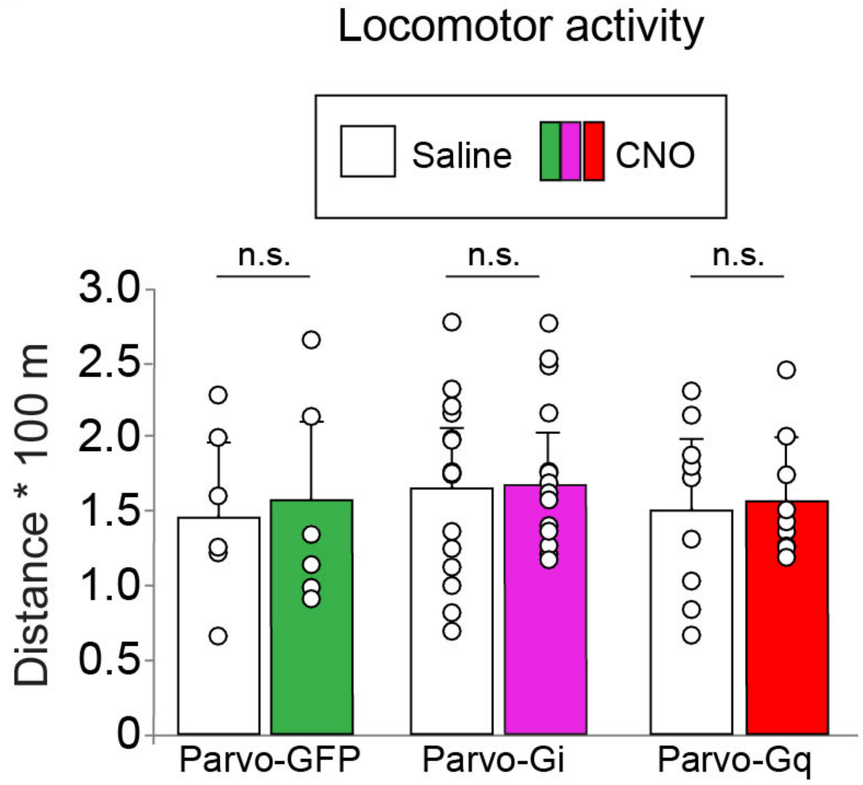

c

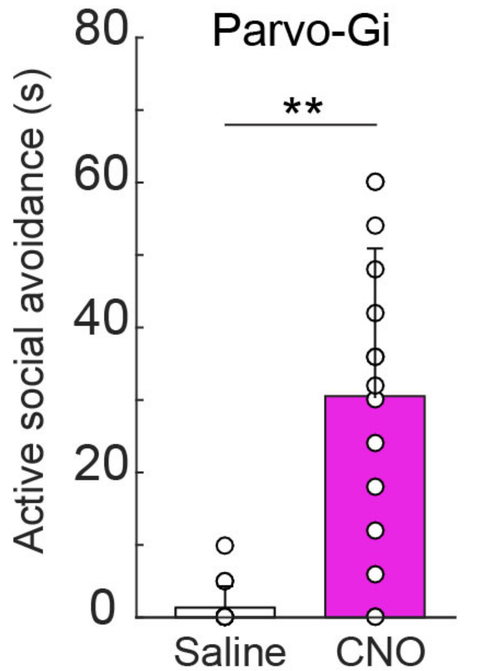

d

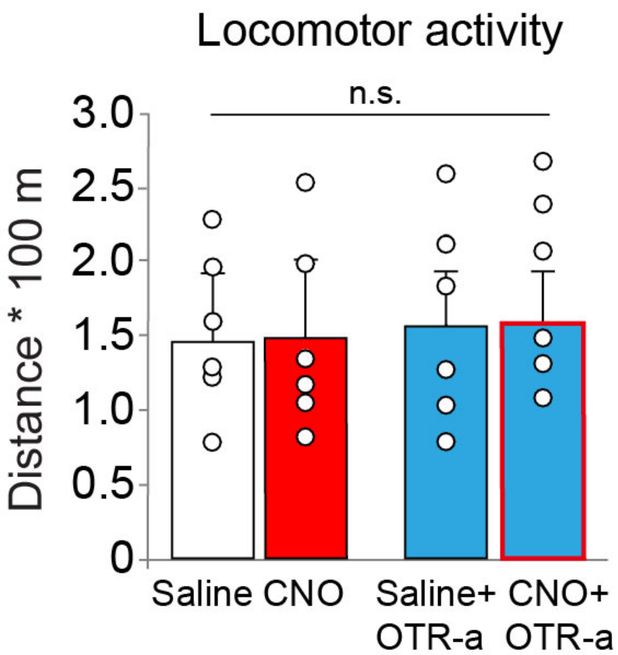

e

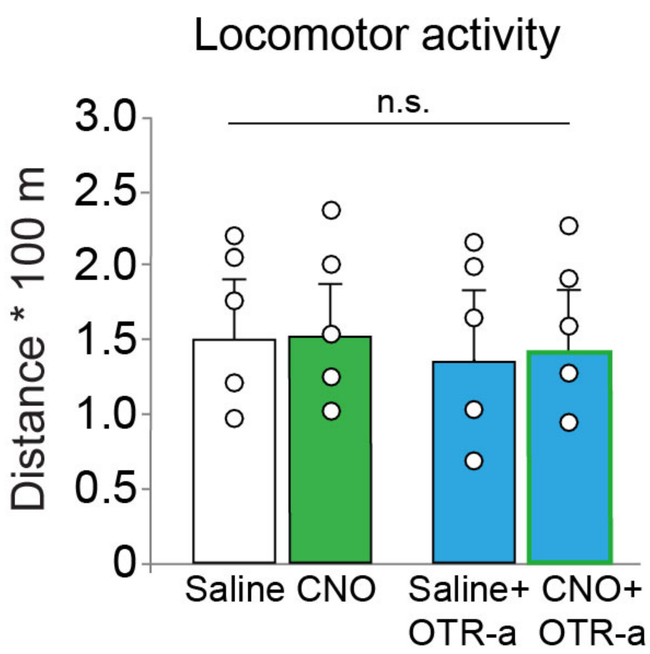

f

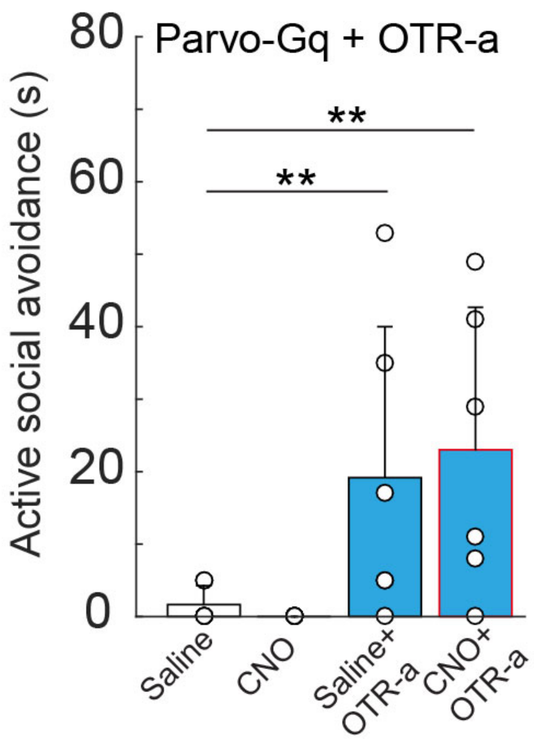

g

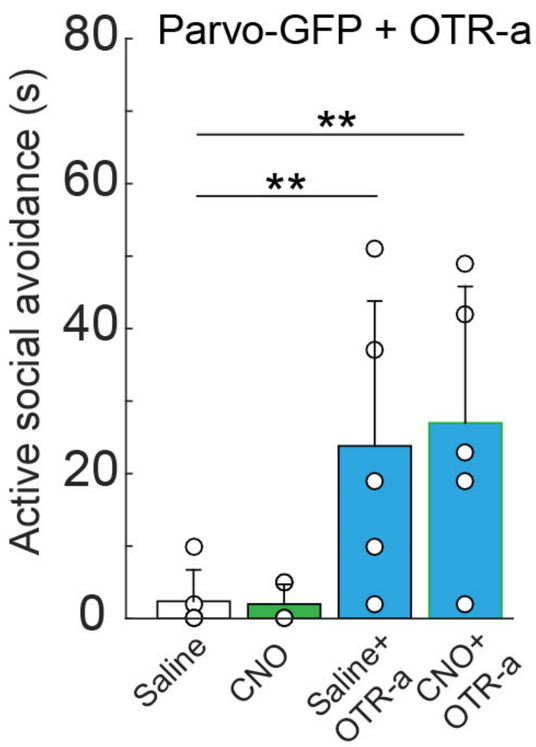

h

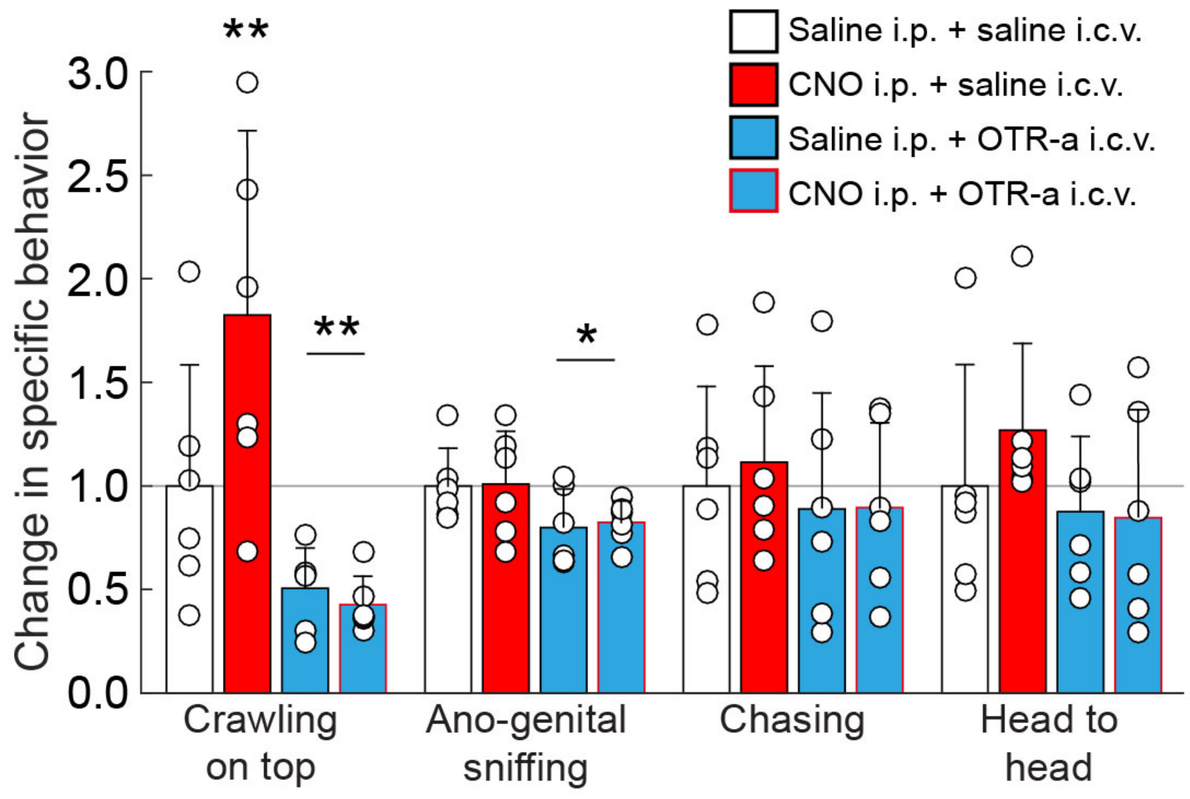

i

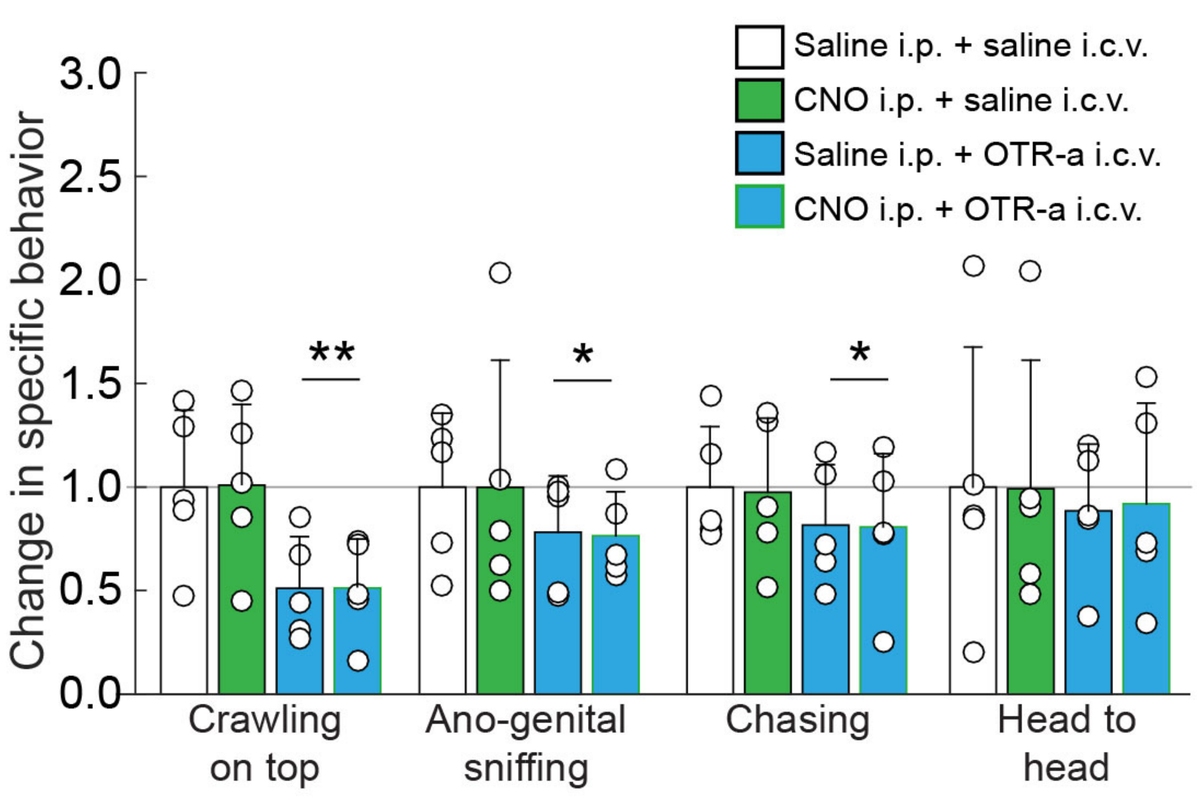

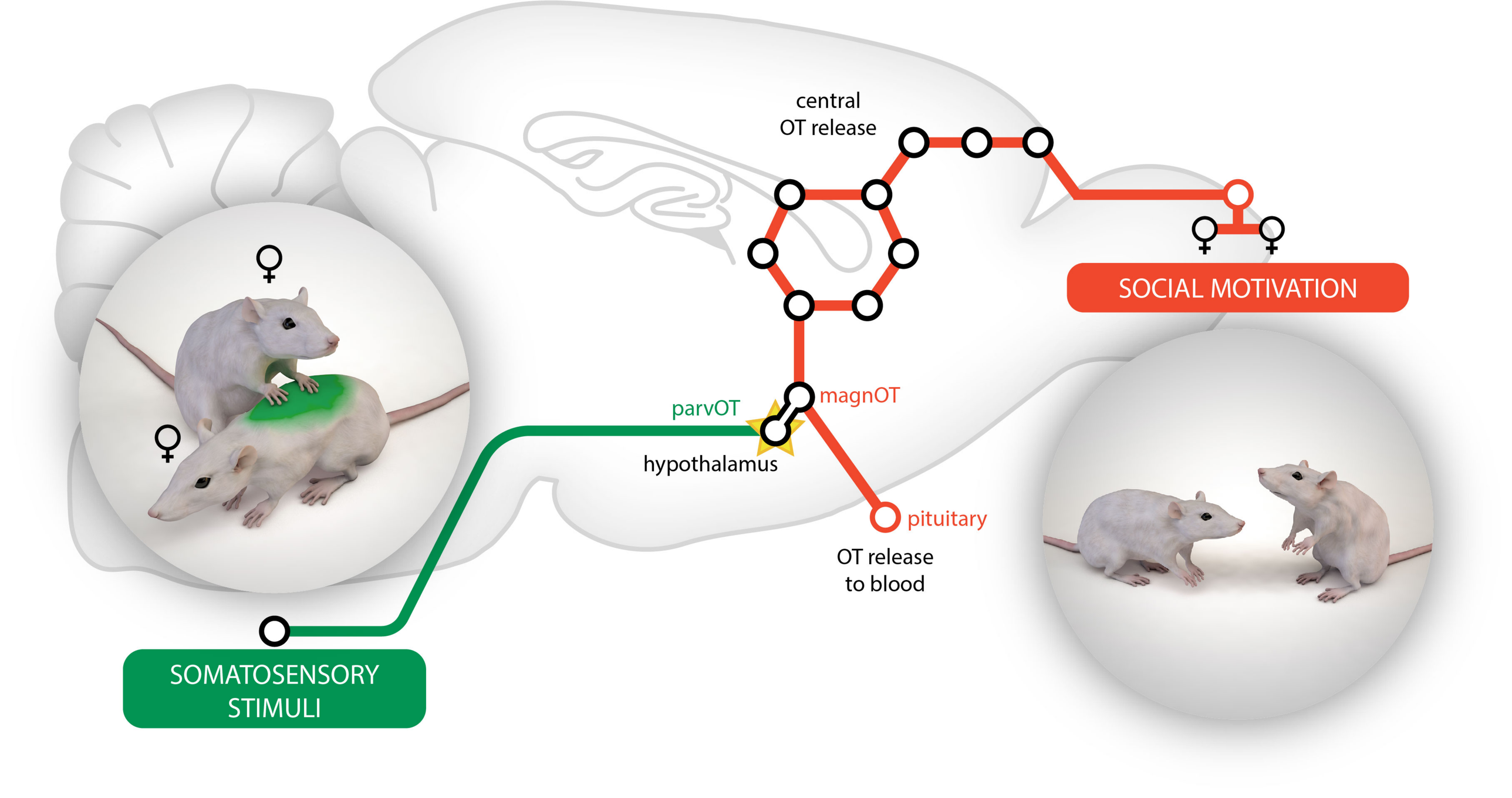
central
OT release
SOCIAL MOTIVATION
parvOT
magnOT
hypothalamus
pituitary
OT release
to blood
SOMATOSENSORY
STIMULI